UNIVERSITY OF SOUTHAMPTON

FACULTY OF ENGINEERING AND APPLIED SCIENCE

DEPARTMENT OF ELECTRONICS AND COMPUTER SCIENCE

ELECTROSTATIC CHARGES GENERATED ON AEROSOLISATION OF DISPERISONS

By

Yanyang WANG

A Thesis Submitted for the Degree
of
Doctor of Philosophy

Oct. 2001

UNIVERSITY OF SOUTHAMPTON

ABSTRACT

FACULTY OF ENGINEERING AND APPLIED SCIENCE
ELECTRONICS AND COMPUTER SCIENCE
Doctor of Philosophy
ELECTROSTATIC CHARGES GENERATED ON AEROSOLISATION OF DISPERSIONS
By Yanyang Wang

In responding to the international community's agreement of phasing out chlorofluorocarbon (CFC) propellants by the year 2000, hydrofluoroalkane (HFA) has been chosen to replace CFCs. Intensive investigations related to the new propellant products have been carried out. Aerosol electrostatics is one of the topics investigated. To understand and subsequently control the charging processes is the motive of the research reported here.

To help elucidate the complex charging process occurring naturally during atomization of liquids from pressurised Metered Dose Inhalers (pMDIs), it has been broken down into a sequence of related, simpler sub processes-drop charging, streaming current charging (coarse spray), splashing charging and fine spray charging.

Our initial studies are of single drops forming at and breaking away from the tips of capillary tubes. The drop forming processes are so slow that any hydrodynamic effect can be dismissed. Then the charge on the drop is measured. It is found that the charge on water drops is always negative (~ 10^{-14}C) at field-free condition and the magnitude of the charge increases as the drop size increases and the surrounding tube diameter decreases. With salt solutions, the charge on drops is negative at dilute solutions, decreases in magnitude as the concentration of electrolytes increases and finally reverses the sign of charge at approximately 1 M – drop charge becomes positive. All these experimental results can be explained in terms of contact potential between liquid and the inner wall of the capillary, which sets up an electric field between the pendant drop and the surrounding tube. Then computational simulation work is carried out and the data are compared with experimental results. It is found that the computer simulation data are in accord with experimental observations. This is a potential method to measure absolute potential difference between a liquid and a solid.

Secondly, the hydrodynamic processes are investigated by increasing the liquid delivery speed so that a jet is formed. The streaming current is monitored in this case. It is found that the streaming current is always negative for water and increases linearly in magnitude as flow rate increases. With salt solutions, the streaming current is negative at dilute solution, decreases in magnitude as the concentration of electrolytes increases and finally reverses the sign of streaming current at approximately 1 M – streaming current becomes positive. Then similar experiments are carried out with model propellant 2H, 3H-Decafluoropentane(HPFP). The streaming current is negative and firstly increases linearly, then increases dramatically and finally reaches another linear relationship with the flow rate. Furthermore the effects of pressure inside a can and concentration of salts on jet charge density are investigated using aqueous solutions

and HPFP. It is shown that the magnitude of jet charge density increases as the can pressure increases and the charge sign changes from negative to positive as the salt concentration increases from 0.01M to 0.1M. Finally jet charge density of pure HFA134a, HFA227ea and their Formoterol formulations are examined. Similar experiments are carried out with pure HFAs and their respective Formoterol MDIs.

The spray charge simulation experiments are carried out for both aqueous solutions and HPFP with standard plastic actuators at different pressures inside cans and different concentrations of salt solutions. It is shown that the charge sign also changes as the concentration increases from 10^{-5}M to 1M, but the polarity is the opposite of the charge on the jet. It means that the actuator actually changes the charge polarity of the spray. The spray charge density on pure HFA 134a, HFA227ea and their Formoterol formulations MDIs with both aluminium and plastic actuators are investigated

Charge that occurs when liquid splashes against different materials is measured. The effects of air blow rate and different materials on the splashing charge are investigated. This is implemented to simulate the splashing process inside the expansion chamber, which is the dead space between the actuator orifice and the metering chamber.

Finally spray size distribution is measured with a Malvern size analyser for aqueous solutions, HPFP, pure HFA134a, HFA227ea and Formoterol MDIs (HFA 134a and 227ea formulations) at different pressures inside cans to relate the effect of spray size distribution on charge density. It is found that the size distribution within the spray cloud has a close correlation with the spray charge density.

A syringe pump was used to deliver liquids to capillary tubes and a digital Keithley electrometer was used to monitor charge on drops and current on jets. A self-designed software was used to control the whole system to allow the desired delivery patterns to be implemented and record the results achieved as well. For the jet charge simulation experiments cans were modified so that the pressure inside the cans could be controlled by a pressurised nitrogen cylinder and also the liquid inside the cans can be changed to investigate the effect of different liquids on the charge density. A dose capturer was modified to capture the drug particles and also monitor the charge on them.

CONTENTS

LIST OF FIGURES:

Page

LIST OF TABLES:

Page

ACKNOWLEDGEMENTS

The success of this project would not have been possible without the continuous encouragement from my supervisor, Professor Adrian Bailey, of the Department of Electrical Engineering at the University of Southampton. I would like to thank him for all his interest and valuable advice given in the supervision of this research work.

I am grateful for the studentship provided by AstraZeneca and wish to express my gratitude to Dr Philippe Rogueda and Martin Grosvenor for their support and the efforts they have put in to make this research work successful.

I would also like to thank my colleagues in the Applied Electrostatics Research Group, particularly Dr T.J. Williams for his constructive suggestions and valuable discussions regarding many aspects of this work.

PRINCIPAL NOTATION

c	Concentration (M)
C	capacitance (F)
D	Diffusion coefficient (m^2/s)
D_{dia}	Diameter (m)
D_v	Volume median diameter
e	Charge on an electron
E_c	Bottom of the conduction band
E_f	Fermi energy level
E_{mod}	The modulus of the electric field strength at the field point
E_v	Top of the valence band
f	Volume flow rate
g	Acceleration due to gravitational
I	Current (A)
I_{cs}	Coarse spray current
I_{fs}	Fine spray current
I_{ftur}	Streaming current at fully turbulent flow
I_{lam}	Streaming current at laminar flow
I_{ptur}	Streaming current at partly turbulent flow
I_{sp}	Splashing current
I_{st}	Static charge current
I_{str}	Streaming current
I_t	total current carried by aerosols
k	Boltzmann's constant
K	Degree Kelvin (Temprature)
l	Litres (Volume)

min	Minutes(Time)
M	Mole per Litre (Concentration)
P	Pressure
s	Seconds (Time)
S	Schmidt number
v	Velocity
V	Volts (Potential difference)
V_{aw}	Potential difference at air/water interface
V_{ca}	Potential difference at capillary/air interface
V_{ex}	Applied external potential difference
V_{ls}	Potential difference at liquid/solid interface
V_{ma}	Potential difference at metal/air interface
V_{ta}	Potential difference at tube/air interface
V_{wc}	Potential difference at water/capillary interface
V_{wm}	Potential difference at water/metal interface
δ	Double layer thickness
λ	Debye Length
ε_0	Permittivity of free space
ε	Dielectric constant
η	viscosity
γ	surface tension
ρ	charge density
σ	conductivity
τ	relaxation time
ζ	zeta potential
μ	charge carried mobility

ABBREVIATIONS

Ca-dips	Calcium diisopropyl salicylate
CFC	chlorofluorocarbon
DI	Deionised
HFA	Hydrofluoroalkane
HFA134a	1,1,1,2-Tetrafluoroethane
HFA227ea	1,1,1,2,3,3,3-Heptafluoropropane
HPFP	2H, 3H-Decafluoropentane
KCl	Potassium chloride
MDI	Metered dose inhaler
MMD	Mass Median Diameter
m.p.	Melting point
NaCl	Sodium chloride
OPERA	A software
POT	The solution potential at the field point
zcp	Zero charge point

CHAPTER ONE

GENERAL INTRODUCTION

Epinephrine was the first drug to be incorporated in a chlorofluorocarbon (CFC) propellant driven metered dose inhaler in the 1950s [1]. This aerosol delivery device was a forerunner of current inhalers used in the treatment of asthma [2]. In recent times, the success of CFC propellant driven metered dose inhalers has been overshadowed by their contribution to ozone depletion in the upper atmosphere and the concomitant health effects [3]. Therefore, the international community has agreed to phase out CFC propellants by the year 2000 [4]. Pharmaceutical scientists have been responsive to the concerns over the environmental effects of propellant and have sought alternatives for the delivery of drugs to the lungs. The three major alternatives are the use of propellants that do not deplete the ozone layer [5][6]; aqueous droplet aerosols delivered by nebulizers [7] and dry powder inhalers [8][9]. Each of these approaches has its merits and their uses have been discussed in detail in the literature [10][11]. In this work, non-ozone-depleting propellants Hydrofluoroalkanes (HFAs) are objects, which we are dealing with.

When MDI and other liquid dispersion processes produce aerosols the droplets or particles within the aerosol clouds almost always carry electrostatic charge. The natural charging during these processes are exceedingly complex involving mechanisms including hydrodynamic and hydrostatic effects.

The charging processes of atomization of an MDI might include the following processes as shown in Fig.1.

- Charging of drops by "water-dropping", known as the effect of Kelvin[12].
- Electrification by friction of the liquid at the nozzle (streaming current).
- Electrification by splashing.

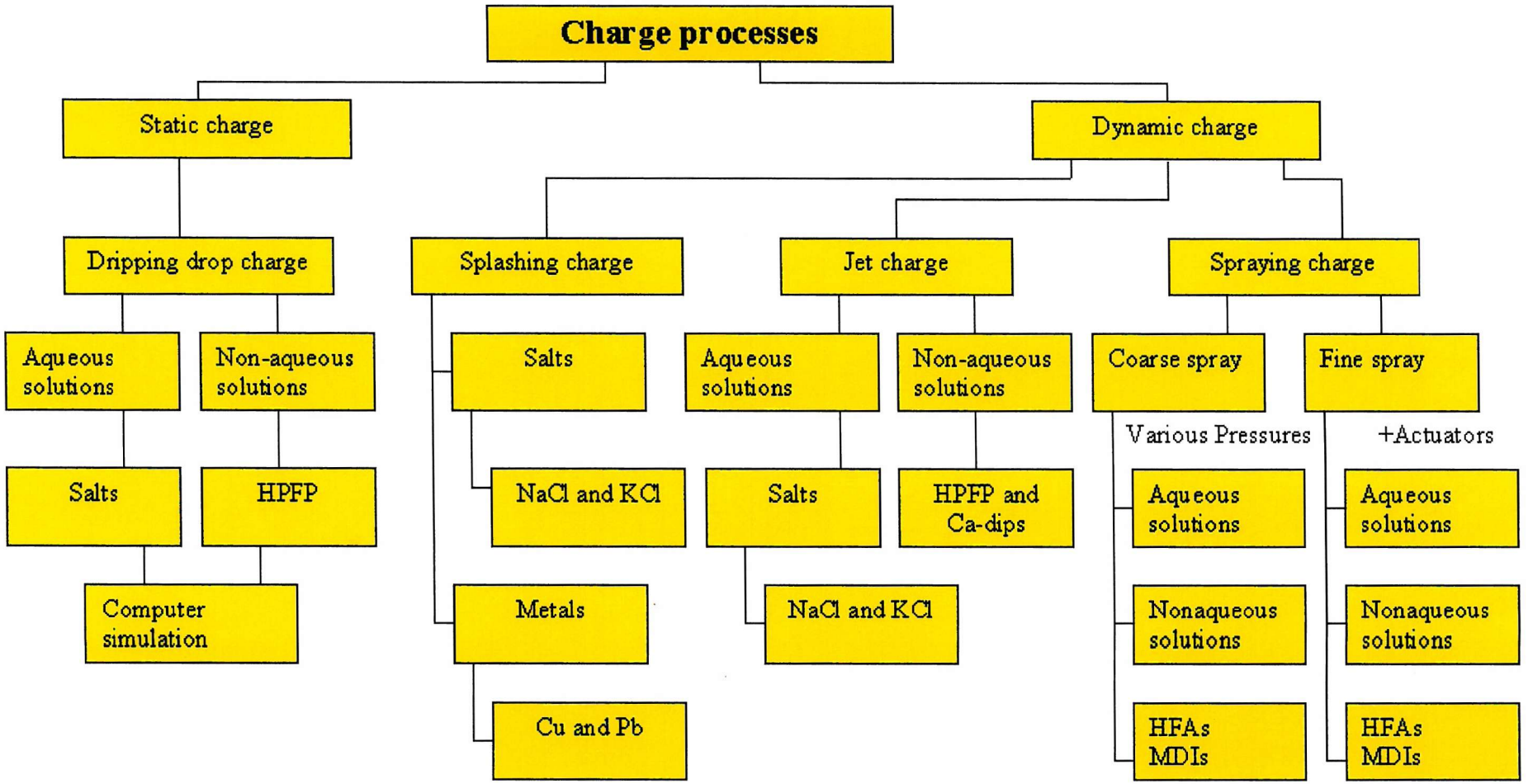

Fig.1 Diagram of major investigation of charge processes of MDIs

This thesis is presented in seven chapters:

I. Chapter one gives an overall review of previous experimental work and related theories proposed by different workers on drop charging, jet streaming current and spray charging. The purposes of this investigation are also outlined in this chapter.

II. Chapter two describes the setup and equipments used in drop charge and jet charge measurement experiments.

III. Chapter three describes drop charge in both experimental work and computer simulation. Experimental apparatus, associated procedure and experimental observations with regard to the measurement of drop size and electrical charge are described in this chapter. Comparisons between the experimental results and computer simulation data are also discussed.

IV. Chapter four deals with jet streaming current carried by liquid when liquid is pushed through a capillary.

V. Chapter five describes splashing charging processes and explanation is given regarding splashing electrification.

VI. Chapter six contains a great deal of work, including coarse spray and fine spray for aqueous solutions, model propellants, pure HFAs and Formoterol HFA formulation systems.

VII. Chapter seven, an overall discussion and conclusion on spray charging mechanisms are given.

1.1 Review of previous experimental work

The various methods of studying the drop, jet and spray chargings which arise during dispersion are reviewed and discussed under the following headings:

I. Electrification produced by dripping: a liquid drop detaching from an orifice into a gas.

II. Liquid jet: A liquid column issuing from an orifice into a gas and breaking under the action of surface tension.

III. Electrification produced by drop-splitting: the shattering of drops by the impact of a flowing gas.

IV. Waterfall electricity: Liquid columns falling through a gas on a solid or liquid surface, after breaking up under surface tension.

V. Electrification produced by spraying a liquid: spraying of a liquid by a gas, as in the action of a scent-sprayer.

VI. Electrification generated by pressurised metered dose inhalers (pMDIs).

An attempt is made to co-ordinate the material obtained from this vast area of research. Many of the results may be explained in terms of the modern theory of orientation and polarisation at the interfaces, but there are other factors, which do not appear to come within the scope of any established principles.

Free surfaces of compact matter-whether solid or liquid –are the regions which give rise to molecular adjustment, film formation, and possibly electrical separation. As such surfaces are easily accessible, they provide a promising field for the study of the constitution of matter.

There are five types of definite interfaces: Solid–solid, solid-liquid, solid-gas, liquid-liquid, liquid-gas. Of these, except liquid-liquid, almost all of them have been discussed in this thesis, and we have attempted to give a summary of existing knowledge of these subjects.

I. Dripping

Dripping charging is well illustrated by Lord Kelvin's [12](1867) famous water-dropper apparatus as shown in Fig 2. Water from an earthed reservoir drips simultaneously from two glass or metal nozzles. Two metal receiving cups are electrically cross-connected to two ring electrodes which are surrounding the tips of the nozzles respectively. When the system is switched on, the falling drops carry a small net charge. Any slight imbalance between the nozzles, drip rate, drop size, etc. leads to a slight difference in the charges that build up in the two cups, and hence the potential of the two ring electrodes differs slightly. A ring electrode at a positive potential with respect to its adjacent nozzle causes the drops that break away to be negatively charged by induction, and vice versa for a negative

electrode. The falling water drops of the Kelvin generator spontaneously produce a potential difference between the collecting cups, the feedback effect of cross connecting the ring electrodes causing the voltage to rise very rapidly to between

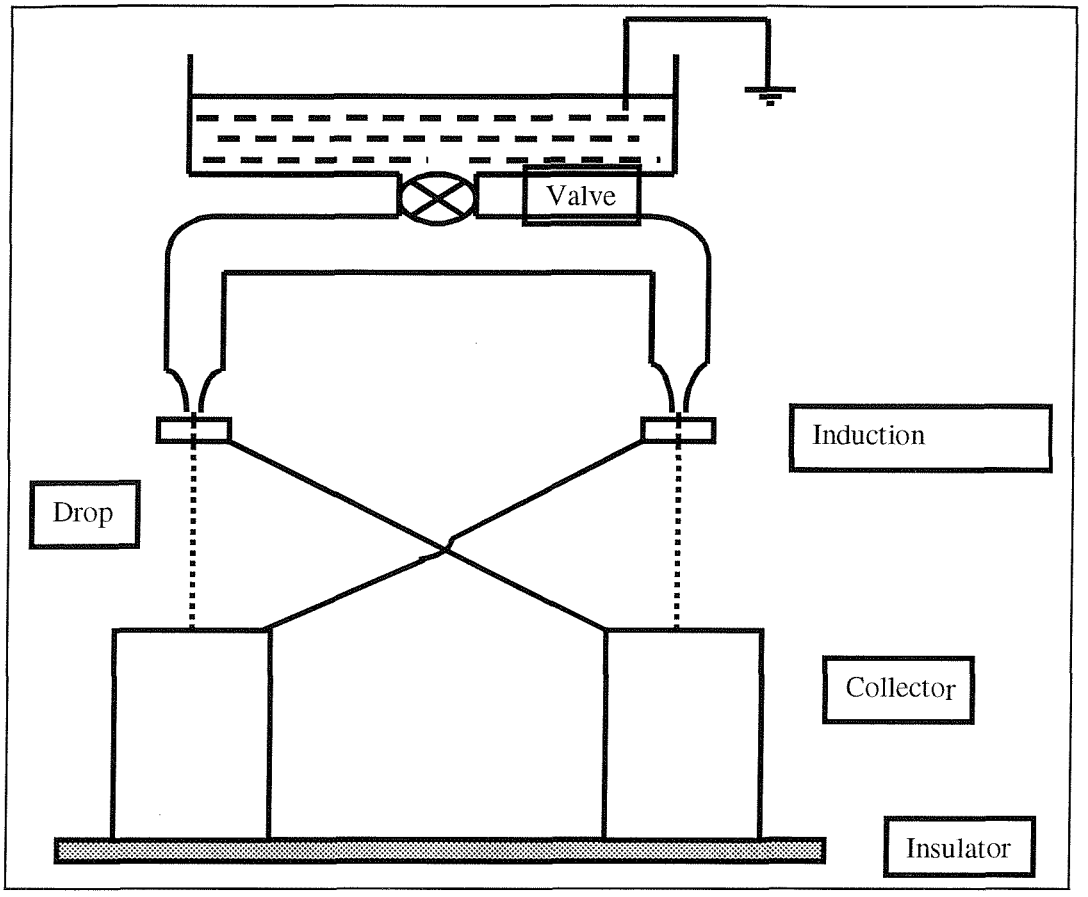

Fig.2 Kelvin's water dropper generator

10 and 20 kV within a minute. A notable characteristic of the Kelvin generator is that as the voltage builds up, the electrostatic fields at the nozzles rise and not only induce appreciable amounts of charge on the detaching drops, but also exert downward forces on the drops so that the dripping rate increases noticeably. The total effect is initiated by the dropping charge.

Chalmers and Pasquill (1937)[13] carried out an experiment in which the charging of drops in the Kelvin water dropper was studied. Their apparatus, as shown in Fig. 3 consisted of a metal reservoir and a dropper tube, the latter being surrounded by a

metalic shield tube. Water was allowed to drip into a collector arrangement, and the charge was measured on the drops. Experiments were carried out at different power-supply voltages. Several experiments were carried out in which both the tube and the dropper were made of copper. It was found that the drop charge Q and the applied potential V at the capillary in general had the same sign, and that Q plotted

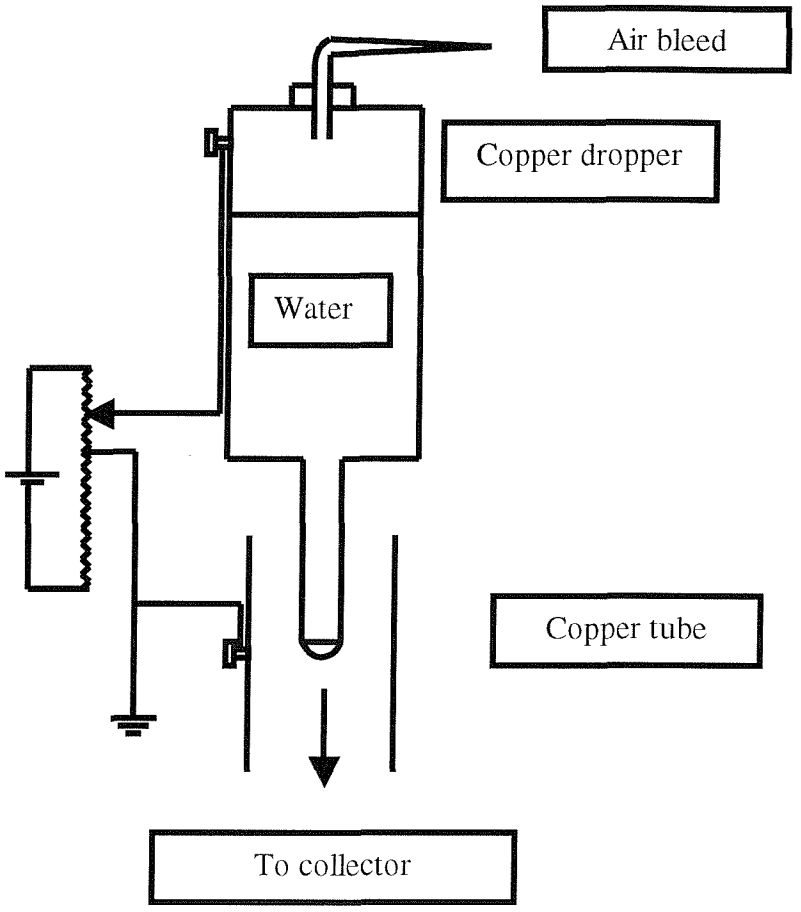

Fig.3 The apparatus of Chalmers and Pasquill (1937)

against V gave a straight line, which just failed to pass through the origin, missing it by about 0.26 volt. Therefore, negatively charged drops detached from the capillary tube when there was no applied potential around the circuit. In order for the drops to carry no residual charge, it was necessary to adjust the external potential to a value of –0.26V. Chalmers and Pasquill[13] considered that this

external voltage was exactly equal and opposite to the voltage that would otherwise have been acting at the water/air interface and resulting in a residual charge on the drops.

Chalmers and Pasquill [13] investigated several possible mechanisms other than the water/air interface voltage mechanism. They tried altering the size of the drops, using hot water, drops of tap water and distilled water and even adjusting the fall height of the drops. Under all circumstances, they found that a voltage of –0.26 V was required to ensure that drops falling from the capillary tube carried a zero charge. Chalmers and Pasquill [13] results lent strong support to the concept of an electrical double layer existing at water/air interfaces, and having a potential drop across it of 0.26 V. The water surface is negatively charged and the inner region positively charged.

Gill and Alfrey [14] [15](1949) measured the charge on drops breaking away from a vertical metal capillary using an apparatus similar to the one Chalmers and Pasquill[13] (1937) used and this time the potentials applied between the copper

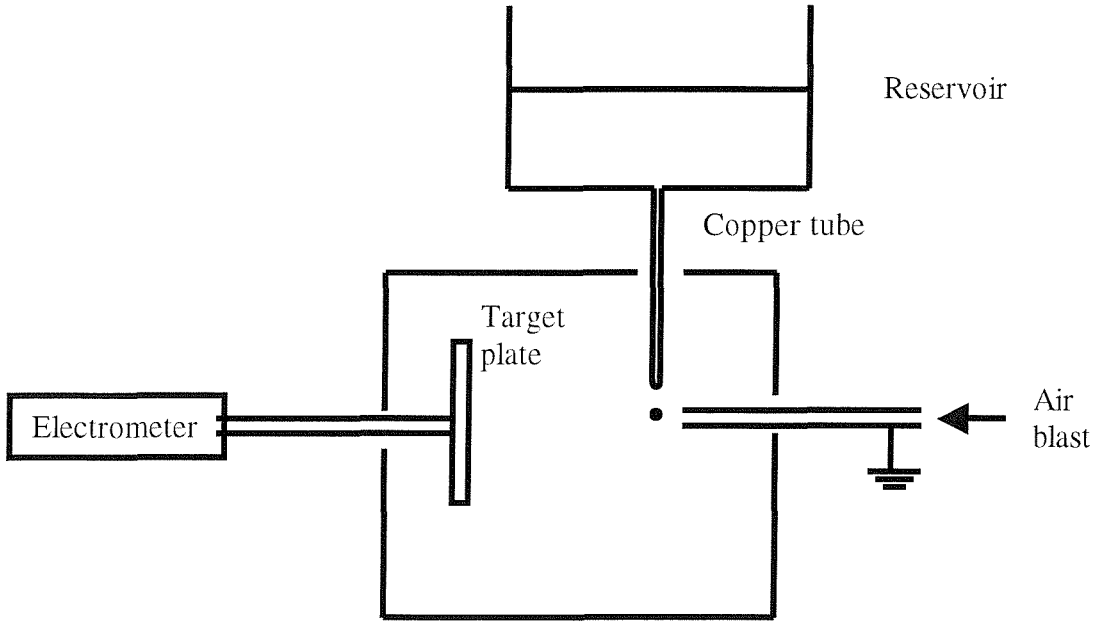

Fig.4 The apparatus of Gill and Alfrey (1952)

capillary tube and the surrounding tube varied from-1000 V to +1000 V. The copper reservoir was kept at earth potential. The relationship between applied potential V and the charge on drops Q also gave a straight line but missing the origin by about 0.1 volt. Similar experiments with carbon tetrachloride and transformer oil showed that in these cases an applied field had no effect whatever.

Gill and Alfrey [15](1952) carried out experiments on drop break-up and splashing against a metal plate using similar equipment to that used in 1949 but using a metal box instead of a surrounding tube, as shown in Fig.4. It was found that water falling through a narrow vertical tube and breaking into drops a few centimeters below the exit acquired negative charge and of the order of $0.3*10^{-14}$ C. It was explained by the contact potential between water and the capillary tube, which cannot be electrostatically shielded by any means.

Iribarne and Klemes [16] (1970) found that the drops had a small initial charge when breaking away from the needle during their experiments on electrification accompanying the break-up of large drops falling in air in the absence of electric field. This was checked by lowering the air speed so that a number of drops could be allowed to fall onto the metallic mesh underneath it, which was connected to an electrometer. The average charge was found to be from –0.4 to $-0.6*10^{-14}$ C, depending on the concentration of the solution.

II. Jet

When a hydrocarbon oil is pumped through metal pipes the streaming current may set up large potential differences, with consequent risk of a spark discharge and an explosion. Since these potentials may reach 70 kV, the streaming current can be used as a liquid high-voltage generator (Boummans[17]). Klinkenberg and van der Minne [18] (1958) in the book "Electrostatics in the Petroleum Industry" reported that the typical results of streaming current carried by low dielectric constant materials using a jet producing apparatus are as follows:

10^{-6} M-Ca(di-isopropyl-salicylate) in benzene, Istr. = -1 x 10^{-9} A.
10^{-3} M-Ca(di-isopropyl-salicylate) in benzene, Istr. = -5 x 10^{-10} A.
10^{-6} M-Al(alkyl-salicylate) in gasoline, Istr. = -1 x 10^{-9} A.
10^{-6} M-Cr(alkyl-salicylate) in gasoline, Istr. = -2 x 10^{-11} A.

The precise values depend on the flow rates. That these streaming currents are negative shows that the mild-steel wall is positively charged, presumably by adsorption of a monolayer of ions such as Ca (di-isopropyl-salicylate)[19].

Rutgers, de Smet and de Myer [20] (1956) measured streaming current through a glass capillary with distilled water and they found that the streaming currents were negative and strict linear proportionality between streaming current and pressure was also found.

III. Drop-Splitting

Two cases, very similar, arise in this section:
A. The impact of falling drops on a vertically rising current of gas.
B. The impact of falling drops on a horizontally moving current of gas.
The first case has been employed in many experiments.

A. Impact of falling drops on a vertically rising current of gas

Simpson [21], in 1909 and later, established that, for water drops of a certain average size (~0.6 mm in diameter), an uprush of air causes the drops to shatter. No shattering of such drops occurs unless the air speed exceeds 8 m/s, but if it does occur the droplets acquire (+) charges and the surrounding air (-) charges. The charge found on the water droplets is about $5*10^{-12}$ C/ml.

The results were directly opposed to Lenard's view, expressed in 1892[22], that mere dispersion of water is ineffective in producing charge. But later in 1915 [23] [24], in his comprehensive review of the subject, Lenard modified his theory, and considered that while a *steady* air stream of 8 m/s will not cause splitting and

electrification, it will do so if it be sufficiently *turbulent* to give large tangentially-directed forces on the surfaces of the water drops.

Iribarne and Klemes [16] studied the electrification produced by large drops (diameter 7.3 mm) undergoing "bag" type break-up in a steady up-draught of air,by allowing the large drops produced (diameter>1mm) to fall on a copper collector connected to an electrometer. The small droplets, mostly of diameter between 100 and 250 μm, produced by the bursting of the bag were caught in a steel wool filter and rough measurement of the charge was made in order to determine the sign. It is probable that this filter also collected any ions present. They found in agreement with Simpson [20] that the large drops were positively charged. With the addition of electrolyte the charge decreased and became negative for concentrations in excess of 10^{-4} mol L^{-1}. All the electrolytes used caused the charging to change in a similar manner. Their results are unusual in that the same magnitude of charge was separated at both low and high concentrations of electrolyte; usually in spray electrification experiments the charge separated at high concentrations is very much smaller than that with pure water. However their readings showed considerable spread, the standard deviation being of the same order as the maximum reading itself.

Zeleny [25] measured the concentrations of ions produced when water drops (diameter 5.8mm) were disrupted by air and found large concentrations of negative ions. The highest positive ion concentration measured was only 10 per cent of the negative and under some conditions the positive ion concentration was practically zero.

Considering these results with those of Iribarne et al [16] [26] it would appear that the charge separation occurring when drops burst, is between negative ions and positive drops, some of which are larger than 1 mm in diameter and not between small droplets of diameter 100 to 250 μm and drops greater than 1 mm as apparently implied by Iribarne et al [16] [26].

B. Impact of falling drops on a horizontally moving current of gas

Experiments were made by J.J.Nolan [27], in which the falling drops encounter not an uprising, but a horizontal air blast. Doubtless the effect is similar to that produced in the experiments of Simpson [21] and Hochswender [24], though the relative speed of drops and air, other things being equal, is less; and yet the resulting movement is not vertical but inclined. The drops would in that case be distorted and hollowed out, as in Hochswender's photographs, though in the present case the cup would be turned sideways-not inverted. Nolan found in the emergent stream of air both (+) and (-) ions, the negative being in excess.

One significant result arising from J.J.Nolan's [27] work is that the total charge on the droplets varies as the new area of liquid formed. Though in later work he expresses doubts as to the exact truth of this law, it appears from his results that, at least for rapid air blasts, this quantitative law is valid. Nolan's [27] result was interpreted thus: when a new surface is very rapidly formed, some of the electrons left on "raw" surface are able to escape and charge the air (-). In that case charge varies with the new area. When, however, new area is slowly formed, electrons cannot escape, and no charge arises. For intermediate speeds of surface formation, the charge cannot be strictly proportional to the new area formed.

IV. Waterfall Electricity

Lenard [22][23] is the pioneer in the subject of Waterfall Electricity. Here we deal with the conditions arising when columns of liquid in passing through a gas break under surface tension into drops and then strike a solid or a liquid surface. Lenard and Aganin[28] have shown that no charges arise unless the column breaks before striking occurs.

The influence of the gas through which the liquid (water) passes was investigated by Lenard[23] and by Sir J.J.Thomson[28] with proportional charges below:

	Thomson	Lenard
Air	+1.0	+1.0
Coalgas	+0.41	+0.86
Hydrogen	-0.11	+0.65

These figures show the relative charges developed in the water after impact. The results differ greatly in amount, and in one case in sign, and we have an instance of the great influence exerted in this class of experiment by small –scarcely detectable-differences in the composition of the water or of the gases used.

Lenard [23] allowed various liquids to descend through air, the results for the charges found in the liquid being, e.g., water (+1.0), ether (+0.01) and mercury (+1.43).

In the above experiments the charges in the liquid are measured. Other investigators, Becker [30], Aselmann [31], Kahler [32] have measured the charges in the air over the liquid. For pure water Aselmann and Kahler found only (-) ions; but for solutions of common salt, both (+) and (-) ions in the air. Becker experimented with mercury falling through various gases (air, carbon dioxide and hydrogen) on to the surface of various metals. The resulting ions in the air are in some cases (+), in others (-), the numerical values also differing very greatly according to the metal employed. He concluded that each metal has its own peculiar double electric layer in air, and that the resulting charges are brought about by the joint action of the double electric layers of the mercury and of the metal struck. Becker drew up a balloelectric (waterfall electrification) series, analogous to the electrochemical series, as follows:

+Zn, Al, H2, Hg, Air, CO2, Fe, Cu, Pt-

The interpretation of this series is as follows:
If mercury falls on mercury in hydrogen, the gas becomes (+), but in air or carbon dioxide (-). If, however, mercury falls through carbon dioxide and falls on iron the gas is (-); if on aluminium (+).

Lenard [23], J.J.Thomson [29] and Rey [33] have shown that an electrolyte such as sodium chloride, when in small concentration in water, reduces the (-) charge in the air, and when more concentrated reverses the charge to (+). Rey has also shown that raising the temperature of the solution in such cases gives rise to increased air charge, unless the concentration of the salt is at the critical point required to give a balloelectrically neutral solution.

V. Spraying

Research in this section has been particularly extensive. Faraday [34], working with an Armstrong electrostatic machine, proved that *dry* steam rushing along narrow passages does not produce electrification, but that it is essential for production of charges to have *water droplets* included in the blast. Doubtless these droplets have a rough journey in the narrow passage; so that both the turbulent steam and the walls of the passages through which they pass will contribute to their decimation. The principle thus established should be borne in mind in the experiments with apparatus like ordinary scent sprayers, with which we now have to deal, since we cannot look to the rush of mere dry gas through the tube to account for any of the charges produced.

Nolan and Enright [35] measured the overall charge on all the droplets of water of diameter greater than 30 μm produced by an atomiser and found them to be positively charged, thus indicating that at least some of the charge separation is occurring between particles of diameter less than 0.01μm and greater than 30μm. Unfortunately as they did not simultaneously measure the ion concentration, there was in fact a surplus of negative ions. However if the ion concentrations were equal as found by Chapman[36] it would be necessary to assume that the compensating negative charge resided on droplets with diameters between 0.01μm and 30 μm. But Chapman measured the charge on water droplets produced by spraying with diameters varying from 3 μm to 10 μm using the Millikan [37]method of suspending them in electric fields, and found that although the average charge

varied from 129 electronic units of charge for the smallest droplets, to 600 units for the largest, the droplets were not preferentially charged. This suggests that the positive charge on droplets ≥ 30 μm be in fact balanced by a negative charge on particles < 0.01μm.

Byrne (1977) [38] studied the spray electrification produced by an air-blast atomiser. The atomiser consisted of two narrow stainless-steel tubes, which were arranged at right angles to each other. Water issuing from one of the tubes was sheared by an air blast from the other. Liquid flow rate and air-flow rate could be varied independently, so as to alter the spray physical characteristics. The outlet ports on the side of the chamber enabled a portion of atomiser spray to be sucked through measuring instruments. One of these was an ion counter, which enabled all ions having mobilities greater than $4 * 10^{-7}$ m^2 V^{-1} s^{-1} to be captured. The other instrument was a total air monitor which consisted of a fine steel-wool collection system which was able to intercept all of the particles which were sucked into it, allowing the total charge of all particles intercepted to be measured. The sampling port and air flows were arranged such that the absolute charge on all drops smaller than about 10 μm was measured. To complete the instrumentation, a circular tray at the bottom of the spray chamber was used to collect large drops. All drops larger than about 30 μm were collected, and their charges were monitored by means of an electrometer. Particles up to a maximum size of about 300μm were detected.

Considering the differing results of the various investigators on the ratio of the ion concentrations produced by spraying, the question arises as to whether the spread in the data reported is due to impurities, experimental difficulties or some other reason.

From this survey it was decided that further investigation was warranted in order to try to establish why differing ion concentration ratios were obtained by different workers particularly between film bursting on the one hand and spraying on the other, and even when water was being used if the relationship between the various disruption processes which caused these differences could not be established, it could mean that a different theory would be required for each one. In fact Iribarne

[16][26][39] suggests a number of different mechanisms to account for the electrification produced by the different disruption processes. If the measurements, which indicated that the ion concentrations produced by spraying were equal, could be verified, it would indicate that the charge separation was occurring among larger particles in contrast to some of the other forms of disruption. Much of the earlier work was done with water which would now be considered as quite impure, therefore it was important to determine if this work was still relevant and whether the basic results were fundamentally different with pure water.

VI. pMDIs

There are very few reports on the electrification produced by pMDIs [40][41][42]. However no reports on the explanation of the charging mechanism of pMDIs have been published yet.

Carter, P.A. et al (1998) [40] reported the phenomenon of drug deposition inside spacer devices and they interpreted this phenomenon in terms of electrostatic charges produced by pMDIs. After investigation of drug deposition inside spacer devices using a salbutamol pressurised metered dose inhaler, they revealed: "aerosol particles generated from a pMDI are likely to be charged and may be attracted electrostatically to the inside surface of the polymer spacer devices. In addition, the material of the spacer device may contribute significantly to drug adhesion inside the spacer as a result of charging since charge accumulates on devices during use. Electrostatic charge accumulation on the surface of a polymer spacer device has been shown to affect the delivery of drug from that device and antistatic materials have been shown to reduce this problem. Spacer devices manufactured from metals have been shown to improve output in a similar way to antistatic liners."

Clayborough, R. and Nichols, S. C. (1998) [41] studied the characterisation of the electrostatic properties of CFC and HFA aerosols emitted from MDIs and MDIs plus spacers. They found that there were significant differences between the CFC and HFA MDI products; CFC products were electropositive whilst HFA products were electronegative.

Peart, J. et. al. (1998) [42](1999) [43] investigated electrostatic charges generated by commercial and experimental CFC and HFA MDIs. They found that both Ventolin and Airomire MDIs produced net electronegative charges on their fine particle clouds of the order of –160 pC, despite their different propellant systems, drug salt forms, drug concentrations and metering volumes.

1.2 Review of the theories of spray electrification

Chalmers and Pasquill (1937)[13] interpreted their results on drop charge in terms of a double layer existing on the interface between water/air in which water surface is negatively charged and the layer underneath positively charged.

Gill and Alfrey (1949 and 1952)[14][15] concluded from their work that the charges on dripping drops and after splashing against solid plates are caused by contact potential existing between the water and inner wall of the capillary in which the water is going through or between water and solid against which drops are splashed.

Iribarne and Klemes (1970) [16] did not give any explanation on the phenomenon of dripping drop charging that they observed.

Lenard [23] postulated that the spray electrification originated in the disruption of a double layer of charge residing on the water surface. He supposed that both positive and negative components must be just inside the water surface. The excess of negative charge found with distilled water was thought to come from the outer negative layer and he appears to have visualised some process capable of peeling the negative layer neatly off the positive because he accounts for the positive particles, formed in a minority, as arising from electrostatic induction in the field of the more numerous negative particles. Busse [44] discussed this explanation but rejected it, preferring to account for the positive particles as having been formed from parts of the surface that had already been denuded of negative ions.

Matteson [45] takes account of the liquid phase ion-pair separation arising from an imbalance of force fields responding to a bulk phase attraction for ions at a suddenly created surface during spraying.

The physical basis for this electrical double layer has not been formulated as yet, but presumably if it exists, it owes its origin to the dipolar properties of the water molecule. Some have considered it to be an ionic double layer such as that which exists at the interface between an electrolytic solution and another phase, where one set of charges is fixed to the interface and the compensating charge is in a diffuse layer extending towards the bulk of the electrolyte. However from classical electrostatic theory [46] electrolytic ions should be repulsed from the low-dielectric constant air phase to the high-dielectric constant water phase and so be crowded away from the interface to the interior of the solution. From a consideration of the solvating energy of the hydrogen and hydroxyl ions in water, Harper [47] shows that they should be approximately 200Å from the surface. Furthermore since the deficiency of solvating energy as ions approach the interface is the same for all singly charged ions because it comes from lack of dielectric polarisation at a relatively great distance from the ion, there is no reason to suppose that the negative ions behave any differently from the positive, hence it would not be expected that an ionic double layer would be formed.

It is generally agreed that at the interface the H_2O molecules are aligned with the oxygen pointing to the air and the hydrogens to the water phase. Fletcher [48] has calculated that the energy gained as a consequence of the water dipole orientating itself in this manner is about 10^{-19} J/mol. This preferred orientation decays exponentially and the surface zone has been estimated to have a thickness of only about 26 Å. However this could not be the physical basis of Leonard's double layer because the separation of the outer negative charge would imply the physical splitting of the dipole water molecules. As water is disrupted, the hydrogen bonding would be preferentially disrupted due to its much lower strength in comparison with the oxygen-hydrogen bonding. In any case there is no reason to suppose that a molecule would split into ions rather than two neutral fragments.

In spite of the theoretical difficulties an ionic double layer apparently exists at a gas-water interface because Bach and Gilman [49] measured its zeta-potential and found it to be in the range -30 to -35 mV; the negative sign is indicating that the negative layer is nearest to the gas phase. Assuming that this ionic double layer consists of a fixed negative layer of absorbed ions at the surface and an underlying diffuse positive phase, the Debye-Hückel theory indicates that the thickness is of the order of ($3\ c^{-1/2}$) Å where c is the concentration of electrolytic ions in mol L^{-1}. For chemically pure water this thickness is of the order of 1 μm (with H^+ and OH^- as the only ions, in concentrations of 10^{-7} M at room temperature). The addition of electrolytes caused the thickness of the layer to decrease and it is about 100 Å at a concentration of 10^{-3} M.

If this ionic layer is in fact Leonard's double layer then in order for charge separation to occur a velocity gradient must exist between the two layers as the water disrupts. For the "fixed" negative charge alone to be separated a layer only a few molecules thick must be sheared off and as the nature of fluid flow on this scale is complex, no quantitative estimate of the charge separation expected can be made.

Iribarne and Mason [39] and Iribarne [16] [26] made quantitative calculations, using ionic layer theory and assuming laminar flow, of the charge separation expected when water disrupts. There are a number of theoretical and experimental objections to their theory. For example when a drop is disrupted by the bag-bursting mechanism it first forms a thin film shaped like a bag, which is connected to a toroid. Iribarne [16] [26] considers that the charge separation occurs as the liquid from the film drain back into the toroid. He assumes that a portion of the positive diffuse layer flows into the toroid, thus making it positive. However, as the film is a few microns thick before disruption, it probably contains both parts of the double layer, as velocity shearing over a distance of about 0.1μm would be required to separate part of the diffuse layer at a concentration of 10^{-5} M.

In applying their theory to bubbles bursting, the film cap is ignored. It would seem reasonable to assume that the greatest velocity shearing occurs with the film when

the greatest charge separation occurs rather than with the jet. In fact Jonas et al's [50] experimental results on liquid jets and filaments support this view as the magnitude of the charges measured were about one thousand lower for disruption processes where the water was not first stretched into a film.

Jonas and Mason [50] measured the charge on two droplets of radii 23 and 37 μm produced by a single jet disrupting and found that the smaller droplet was slightly positive. They account for this result by assuming that the larger droplet contained more of the surface negative layer. However it seems more reasonable to assume that the underlying positive charge drains into the larger droplet by analogy with the theories given for bag bursting of drops and for filaments breaking into three droplets. However this would predict that the larger droplet would be positive which disagrees with experiment. As the separated charges are very small it is possible that this is not a manifestation of spray electrification.

Iribarne [16] [26] proposed that two spraying mechanisms must be used to account for the polarity change normally found as the concentration of electrolyte is increased. He suggested that one mechanism (termed droplet formation) was common to almost all disruption processes and occurred at the higher electrolyte concentration giving the final persistent electrification. A number of different mechanisms were proposed for bubbling, drop bursting and splashing but no attempt was made to suggest a mechanism for spraying.

The existence of spray electrification as a separate charge generation mechanism has been questioned. Gill [14] has emphasized the inherent improbability of Lenard's hypothesis and with Alfrey [14] [15] has supposed that other investigators have been misled when interpreting their experiments as being in accord with this hypothesis. They suggested that others have overlooked the importance of the induction charging of drops when they impinge and rebound from a solid surface

1.3 Objectives of the present Investigation

The experimental objectives of this study are to examine the electrostatic charges generated on aerosolisation of dispersions; to understand and subsequently control the charging processes that occur during the production of aerosols from Metered-Dose Inhalers (MDIs).

It is not generally a difficult task to determine the electrostatic charges when an artificial electric field is used to stimulate or dominate charging processes, and the results can be explained in terms of electrostatic induction. However, to determine the natural charging processes is rather difficult. This is because, first of all, it must be certain that any external field has been shielded so that any artificial results can be eliminated; secondly, it is extremely difficult to eliminate all other undesired naturally occurring fields to leave only the one which is to be investigated; Finally some of the signals involved in natural charging processes are very small making the determination of the charge even more difficult.

Therefore, in order to investigate the natural charging occurring during aerosolisation of a dispersion, it is very important to break down the complex processes into related simpler sub sequences.

In this study, the spray processes of MDIs are broken down to the sequences as below:

- Charging of drops by "water-dropping" effect of Kelvin.
- Electrification by friction of the liquid at the nozzle (streaming current or coarse spraying).
- Electrification of splashing
- Fine spray charging

Therefore, the purposes of this study, in the first stage, are to examine the charges generated when liquid drops detach very slowly from the tips of vertically mounted capillaries. The drops break away from the tips in such a way that any dynamic effects on the drop charges would be dismissed, leaving only static effects which

dominate the whole charging processes. Up to date no report of thorough investigation on this subject has been seen except Chalmers'[13] work and in two or three papers this phenomenon is mentioned only in a few lines.

In the second stage, liquid is forced with greater pressure through the capillary so that the liquid comes from the orifice in a continuous manner- a liquid jet. In this case, the hydrodynamic effects become dominant in the charging processes, making the hydrodynamic role played in the whole charging processes possible to be examined.

Thirdly, the dripping drop is blasted by air against a metal plate and all the droplets are bounced back away from the metal plate. The charge left on the metal plate is investigated. This phenomenon is called splashing electrification, which is closely related to the charging processes of a pMDI device.

Finally, spray charging processes are investigated. These processes are divided into two parts: coarse spray, which refers to the spray produced by liquid or suspension coming from the valve stem and fine spray, which refers to the spray coming out of the orifice of the actuator after the coarse spray splashing against the extension chamber of the actuator. In both coarse and fine spray sections, the charging processes of aqueous solutions, model propellants, HFAs and Formoterol HFA formulations are investigated.

CHAPTER TWO

DESCRIPTION OF APPARATUS

2.1 General Layout

The experimental arrangement is shown in Fig.5. The experiments required a liquid delivery system to make the liquid flow inside the capillary at a desired flow rate. Therefore a syringe pump was used which can be controlled by a designed software. The programme and flowchart used to control the syringe pump are attached in the Appendix I at the end of this thesis. A syringe was used as a reservoir and needles of various sizes may be fitted to the syringe. In this work stainless steel needles of different outside diameters as shown in Table1 were used and their tips were especially made flat to produce the typical shape of drops.

In order to collect the liquid and measure the charge it carried with it, a digital electrometer was used which also had been connected to the computer and controlled by a designed software. As the experiments were carried out, the data taken from the charge collector was stored in the computer as *.dat file which would be analysed by using Excel and at the same time the results were displayed on the screen to be observed. This programme and flowchart can be seen in Appendix II.

A Faraday cup was used to collect the liquid and was connected to the electrometer. In order to avoid the influence of the Earth's natural electric field (which under fair weather condition is about 130V/m at the Earth's surface [51]) and other interfering signals, the whole set-up was put in a Faraday cage (60cm x 60cm x 60cm); apart from that, a metal tube was used so that the pendant drop at the tip of the needle would be in a properly symmetric electric field. The needle was positioned along the axis of the surrounding metal tube and at the centre and a set of metal tubes of inner diameters 5.6mm, 8.9mm, 16.5mm and 30mm were used. In order to avoid contact potential between the metals, stainless steel was chosen to use for the materials of capillary needles, surrounding tubes and connection wires.

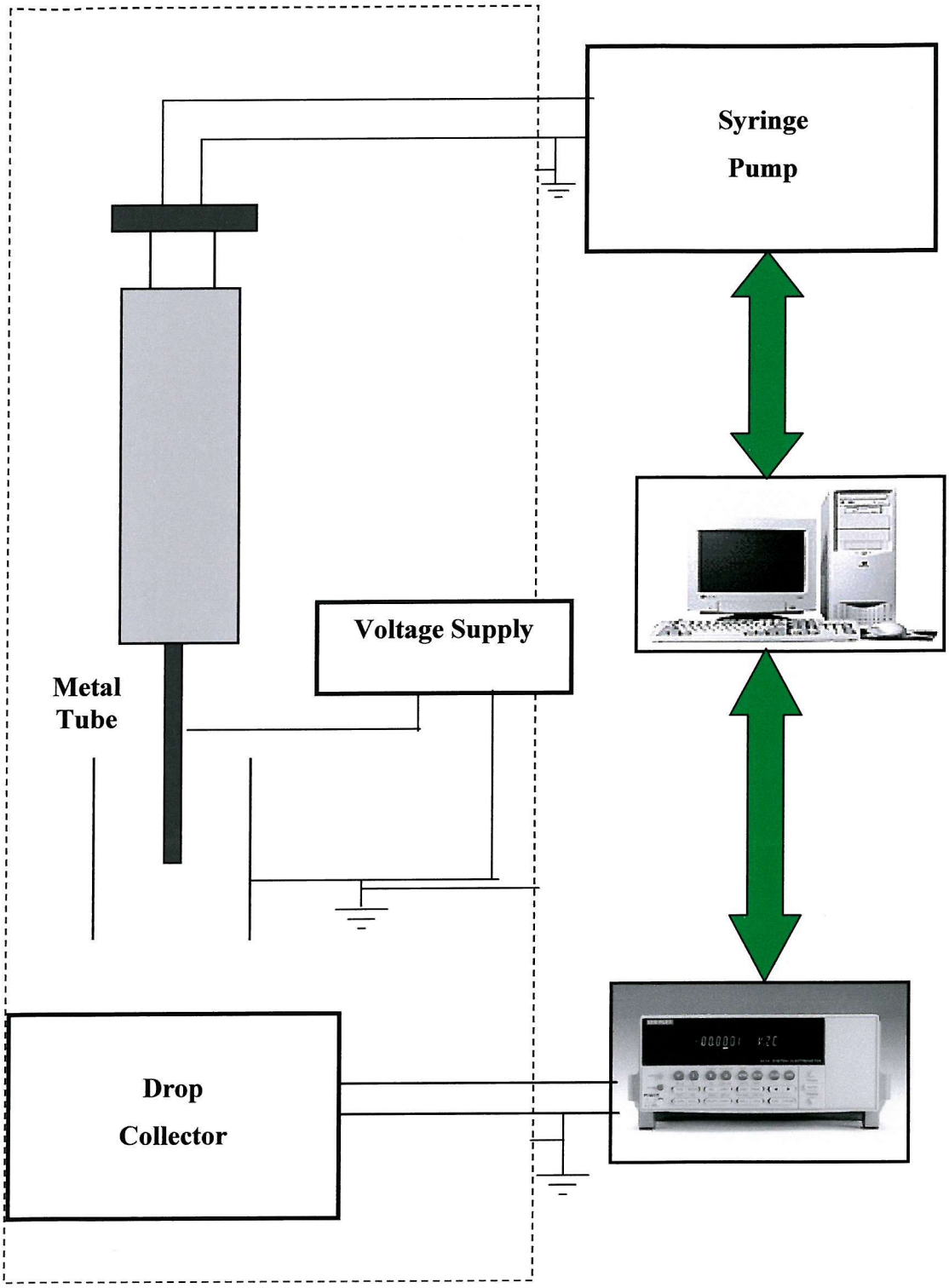

Fig. 5 Diagram of Apparatus of generating drops and jets

During all experiments, the flow rate was set to be 6 μl/min so that not only every single drop reached its maximum shape very slowly before it was broken away from the tip of the needle, but also, at this low flow rate, electrokinetic effects on drop charging processes could be ignored. DI water (deionised water, ~ 18.2 Megohm-cm resistivity) and aqueous solutions were used. The charged drops detaching from the tip of the needle fell into the Faraday cup. Drop charge was averaged over the individual charges. In our case nine drops were taken to average the drop charge. The drop size was calculated from the volume of delivered liquid, which would be displayed on the screen.

2.2 Sample preparation

During the experiments, DI water (deionised water) from a Corning Mega-Pure System (MP-6A) distillation column was used and its conductivity was ~ $1.02*10^{-6}$ S/m. Salts and alkaline stock solutions were prepared by dissolving Fisher Scientific pellets in DI water. Acid solutions of different concentrations were diluted in DI water using concentrated acids from Fisher Scientific Company.

Chemicals used during the experiments are as follows:

DI water ($1.02*10^{-6}$ S/m)

Tap water ($2.65*10^{-2}$ S/m)

Salts: Potassium Chloride (10^{-6}~3M)

Sodium Chloride (10^{-6}~6M)

Ammonium Chloride (10^{-6}~1M)

Lanthanum Nitrate (10^{-6}~1M)

Salts were chosen in such a way that KCl, NaCl and NH_4Cl to give mono-valence effect and $La(NO_3)_3$ to give multi-valence effect.

Alkalis: Potassium Hydroxide (10^{-6}~10^{-2} M)

Sodium Hydroxide (10^{-6}~10^{-2} M)

Acids: Sulphuric acid (10^{-6}~10^{-2} M)

Hydrochloric acid (10^{-6}~10^{-2} M)

Table1. Needle (capillary) diameter table

Needle Gauge	G30	G27	G26	G24	G22	G20	G18	G17	G16	G12
OD*(mm)	0.305	0.406	0.457	0.559	0.711	0.889	1.271	1.499	1.651	2.769
ID *(mm)	0.152	0.203	0.254	0.305	0.406	0.584	0.838	1.041	1.194	2.159

* OD and ID refer to the outer diameter and inner diameter of the needles respectively.

Table2. Surrounding tube sizes

Tube Length (mm)	22.4	35.6	66	136
Tube Inner Diameter (mm)	5.6	8.9	16.5	30

2.3 General equipment

A digital Keithley electrometer (Model 6514) and a Harvard apparatus syringe pump (PHD 2000 Infusion) were used, which can deliver up to 220.82 ml/min with a single 140 ml syringe and down to 0.0001 μl/hr with a single 0.5 μl syringe. Maximum pressure is dependent on syringe size. A Viglen computer (Contender P2 400) was used to control both the syringe pump and electrometer. A whole set of stainless steel needles ranging from Gauge 30 to Gauge 12 (Hamilton Needles) were fitted to the syringe to produce drops and jets. A set of stainless steel tubes of inner diameters 5.6mm, 8.9mm, 16.5 and 30mm were used. Two Aluminium Faraday cup were used to collect liquid and a digital Thurlby power supplier (PL310) was used to give an external field between needles and the surrounding tubes.

OPERA-2D was used to analyse drop charge and Borland C++ was used to compose programme software.

CHAPTER THREE

DROP CHARGE

First of all, the charge on a single drop, breaking away so slowly that any hydrodynamic or electrokinetic effects can be dismissed, was examined under different conditions with different liquids and tubes of different sizes. The experimental results were compared with computer model simulation data.

3.1 Introduction

Basically, six kinds of experiment were carried out. First of all, under the conditions of an external electric field being applied between the needle and the surrounding tube, single drop charge is measured using DI water and needles of various outer diameters. In this case, the needle and the surrounding tube were both connected to a power supply (Thurlby, PL310) and voltage from -1V to +1V was applied during the experiments. Secondly, in the absence of an applied electric field between the needle and the surrounding tube, drop charge was measured using various electrolyte solutions at various concentrations. The field-free condition was obtained by connecting the needle and the surrounding tube with a stainless steel wire which was grounded all the time during this kind of experiment, with the whole set-up being put in a Faraday cage. The electrolyte solutions of potassium chloride, sodium chloride, ammonium chloride and lanthanum nitrate were used and the concentration is changed about from 10^{-5}M to 1M. Then gas friction on drop charge was examined. Finally, the influence of both needle diameter and surrounding tube diameter on DI water drop charge was investigated.

3.2 Basic static theory

- Image charge

It is shown in Fig.6 that real charges induce image charges in adjacent conductors. The sequence of events leading to the generation of charge by induction is shown in Fig.6 In (a) a low resistivity, electrically neutral particle arrives in the space between two electrodes across which a voltage is applied. The electric field in this space causes charges within the particle to redistribute in order to maintain a constant potential throughout its volume. Positive charges are induced on the side facing the negative electrode, negative charges on the side facing the positive electrode.

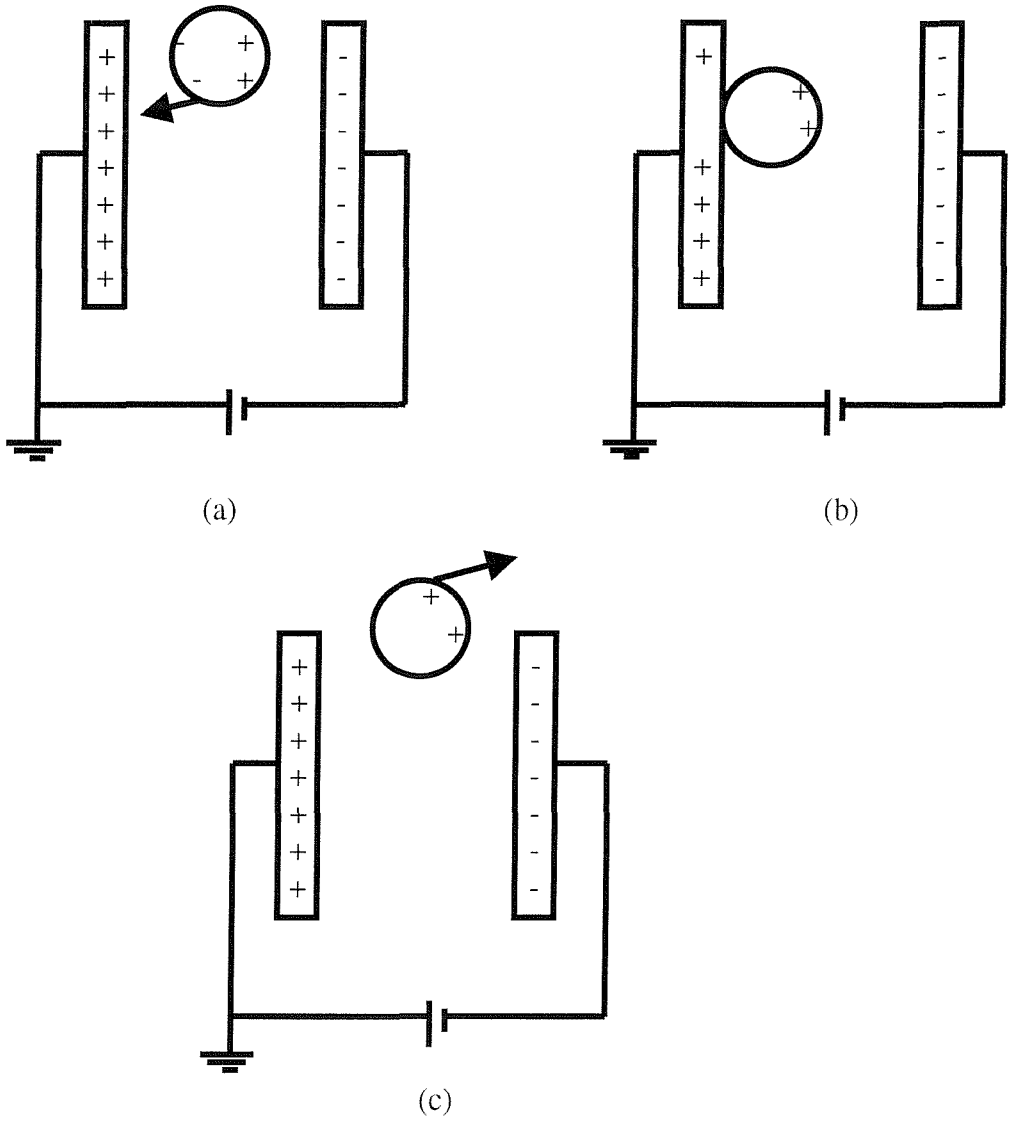

Fig. 6 The three stages in induction charging. (a) Polarisation in an electric field, (b) Charge transfer and (c) Charged particle moves away from charging electrode

The particle is said to be polarised. If, now, the particle momentarily contacts the earthed electrode, negative charges flow out of the particle into the electrode and neutralise an equal number of positive charges in the electrode. The particle is left with an excess positive charge (Fig. 6(b)) and when it breaks away from the electrode this excess charge is retained (Fig.6(c)). It should be remembered that had the particle touched the negative electrode it would have acquired a negative charge.

- Metal-Liquid Contact - The double layer

In order to describe contact potential quantitatively in terms of electron transfer for metal-metal and double layer for metal-solution, accurate knowledge is required of the electronic structure of the materials involved.

It was Helmholtz [52] in 1897 who first postulated that a double-layer invariably formed at a phase boundary. From this basic concept he developed a mathematical theory relating the velocity of electroosmotic flow to the charge separation which occurred in the double-layer. Despite this early success, some thirty years elapsed before Gouy [53](1910) in France and Chapman [54] (1913) in Britain independently presented a theory which was applied initially to the interfaces between solids and weak electrolytes.This has since been added to by Stern [55](1924) and by Grahame [56] (1950).

Ions produced by dissociation of trace contaminants undergo random thermal motion which distributes them uniformly throughout the liquid. This situation changes at a boundary with a solid surface because one type of ion, say positive, is preferentially adsorbed to the surface of the solid (Fig.7). If the liquid was electrically neutral at the beginning, the loss of positive charge to solid surface means that an excess negative charge of equal magnitude must be present in liquid. Thus, a difference in potential is created between the solid and the bulk liquid. With positive ions preferentially adsorbed to the surface, as in Fig.7, the potential of the solid surface must be positive

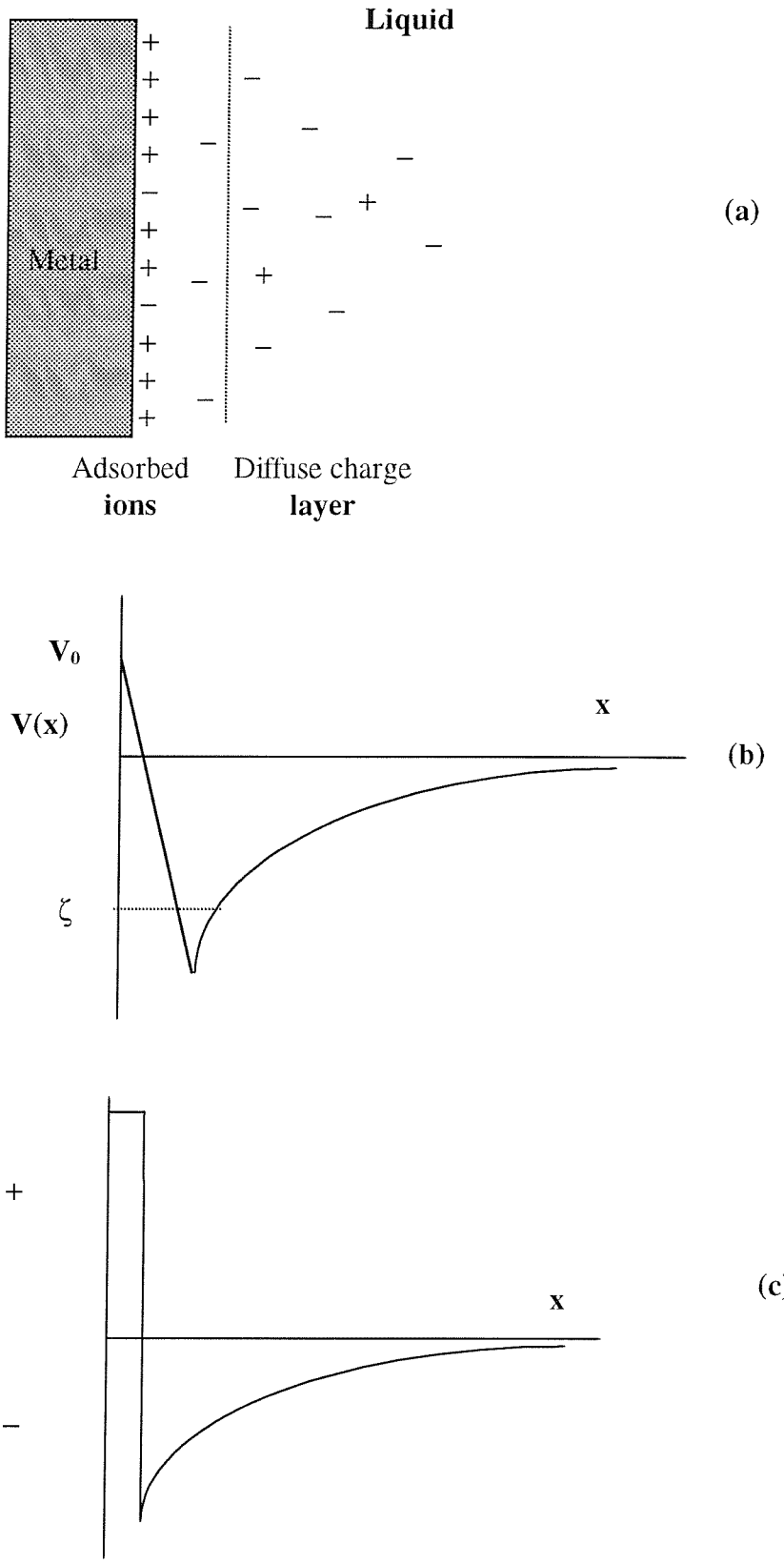

Fig. 7 (a) A double layer at a solid-liquid interface. (b) The potential and (c) the charge distribution across the interface.

relative to the bulk liquid. The magnitude of this potential depends on the density of the ions localised at the solid surface.

The separation of positive and negative charges at the interface gives rise to an electric field in the liquid, which causes the ions in the liquid to redistribute; negative ions are attracted towards the surface, positive ions are repelled. Consequently, the concentration of negative ions near the interface is increased above that in the bulk liquid while the positive-ions concentration is reduced. Diffusion processes now become important. As a result of the concentration gradients set up near the interface, negative ions diffuse away from the interface, while positive ions diffuse towards the interface. This diffusive flow of ions opposes the redistribution (conduction) caused by the electric field originating from the charged surface. Eventually, the diffusive and electrical flows balance and the interface comes into equilibrium.

The immobile surface charge and the diffuse layer of counter ions in the liquid (see Fig. 7) together constitute the double-layer.

In the Gouy-Chapman model of the double layer, it is assumed that the adsorbed surface charge is distributed uniformly over the surface of the solid and that the counter ions in the diffuse part of the double-layer are point charges. The ions in the liquid must satisfy simultaneously both the Poisson equation for space-charge and the Boltzmann equation which provides a mathematical relation between the concentration of ions at a particular location in the liquid and the electrostatic potential there.

Applying the Boltzmann equation to the case in hand enables the concentrations of positive and negative ions, $n(x)^+$ and $n(x)^-$ respectively, at a distance x from the solid surface in Fig 6(a), to be written as

$$n(x)^+ = n\exp\left(-\frac{eV(x)}{kT}\right) \qquad (1)$$

$$n(x)^{-} = n\exp\left(+\frac{eV(x)}{kT}\right) \qquad (2)$$

where n = $n(\infty)^{+}$ = $n(\infty)^{-}$ is the density of ion pairs in the bulk liquid well away from the interface, e the electronic charge, k Boltzmann's constant and T the absolute temperature.(Here assumed the ions to be monovalent). The charge density, q(x), at x is then given by

$q(x) = e\,[\,n(x)^{+} - n(x)^{-}\,]$

i.e.

$$q(x) = -\,en\left[\exp\left(\frac{eV(x)}{kT}\right) - \exp\left(-\frac{eV(x)}{kT}\right)\right] \qquad (3)$$

which on substituting into Poisson's equation yields

$$\frac{d^2V(x)}{dx^2} = \frac{ne}{\varepsilon\varepsilon_o}\left[\exp\left(\frac{eV(x)}{kT}\right) - \exp\left(-\frac{eV(x)}{kT}\right)\right] \qquad (4)$$

For large values of x, the electric field of the charged surface, i.e. the potential gradient in the liquid, must decrease to zero (screened by the diffuse cloud of counter ions). Furthermore, if it is assumed that the potential in the bulk liquid is also zero and that insulating liquids may be considered to be weak electrolytes so that $eV(x) \ll kT$, then equation (4) may be integrated twice (Sennet and Olivier, 1966), yielding

$$V(x) = V_O\exp\left(-\frac{x}{\delta}\right) \qquad (5)$$

where V_O is the potential at the surface of the solid. δ, which has the dimensions of length, is given by

$$\delta = \left(\frac{\varepsilon \varepsilon_o kT}{2ne^2} \right)^{\frac{1}{2}} \qquad (6)$$

According to the Einstein relation, the ratio of mobility, μ, to the diffusion coefficient, D, of ions is given by

$$\frac{\mu}{D} = \frac{e}{kT} \qquad (7)$$

which on substituting into equation (6) yields

$$\delta = \left(\frac{\varepsilon \varepsilon_o D}{2ne\mu} \right)^{\frac{1}{2}} \qquad (8)$$

For a monovalent electrolyte in which both species of ion have identical mobilities, this can be further simplified using equations $\sigma = \sum_i n_i q_i \mu_i$ and $\tau = \rho \varepsilon \varepsilon_o$ to give

$$\delta = (D\tau)^{\frac{1}{2}} \qquad (10)$$

where σ, ρ, n_i, μ_i, q_i, and τ and are volume conductivity, resistivity, densities, mobilities of the free-charge carriers in the material, the charge on each carrier and the dielectric relaxation time of the electrolyte.

Equation (5) shows that the potential in the liquid decreases exponentially from an initial value V_O at the interface to zero in the bulk liquid (Fig 6(b)). If we now substitute for V(x) in equation(3) while retaining the assumption of a weak electrolyte, we obtain the charge density in the diffuse part of the double-layer as

$$q(x) = -\left(\frac{2ne^2 V_o}{kT} \right) \exp\left(-\frac{x}{\delta} \right) \qquad (11)$$

which can be written as

$$q(x) = -\left(\frac{\varepsilon\varepsilon_o V_o}{\delta^2}\right)\exp\left(-\frac{x}{\delta}\right) \qquad (12)$$

We see, therefore, that the charge density in the liquid (Fig.6 (c)) also decreases exponentially into the bulk of the liquid in the same way as the potential.

Since the system as a whole must remain electrically neutral, the net negative charge in the diffuse layer must equal the net positive charge on the solid surface. Assuming, therefore, that the liquid extends to infinity for positive values of x but at x = 0 is bounded by a solid surface of area, A, to which a uniform charge +Q has adsorbed, we may write

$$Q = -\int_0^\infty Aq(x)dx = \int_0^\infty A\left(\frac{\varepsilon\varepsilon_o V_O}{\delta^2}\right)\exp\left(-\frac{x}{\delta}\right)dx \qquad (13)$$

which simplifies to

$$Q = \left(\frac{\varepsilon\varepsilon_o A}{\delta}\right)V_o \qquad (14)$$

This is a particularly interesting result since it shows that a double-layer behaves exactly like a parallel-plate capacitor in which the plate separation is δ and across which a potential V_o appears. Until now, the parameter δ has been considered simply as a characteristic length in the exponential decay of charge and potential through the double-layer. By analogy with the charged capacitor, we see now that it is a measure of the effective width of the double-layer.

- Metal-Metal Contact

Quantum mechanical considerations dictate that electrons in solids occupy discrete energy states. In metals, the states available for the valence electrons form a quasi-continuous band (Fig 8(a)) ranging from Ec to the vacuum level. The vacuum level

is defined as the energy of an electron removed an infinite distance away from the solid and is usually taken to be zero. The density of states per unit energy interval, N(E), increases parabolically as shown in Fig 8(b). The total number of states

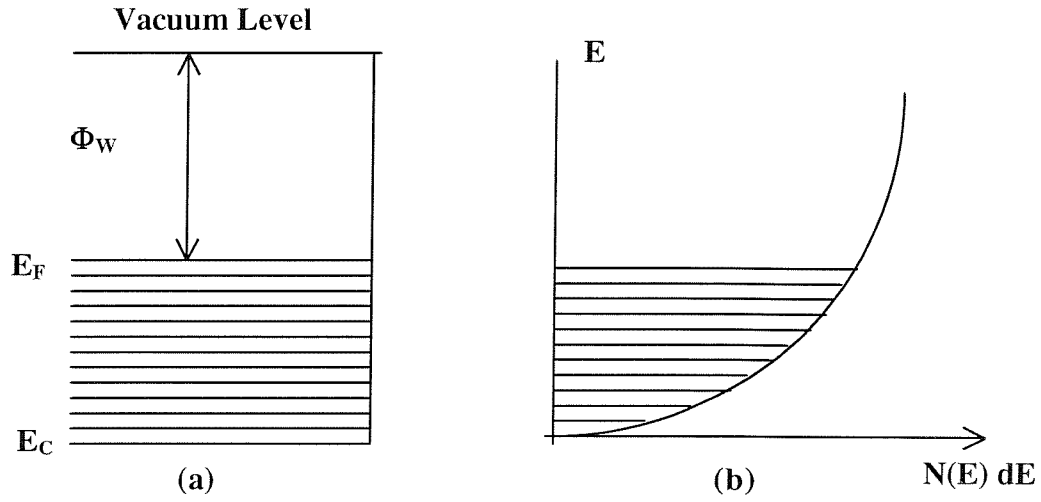

Fig. 8 (a) Simple energy band structure and (b) the density-of-states curve for a metal

greatly exceeds the total number of valence electrons so that only those states below the Fermi energy, Ef are occupied. The energy interval, ϕw, from Ef to the vacuum level is termed the work function (or contact potential) and is an important characteristic of the metal.

As can be seen from Fig 9, ϕw represents the minimum energy that an electron in the metal must gain if it is to escape from the metal (in chemistry ϕw is refered to the electrochemical potential of the metal). For most metals, ϕw is in the range 4 to 5 eV, with Ec some 10 to 15 eV below the vacuum level.

Fig 9 shows a contact being made between metal A of work function ϕ_A and metal B with a higher work function, ϕ_B. In (a) the two metals are far apart so that no interaction occurs between them. When the two metals are brought into contact, electrons in the higher energy states in A transfer by a tunnelling mechanism into the unoccupied lower energy states in B. Consequently, the potential of metal A

becomes more positive, thereby decreasing the potential energy of all the electrons remaining in A. The potential of B becomes more negative resulting in an increase in potential energy of the electrons In B. The transfer of electrons across the

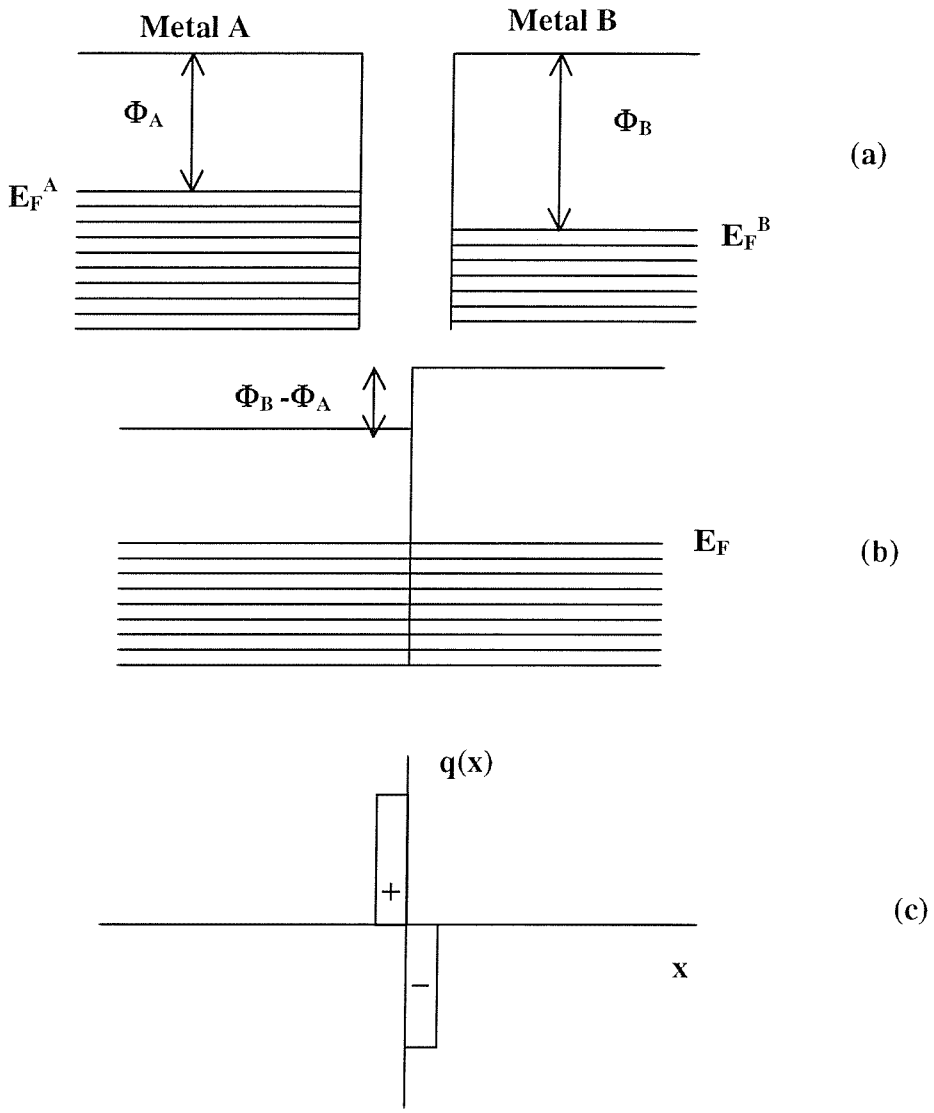

Fig. 9 Contact charging of metals. (a) Two metals of different work functions brought together. (b) At thermal equilibrium the Fermi energies of the two metals are equal.(c) The charge distribution across the interface at thermal equilibrium.

junction is sufficient to cause the two Fermi energies E_F^A and E_F^B to coincide as shown in Fig 9 (b). This potential difference, ΔV, is equal to $(\Phi_B - \Phi_A)$/e volts and is known as the contact potential difference. It is equivalent to the zeta-potential at the solid-liquid interface and again a double layer has formed (Fig9 (c)) albeit very thin.

3.3 Experimental results and discussion

3.3.1 Drop charge dependence on voltage

In order to investigate the charges on water drops, electric potentials from –1 to 1 volt were applied between the capillary and the surrounding tube and the charges on drops were measured. It was found, as shown in Fig 10, that the drop charge Q (DI water) plotted against the applied voltage V (between the capillary needle and the tube, the polarity of V is the sign of the electrode connected to the capillary) gave a straight line which just failed to pass through the origin, giving as intercept the potential that must be applied so that the drop carries no charge.

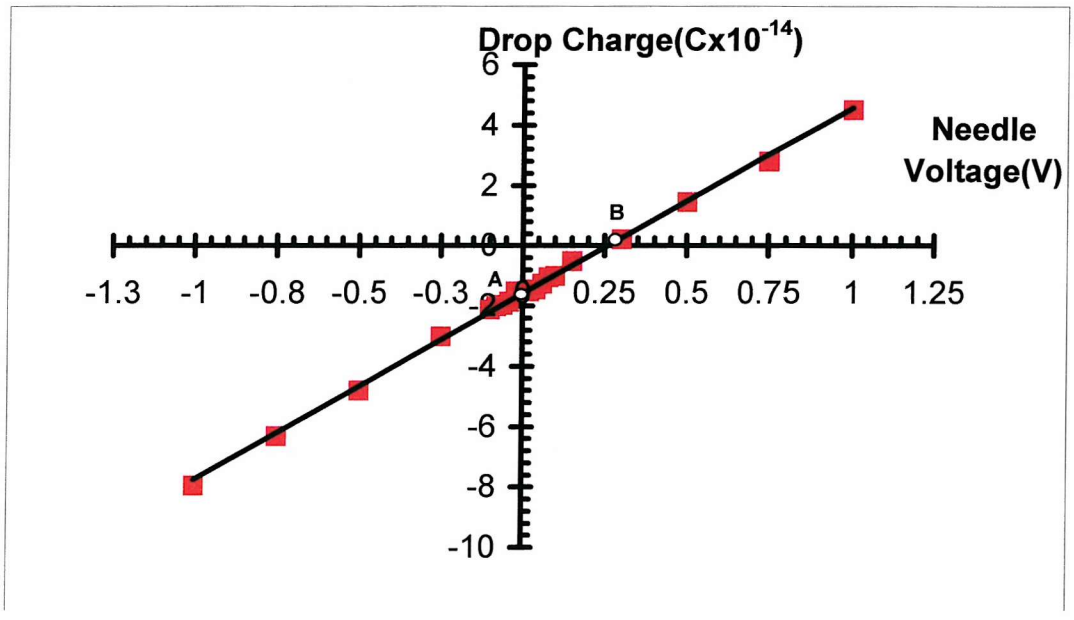

Fig.10 Drop charge vs the applied potential differences between needle (G22) and surrounding tube for DI water

This is a very interesting result in many ways. First of all, the relationship between the drop charge and applied voltage between the capillary and the surrounding tube is linear, indicating that the charge on a drop is due to induction. When the surrounding tube is positively charged (it is connected to the positive electrode of the power supply) it will induce negative charge on the drop surface, while it will induce positive charges on the drop surface if the surrounding tube is negatively charged (it is connected to the negative electrode of the power supply). Moreover, the higher the potential, the greater the amount of charge on the drop surface.

This is true for the whole line in Fig.10 except line between **A** and **B**.

- Firstly, from the graph it can be seen that, in this area, the surrounding tube is still connected to negative electrode of the power supply, but the drop surface is negative charged. According to electrostatics law, this means that there must be another electric force in the system which cancels out the external field and makes the surrounding tube carry positive charge. Therefore, negative charge is induced on the drop surface.
- Secondly, we also notice from the graph that point **A** represents the charge on the drop, which is negative, when there is no external field applied between the capillary and the surrounding tube. Again according to electrostatics law, there must be an electric field existing in the system, which makes the surrounding tube carry positive charge and negatively induced charge is carried by the drop.
- Finally, let's look at point **B**. Point **B** is the zero charge point (zcp). It means that if the surrounding tube is applied negative voltage of –0.27V (or the capillary is positively charged at 0.27V relative to the surrounding tube), the drop carries a zero charge. However, according to electrostatics law, the drop must carry a certain amount of positive charge if the surrounding tube is negatively charged to –0.27V. But the experimental result shows that the drop carries zero net charge under this condition. This also suggests that there must be an internal electric field existing in the system, which is equal and opposite the external field so that the net charge on the drop is cancelled out totally at point **B**.

We also know that the contacts between solid-solid, solid-liquid, liquid-air and solid-air can establish interfacial potentials at the interfaces due to the differences of work functions between them. In the case of this work's system, there are three interfaces involved, steel (surrounding tube)-air, air-water and water-steel. Here we suppose the work function for surrounding tube, capillary and connecting wire is the same because stainless steel is chosen as the material for all of them.

Following the analysis above it can be seen that the total natural interfacial potential differences in the system might be the other electric force balancing the external field.

In the following we shall use abbreviations to denote the potential differences at the interfaces, such as Vca for the potential difference at the capillary-air interface, in each case taking the first name as positive; t, w, m and ex refer to tube, water, metal and external respectively.

Using the setup as shown in Fig. 5, in the circuit when the drop carries zero charge it means that the total natural potential difference is equal and opposite to the external potential, i.e., that

$$Vta + Vaw + Vwc = -Vex \qquad (15)$$

If we use the exactly same metal for capillary and surrounding tube, then we have

$$Vta = Vma,\ Vwc = Vwm \qquad (16)$$

From (15) and (16) we deduce

$$Vma + Vaw + Vwm = -Vex \qquad (17)$$

From (17) we can see that Vex can be read from the power supply. Therefore, if we know any two items of the three on the left side in the equation (17), the third item can be calculated from equation (17). This means a potential way of measuring the absolute contact potentials.

Now let's look at the interfacial potential differences between metal-air Vma, air-water Vaw and water-capillary Vwm respectively:

a) interfacial potential difference between metal-air Vma

As shown in Fig.11 (a), a monolayer of oxygen is adsorbed onto the surface of the metal. Because the electronegativity of oxygen is greater than any metal, the electronic cloud between oxygen-metal (O-M) is dislocalised towards oxygen, i.e. the bond is polarised. Therefore, the metal surface is negatively charged. However, the potential between metal-air is very small because of the great mobility of oxygen, which can easily escape from the surface of metal. Moreover, according to the reports of Faraday (1843) [34] and Matteson (1971) [45] in streaming current measurements, the potential difference at metal-air is so small that there was no streaming current measurable no matter how high the air flow rate is. Therefore, the interfacial potential difference can be dismissed compared to those at air-water Vaw and water-metal Vwm, that is Vma $\equiv$0.

b) interfacial potential difference between air-water Vaw

An equilibrium based on a distribution of potential determining ions is not possible between air and water through lack of ions in the air phase. A double layer, however, may be present at the interface through liquid phase. According to literature [13] [23] the double layer at the interface of air-water is formed with the outer surface (slightly) more negative and the underneath is more positive due to the orientation of water molecules at the surface, as shown in Fig.11 (b). The potential difference at air-water interface is also negligible compared to that at water and metal interface (this will be discussed in detail in next section on the influence of electrolyte concentration on drop charge).

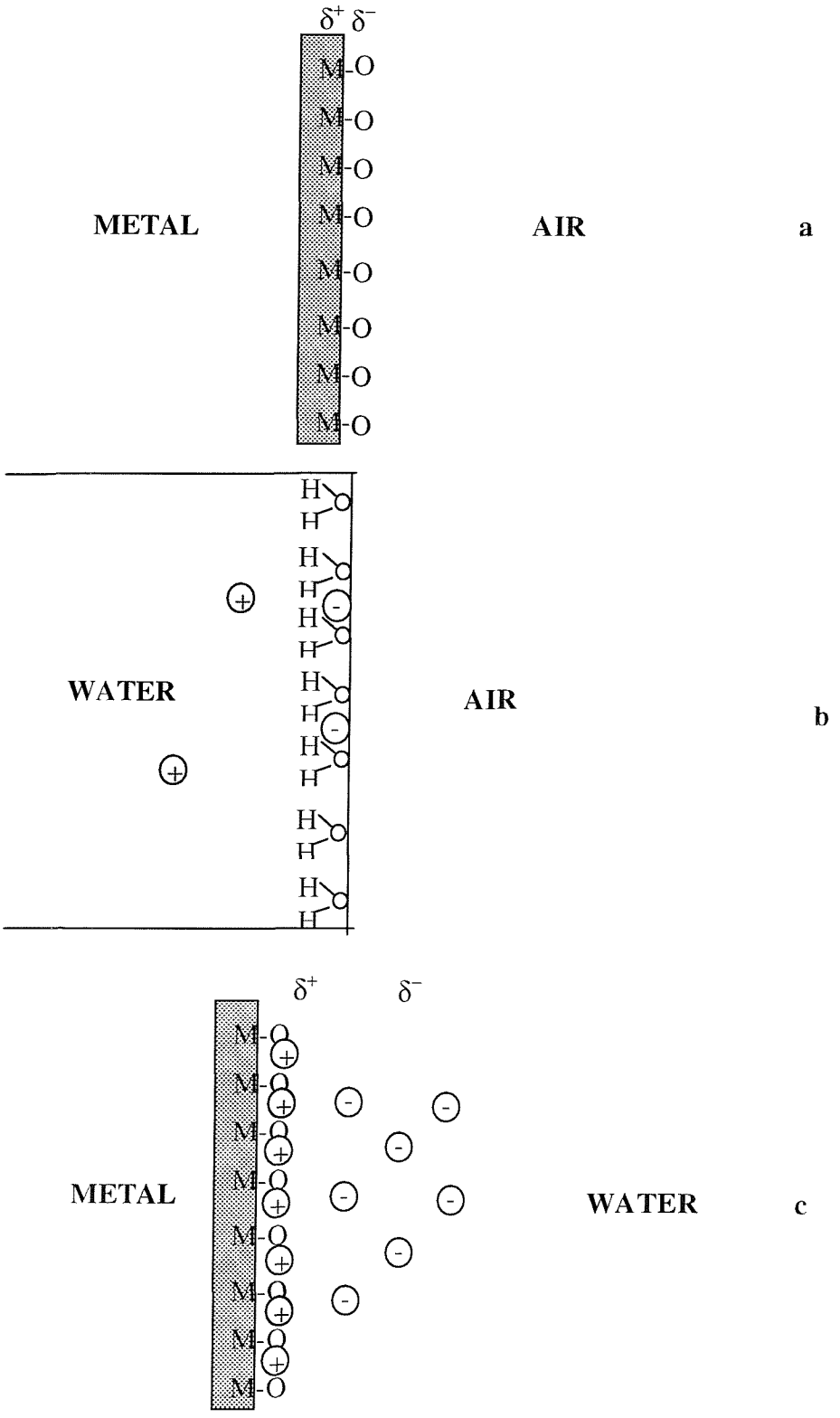

Fig.11 Interfacial potentials at interfaces (a) metal-air Vma, (b) air-water Vaw and (c) water-capillary Vwm Fig.10 Interfacial potentials at interfaces (a) metal-air Vma, (b) air-water Vaw and (c) water-capillary Vwm

c) interfacial potential difference between water-capillary Vwm

At the interface between water-metal, a double layer is also formed, as shown in Fig.11(c). Because the metal surface is always covered by a monolayer of oxygen[57], the metal surface is slightly negatively charged. When the metal contacts with water, it will adsorb positive ions (e.g. H^+, or other cations), which makes the double layer at metal surface positive charged and the liquid side is negative charged.

If we presume it is true that

$V_{ma} \cong 0$,

$V_{aw} \cong 0$

Then according to equation (17), we have

$$V_{wm} = -Vex = -0.27V \qquad (18)$$

If we change the materials of liquid and solid and rewrite equation (18)

$$Vls = -Vex \qquad (19)$$

there l and s represent liquid and solid respectively, the absolute potential difference between any liquid-solid would be calculated with Equation (19).

3.3.2 Drop charge dependence on concentration of electrolytes

If the charge on drops with no external electrical field is really due to the interfacial potential differences, different liquids should produce different interfacial potential differences, therefore different charges on drops. This is based on the theory of contact potential between liquid and solid as stated in section **3.2 Basic static theory**. This is proved to be the fact by experiments. Fig 12 represents the results of single drop charge obtained with solutions of sodium chloride, potassium chloride, ammonium chloride (mono-valent electrolytes) and lanthanum nitrate

(multi-valent) at concentrations from 10^{-5} M to 1 M in field-free and room temperature conditions. For all of these solutions negatively charged drops are produced at low ionic concentrations. As ion concentration increases drop charge reduces and then sign reversal occurs except for NH_4Cl and $La(NO_3)_3$. For the potassium and sodium chloride solution drop charge reverses sign i.e. positive drops are produced, at ionic concentration of about 1 M. For ammonium chloride and lanthanum nitrate solutions similar results are obtained except that charge reversal occurs or would occur at much higher ionic concentrations.

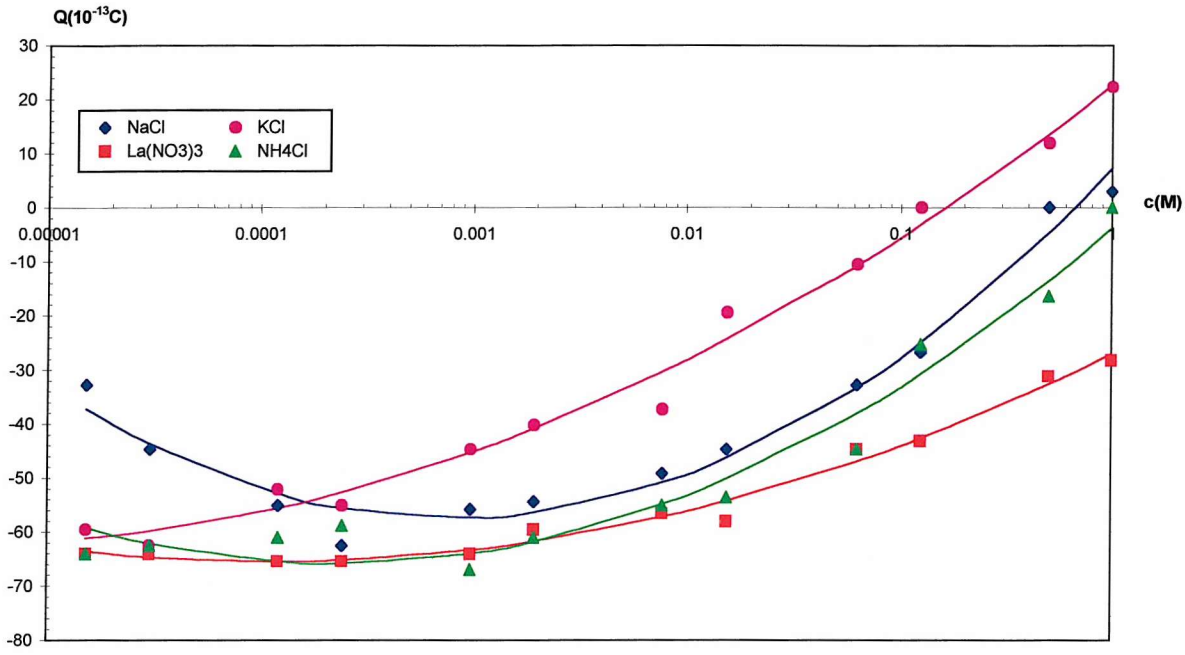

Fig.12 The relationship between drop charge and the concentration of solutions of different electrolytes using needle G22

These results of drop charges depending on electrolyte concentrations prove that the interfacial potential difference at water-metal Vwm is the dominant item amongst the three interfacial potential differences, water-metal Vwm, air-water Vaw and metal-air Vma. This is because:

- Changing electrolyte concentration will not change the interfacial potential difference at air-metal. In other words, the interfacial potential difference of air-metal does not contribute to the change of drop charge. Hence, the influence

on drop charge of the interfacial potential difference of air-metal can be dismissed.

- Changing electrolyte concentration will change interfacial potential difference of air-water Vaw. But the effect should be the opposite of the experimental results. Increasing electrolyte concentration (NaCl, KCl, NH_4Cl and $La(NO_3)_3$) would increase the value of the interfacial potential difference of air-water[54] due to the adsorption of anions onto the surface of liquid, as shown in Fig.11(b). Therefore, the value of drop charge would increase rather than decrease. From this it can be deduced that the interfacial potential difference of air-water Vaw is not the dominant item at the left side of equation (17), therefore can be dismissed from the equation (17). In other words, the interfacial potential difference of water-metal is the really dominant factor in the whole system or the main reason responsible for the drop charge. Therefore, equation (19) is tenable.

3.3.3 Investigation of the influence of other parameters (temperature and gas friction)

a) Hot water (DI water heated up to boiling) was used instead of cold DI water and the similar experiments were carried out as shown in Fig 13 and it was found that there was no significant difference for drop charge between hot and cold DI water.

b) The drop charge when there is no external potential difference applied may be due to the friction between the falling drops and the surrounding air, e.g. the drops might pick up charges from the surrounding air through which it is falling. Therefore, the height of the drop falling before it reached the collector was changed and the charge on the drops falling different height through surrounding air was measured. It was found that variation of the height through which the drop fell did not alter the results, showing that the drop does not acquire an appreciable charge while falling. This is in agreement with the

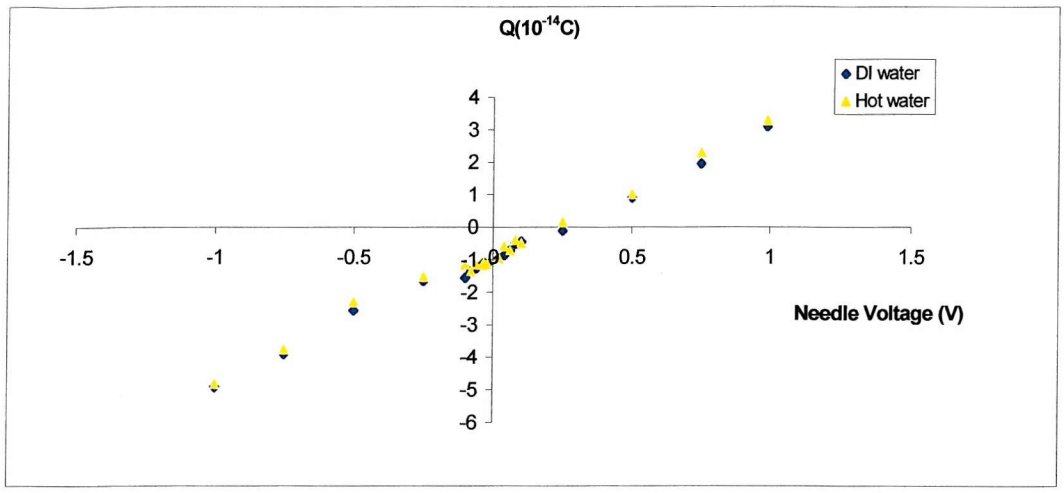

Fig. 13 Drop charge against applied voltage between needle (G22) and surrounding tube for DI water and Hot water

results reported by Lenard [23] and Aganin [28] on a liquid column falling through a gas. Both Lenard and Aganin have shown that if a jet of liquid meets a liquid surface before breaking up under the action of surface tension, no charge is developed in it or in the gas through which it passes.

We learn from this that mere friction between gas and liquid does not, *per se,* cause electrical separation.

3.3.4 Drop charge dependence on geometry of capillary diameter and tube diameter

a) If the charge on drops when there is no external field applied is really due to a potential difference, the alteration in size of the drop should not, on the one hand, alter the potential difference found as intercept. This is found to be so, as indicated in Fig 14, the two lines converge at the same point (0.27 V) on V coordinate axis. On the other hand, the drop charge should increase as the drop size increases. This is also the fact as shown in Fig 14.

b) If the drop charge with no applied external field is really due to the interfacial potential differences naturally occurring when the setup was put together, then the drop charges should change as the size of the surrounding tube alters. This proved to be true as shown in Fig 15 and Fig 16.

With a certain needle, the drop charge decreases as the diameter of the surrounding tube increases.

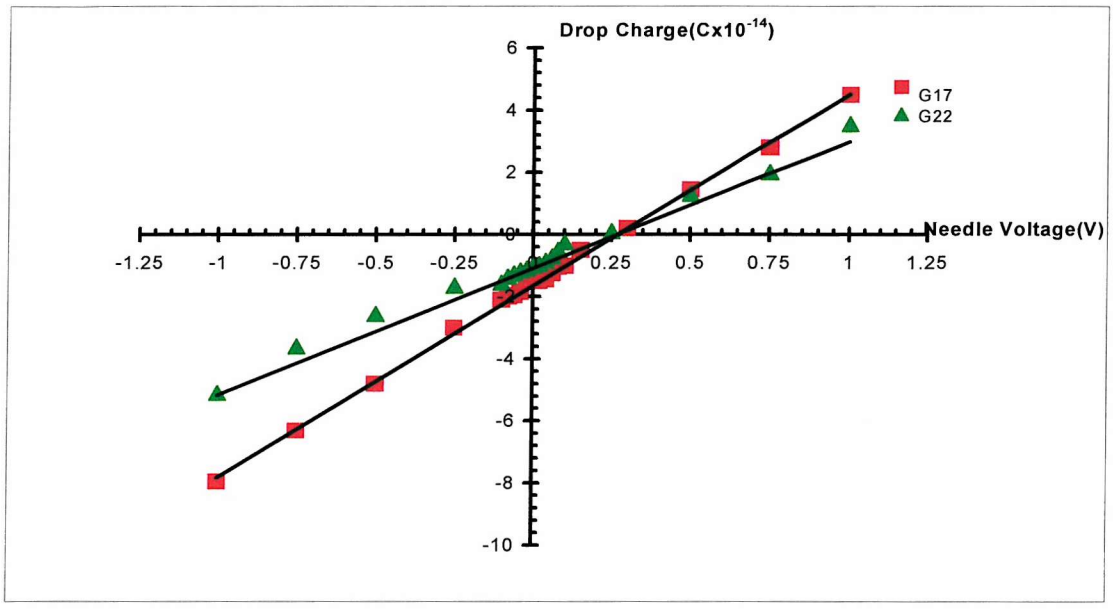

Fig.14 The relationship between drop charge and applied potential between needle and surrounding tube for DI water using different size needles (G17 and G22)

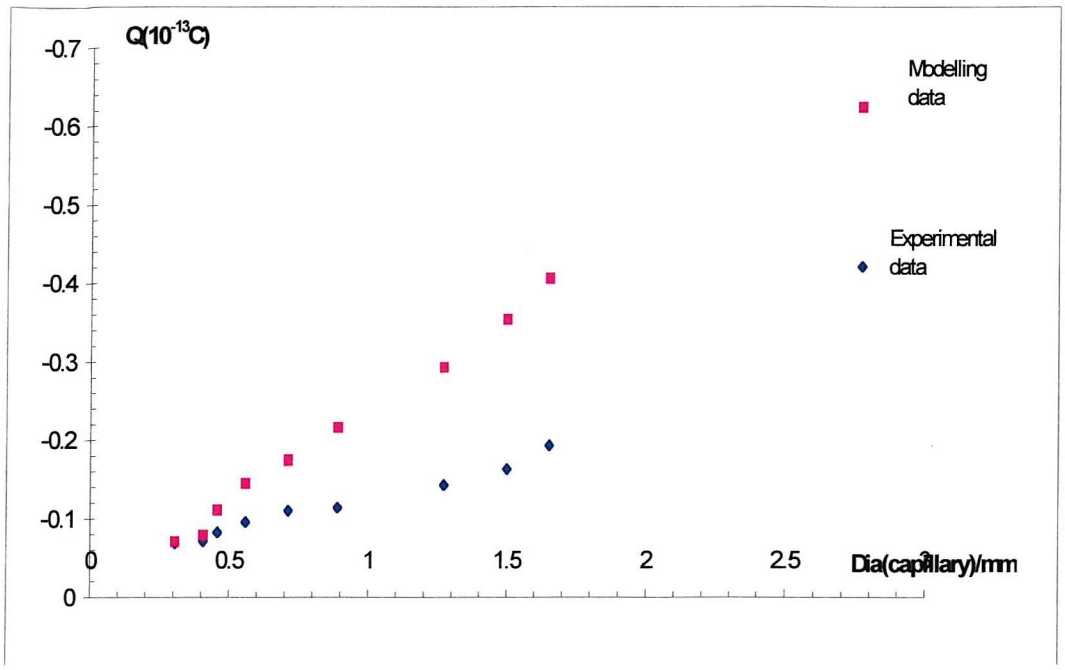

Fig.15 DI water drop charge vs needle outer diameter (For modelling data, see Section 3.5.3.2)

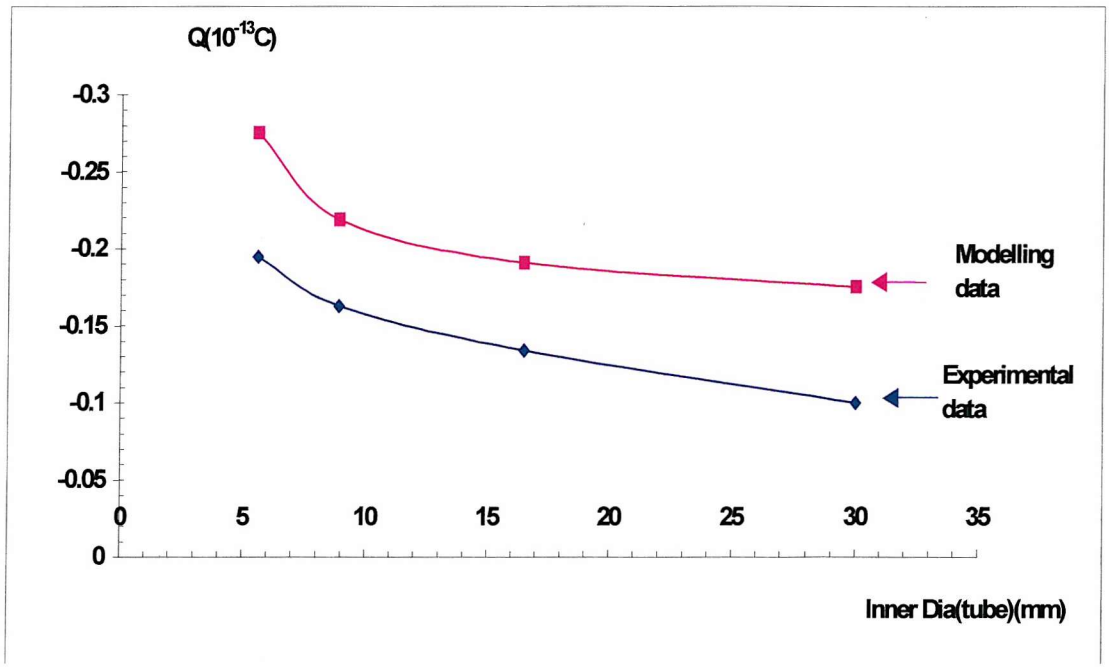

Fig.16 Drop charge against diameter of surrounding tube for DI water using needle G22 (For modelling data, see Section 3.5.3.2)

3.4 Conclusions

From the results and the basic theory above, we can draw conclusions as the following:

- The charge on pendant drops hanging in a surrounding cylindrical tube is mainly caused by naturally formed contact potentials around the system- Vwm(contact potential between water and metal of the needle), Vma(contact potential between the air and the metal of the surrounding tube) and Vaw(the potential between the air and the water).
- According to the results reported by several researchers [23] [28] and our experimental results, we can conclude that the contact potential between air and metal is small enough to be dismissed.
- As for the potential existing between air and water, it can also be excluded because it would have given opposite experimental results if it was the dominant electrical force in the system.
- So far, we can say

$$Vwm = -Vex \qquad (18')$$

or

$$Vls = -Vex \qquad (19)$$

In our case

Vwm=-0.27 V

- We can conclude that the absolute contact potential between DI water and stainless steel is measurable, which is –0.27 V in our case.
- The set-up of the pendant drop charge measurement can be used to measure absolute contact potentials between the liquid and the inner wall of the needle through which the liquid flows.

It must be pointed out that because the contact potential is very much subjected to surface states, the contact potential can vary dramatically due to different materials.

Even for the same material, different crystal planes have different work function so that the contact potential can be very different for different planes of the same material. A slight contamination by impurities could change the contact potential remarkably because they can alter the work function outstandingly, can even change the polarity. Because of this, different researchers reported different results which are difficult to compare.

3.5 Computer simulation

In this section, attention is directed towards the modelling of surface charge distribution of a pendant drop within a surrounding cylinder tube. Computational work has been carried out by using the electromagnetic software OPERA-2D and some of these results are presented and discussed in this chapter. In addition, theoretical considerations on how the pendant drop surface is established and the existence of negative charge along the drop surface despite small positive fields or no fields are applied.

3.5.1 Finite Element Method – A brief History

The basic idea of the finite element method has always been to replace an actual problem by a simpler one [58]. In formulating the simplified problem, use is made of the so-called finite element. If the simpler problem can be solved, and the estimated solution represents the true solution with a reasonable accuracy, this method has obviously served a useful purpose.

The earliest use of finite element method was probably that of geometry. About 2000 years ago, mathematicians were interested in problems such as determining the circumference and area of a circle. Exact solutions had to await the discovery of the calculus. In the meantime, amazingly accurate results were found by introducing approximate problems using finite elements. In the case of the circle, it is obvious that a regular polygon can be chosen as a substitute problem. The straight line then becomes the finite element and it is therefore possible to estimate

the circumference and area of the circle; in another words, to estimate the value of π.

Ancient records show some of the remarkable accomplishments of early day mathematicians and some were unquestionably based on using finite elements. For example, the Ahmes papyrus shows that by 1500 B.C. the Egyptians were using $10^{1/2}$ for π. A still earlier papyrus indicates that by about 1800 B.C. the Egyptians possessed the correct formula for calculating the area of a sphere and the volume of a pyramid. A Chinese book written around the time of Christ, reveals that Chinese were aware of certain geometric theorems at least as early as the Greeks. Based on those theorems, the Chinese engineer Tsu Chung Chih determined the value of π to lie between 3.1415926 and 3.1415927 by 480 A.D. His work was probably based on replacing the area of the circle with slender inscribed and circumscribed rectangles. In fact, the procedure for using these rectangular finite elements and the Chinese proof for Pythagoras theorem is itself an interesting development.

The area of a circle can be replaced by an inscribed or circumscribed polygon. The former method would therefore provide lower bounds and the other upper bounds for both the circumference and area. The accuracy will no doubt increase with the number of faces of the inscribed or circumscribed polygon.

Archimedes, one of the greatest of the early mathematicians, used finite elements for estimating the volume of solids. His work brought him to the very threshold of calculus. As it was, the ultimate fulfilment of his early steps had to await the day of Newton and Leibnitz some twenty centuries later.

3.5.2 Theoretical Background

Solutions of potential or field problems in electrostatics are commonly obtained by solving Poisson's or Laplace's equations. Apart from a few simple cases, these two harmonic equations cannot be solved analytically. Although there are many mathematical functions that can satisfy the differential equations, they rarely

satisfy the required boundary conditions. In a boundary-value problem, it is the boundary conditions as much as the differential equations that determine the solutions. Numerical methods involving discretisations are therefore required.

Within the solution domain, the continuous functions are represented by values at a finite number of points. These values are obtained from a set of simultaneous algebraic equations, which are usually linear. The accuracy of the values can be improved by increasing the number of points. In regions where the continuous functions change most rapidly (e.g. sharp point etc.) additional points are normally required to sustain satisfactory local accuracies.

Various methods are available for establishing the simultaneous equations and the major ones are finite difference and finite element methods.

3.5.3 Computer modelling

Static electric field (or electric potential) within the area between the drop and surrounding tube was simulated by OPERA-2D. This programme is mainly for 2-D electromagnetic problems but 3-D problems can sometimes be analysed if they are axy-symmetric; i.e. the symmetric part of the model is represented on the z-r plane by means of so-called axy-symmetric finite elements. Numerical values obtained for all node points in an analysis will automatically give visual understanding of the problem.

The distribution of electric potentials between a pendant drop hanging at the tip of a needle and a cylinder was simulated. Data from this model were compared to the experimental results.

Also, boundary conditions and the corresponding results in each of the above analyses are presented and discussed.

3.5.3. Pendant Drop Profiles

Attempts to determine the complex profiles of pendant drops of liquid hanging from capillary tubes have been made by several researchers [59][60][61][62][63] due to the importance of drop shapes as a means of determining surface tension. Equilibrium profiles may be determined by solving the pressure balance equation due to gravity and surface tension. A typical pendant drop profile is shown in Fig.17. The pressure balance equation which describes the equilibrium condition of the drop may be written as

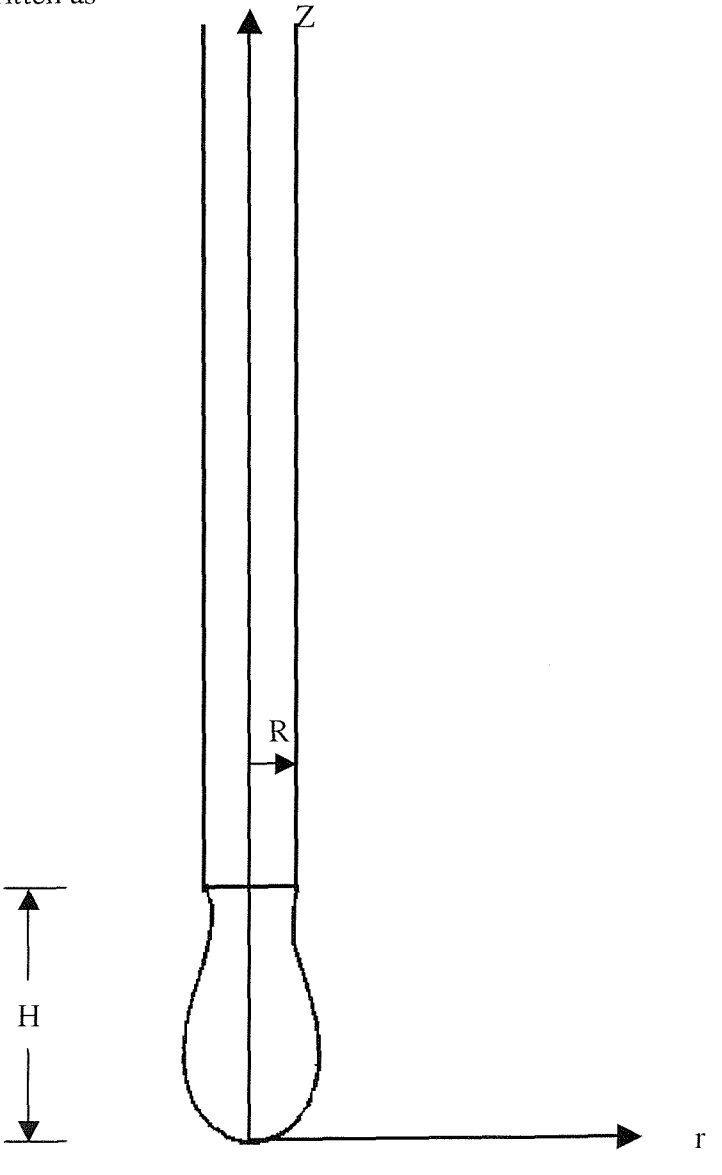

Fig. 17 A typical drop profile hanging at the tip of a needle in field-free conditions

$$\frac{2\gamma}{b} - \rho g Z = \gamma\left(\frac{1}{R_V} + \frac{1}{R_H}\right) \qquad (20)$$

Z is the axis of symmetry of the drop, R_V and R_H are the principle radii of curvature in the vertical and horizontal planes respectively at any point, and b is the radius of curvature at the tip of the drop, ρ the liquid density, γ the surface tension, g the acceleration due to gravity.

There is no analytical solution for equation (20) and it must be solved numerically. Among the recent investigators Padday's[61] extensive tables of solution are given for different parameter β ($=b^2\rho g / \gamma$). Given ρ, γ and the nozzle radius one can find, using the above-mentioned tables, the profile which fits the nozzle geometry. The characteristics of these drops, normalised to the capillary tube outer radius R, for ρ = 1.00 g/cm^3, γ = 72.75 dyn/cm and g = 980 cm/s^2, are [64]:

H/R = 7.0

b/R = 2.32

This was obtained [64] by taking b approximately equal to the corresponding experimental value, and generating the profile, thus proving that experimental and theoretical results match quite well. During all our computer modelling, the profiles used were based on the above-mentioned characteristics.

3.5.3.2 Computer Modelling Geometry and Solutions

The experimental set-up used simply consists of a capillary needle surrounded by a cylindrical tube with their supporting framework as shown in Fig.5. Only a half of the whole geometry was considered in analysis due to symmetry. To analyse the potential distribution in the region between the pendant drop and the surrounding cylindrical tube, a boundary as shown in Fig.18 was chosen. The potential of the surfaces of the pendant drop and the capillary is -0.27V according to the results obtained from experiments and the potential at any point of the surrounding tube is

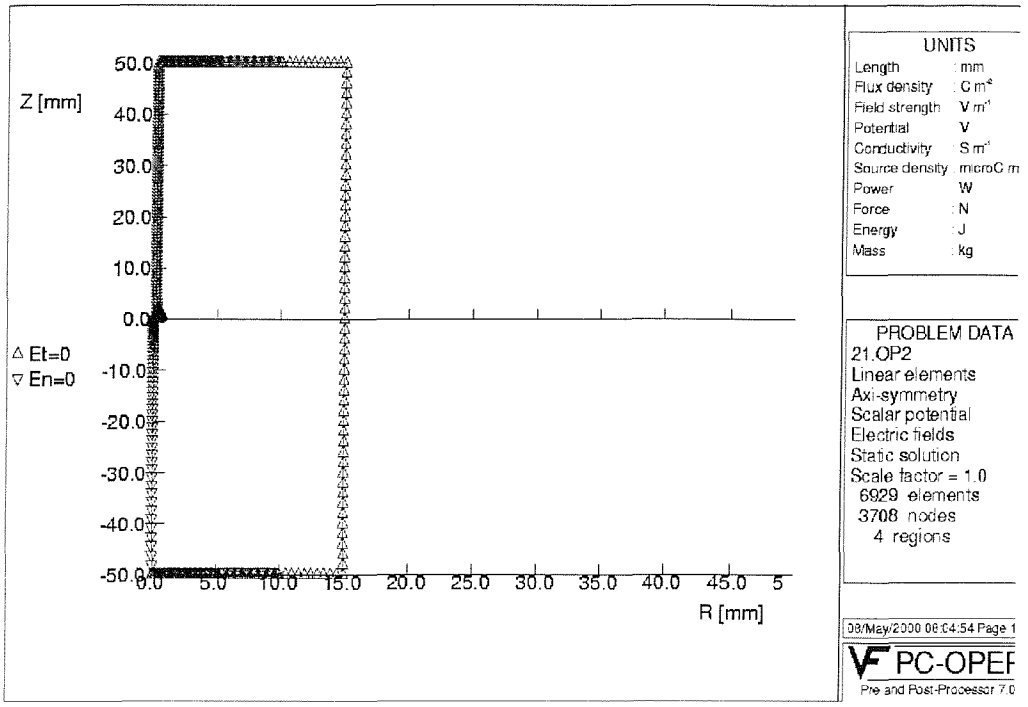

Fig.18 The boundary conditions for drop charge analysis using OPERA

zero, based on the conditions used in the experiments. The mesh was created in such a way that it was fine around the drop surface, which was the area we were with concerned most, and became less fine as it was away from the drop surface, as shown in Fig.19.

Fig.20 and Fig. 21 show the electric potential contours in filled zones and coloured lines respectively when a needle of Gauge 22 and a surrounding tube of 30 mm diameter were used while Fig. 22 and Fig. 23 show the Emod (the modulus of electric field strength at the field point) in filled zones and coloured lines respectively. The data of Emod at the drop surface were extracted and drawn along the surface and shown

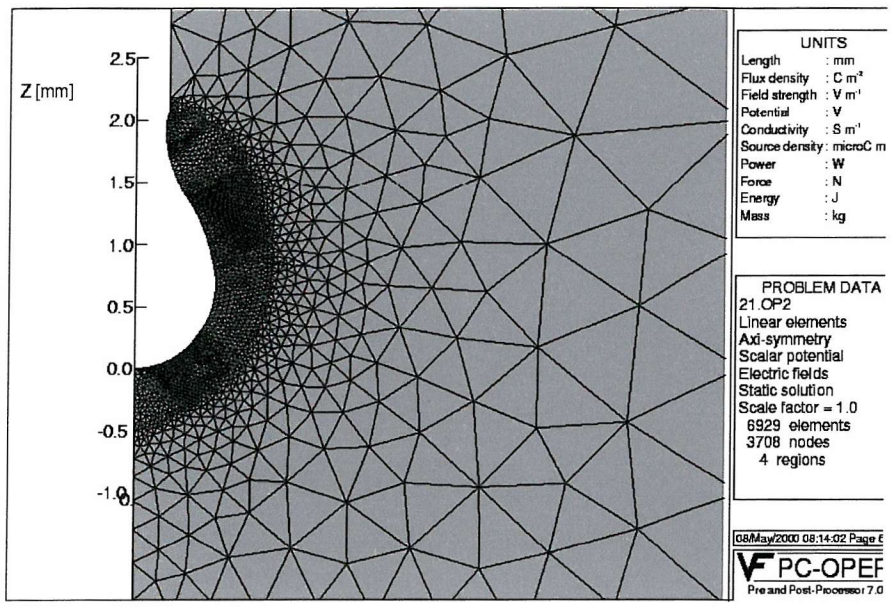

Fig.19 The mesh used in drop charge analysis using OPERA-2D

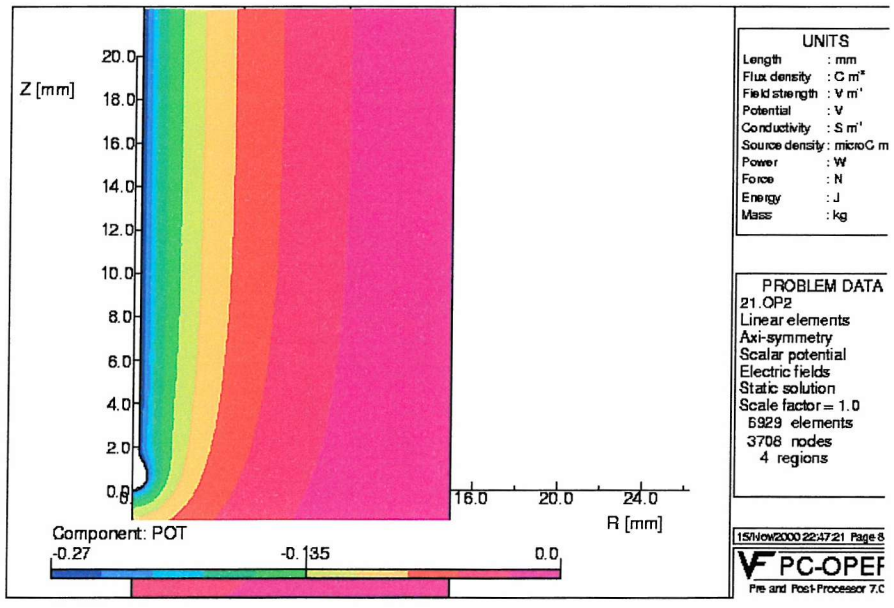

Fig.20 The equipotential contours in field

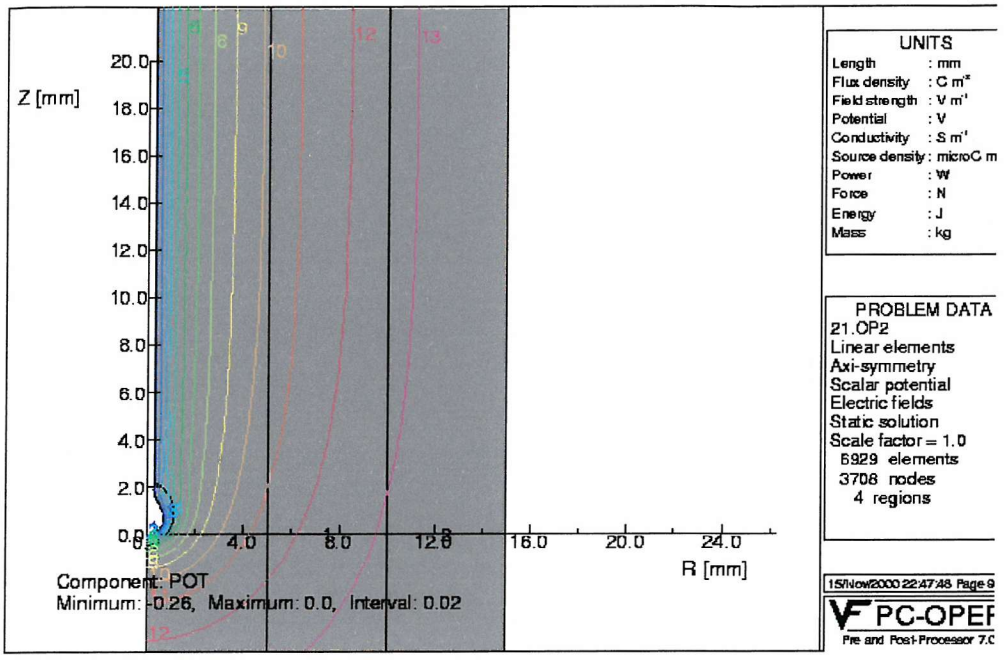

Fig.21 The potential contours in coloured line

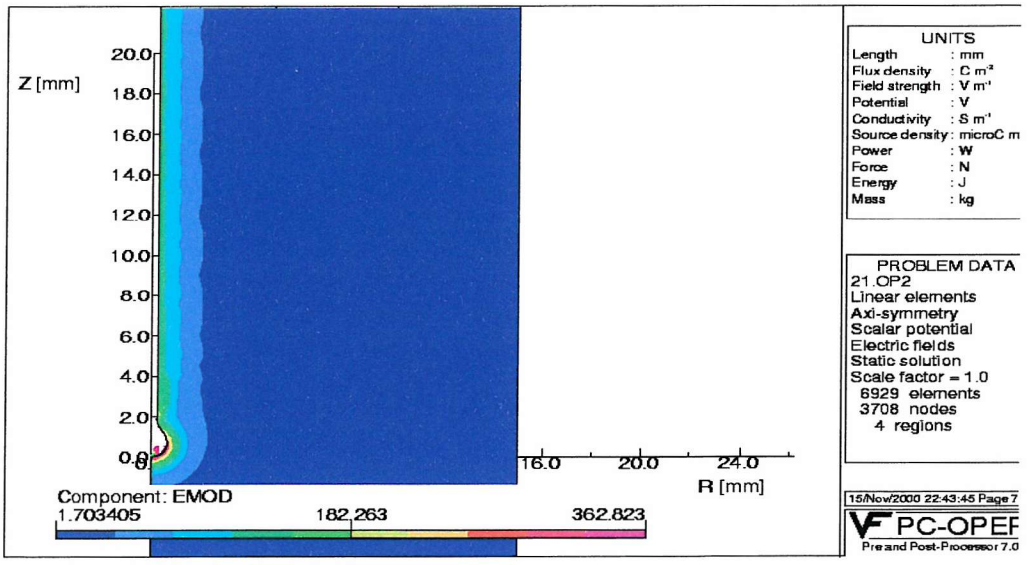

Fig.22 The EMOD in the area between the drop and surrounding tube in filled zone style

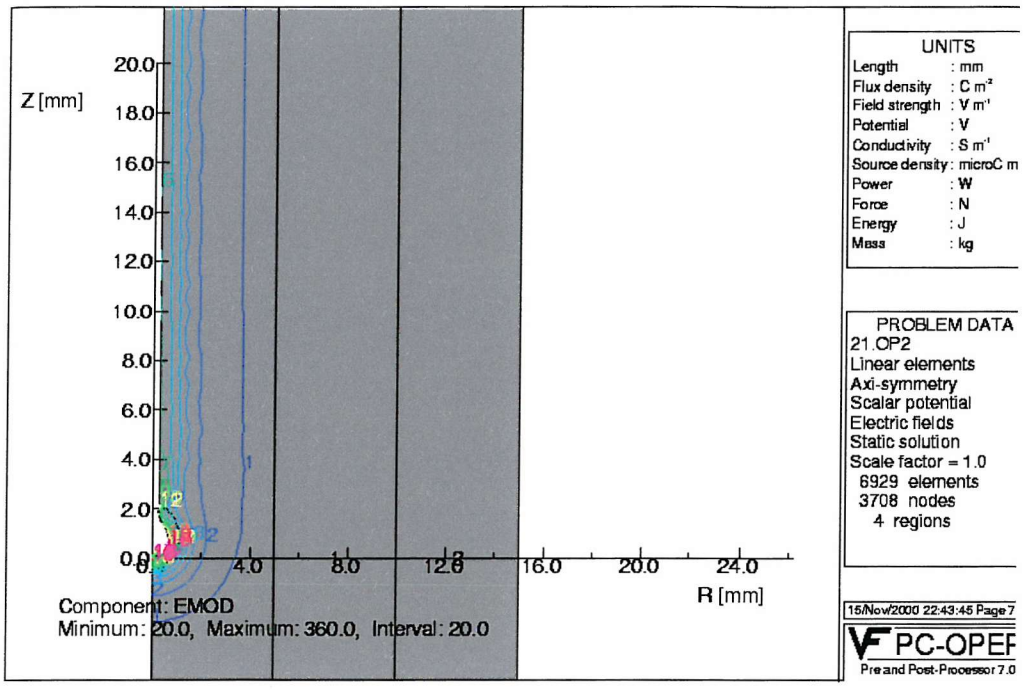

Fig.23 The EMOD in coloured line style

in Fig. 24. From Fig.21, Fig.22 and Fig.23, it can be seen that the electric field inside the tube is concentrated along the drop surface and less strong at the edge of the needle. Because of this, it would not cause too much error when we integrate the drop charge along the surface if we choose a different plane close to the drop "necking" or break off region.

In order to calculate the electric field, the integrate path was chosen such a way that all electric field lines entering the drops were included except at the top line, which can be seen in Fig.25. The top integrate line is chosen at the position at drop radius is minimum because drop is supposed to break away from here. Then the drop charge was calculated. Simulation in the way mentioned above were carried out using the whole sets of needles and tubes. The results were compared with experimental results, as shown in Fig.15 and Fig.16.

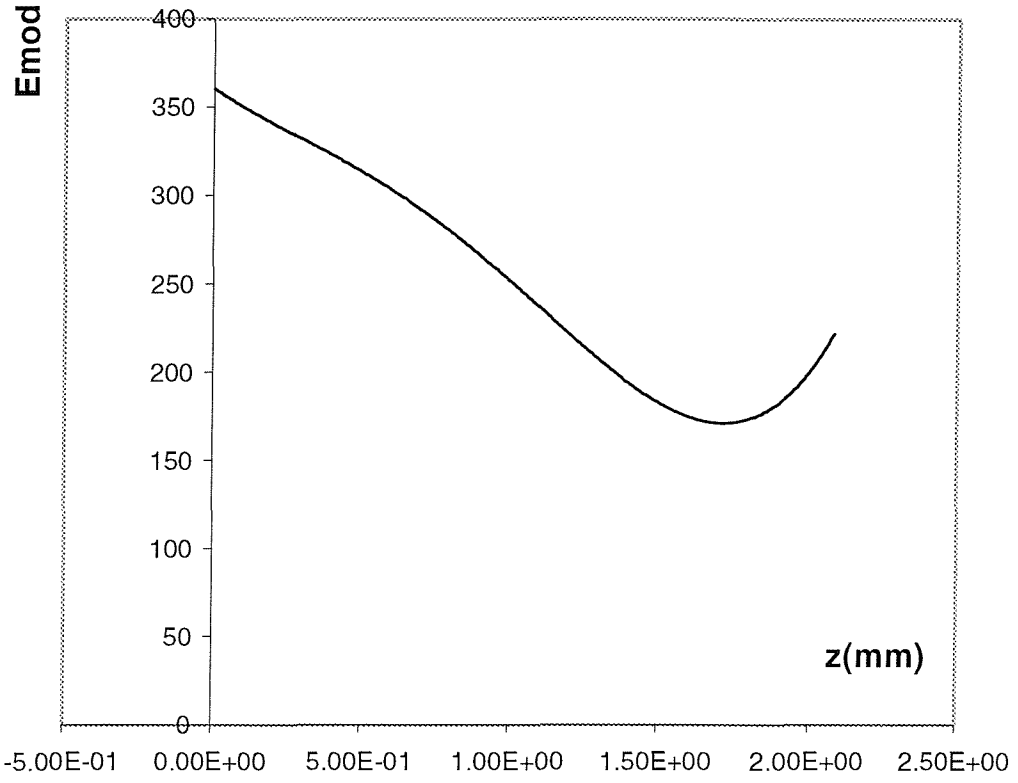

Fig.24 The EMOD value along the drop surface

Fig. 15 shows the drop charge Q against the diameters of needles when a certain diameter (diameter was 30mm) of the surrounding tube was used while Fig.16 shows the drop charge Q against the diameter of surrounding tubes when the needle diameter was fixed to be Gauge 22. From the graphs we can see, as expected from experimental data, that the drop charge increases as the diameter of the needles increases when the size of the surrounding tube is fixed, while the drop charge decreases as the diameter of the surrounding tubes increases when the gauge of the needle is fixed.

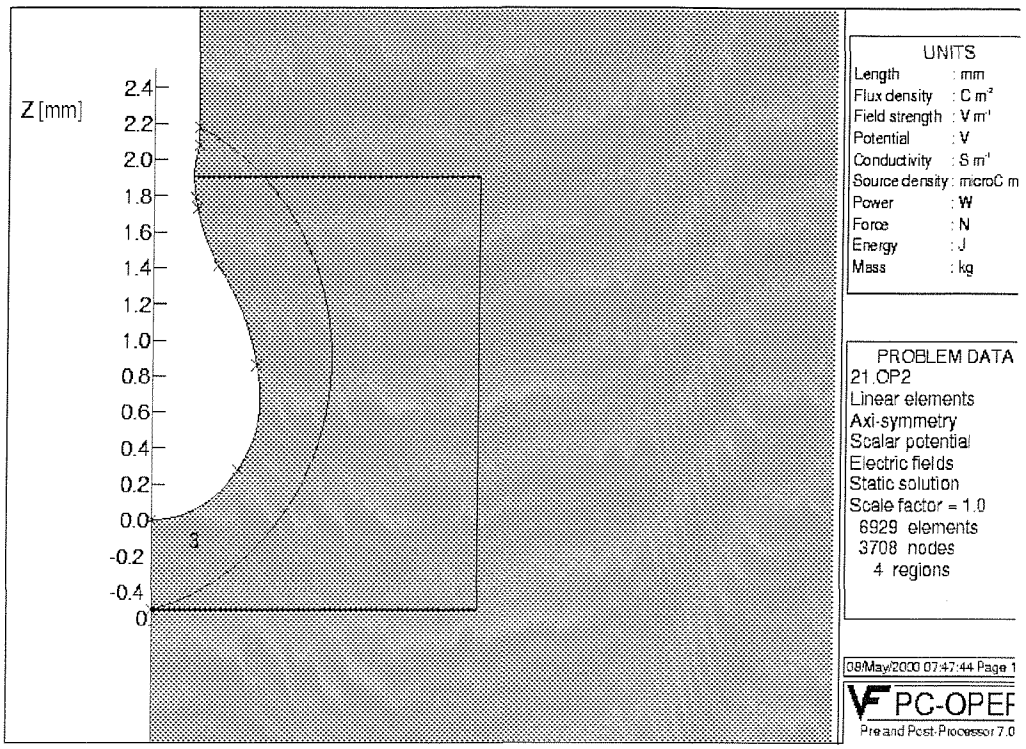

Fig.25 The integration path of calculation of charge on the drop surface

3.5.4 Discussion on the solution Errors

The global r.m.s error involved in each analysis (in Section 3.5.3.2) is about 3 percent. This figure represents the global accuracy of the solutions and also indicates how refined each finite-element mesh was. Very often, a large global r.m.s error could be the direct result of a large local r.m.s error. This normally occurs in regions where geometric details exist; that is, the regions in which the gradient of the unknown quantity changed most rapidly. One simple way to improve the local accuracy is to increase the number of finite elements locally.

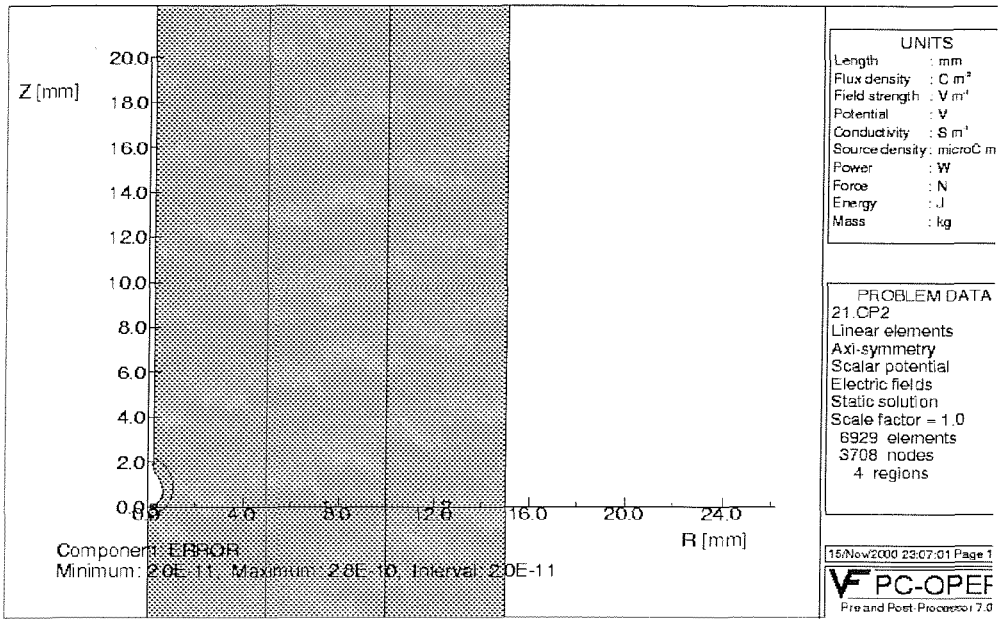

Fig. 26 Error analysis in the region around drop

As a simple example, the region around the edge of the needle required a more detailed mesh than any other spatial regions to obtain an accurate local solution.

To examine the effect of finite element size on a solution, a model should be solved by using two levels of finite element discretisation or with the same discretisation but using two different element types-linear and quadratic. In either case, comparing the two solutions will give an indication on the discretisation error. However, this error does not represent the accuracy of the model. Very often, increasing the number of finite elements will lead to a better solution but a longer processing time would be the result. The computer models mentioned in this chapter have been analysed by using both linear and quadratic elements. Since they are simple models, the discretisation error was found to be about 2 percent on average, especially in the area of drop surface it was only $\sim 10^{-10}$ as shown in Fig. 26. Hence the discretisation error can be dismissed.

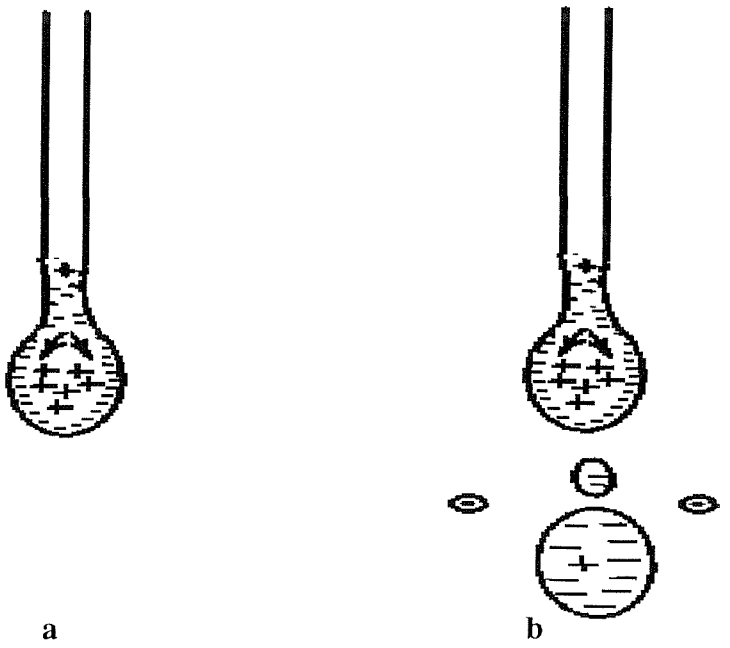

Fig.27 (a) Drop charge redistribution due to dynamic effects and (b) satellite drop formation

However, it should be noted that the global or local r.m.s. error does not represent the accuracy of the models.

3.5.5 Discussion on the data comparison between experiments and computer simulation

Fig.15 and Fig.16 show the results obtained from experiments and computer simulation.

- From the graphs, it can be seen that the computer simulation data are in accord with experimental observations and correctly predicted that the negative charge carried by drops would increase as the capillary diameter increases and the surrounding tube diameter decreases.
- But it also shown that the computer simulation data are always greater than experimental results. And the bigger the drops, the greater the error. This might

due to the dynamic effect during the drop break away. Two factors might contribute to the less drop charge phenomenon than theoretical data:

a) During the process of a drop formation, a very narrow neck part is formed at the final stage of the drop formation as shown in Fig.27 (a). At the moment of the drop is breaking way from the tip, a flow of liquid having a net positive charge passes through the constricting neck into the forming drops and as a result the charge on detached drops may be less negative than would otherwise be the case.

b) If satellite drops are formed during this process, as is sometimes observed in practice, they arise from the pinched-in portion which has surfeit of negative charge and hence such satellite drops are likely to be negatively charged, leaving the detached drop even less negative than would be otherwise. This can be seen more clearly on the diagram shown in Fig 27 (b).

c) It is clear that these factors, mentioned above, would contribute more as the drop size increases, which explains why the error between experimental results and computer simulation data increases as the capillary diameter goes up.

As discussed above, the solution to the problem of pendant drops should be time-varying but not static due to the distribution of charge as the process of drop detaching is going on. Since the mechanism of the charge distribution is, on the one hand, very complex; on the other hand, the moment a drop detaches from the tip of the needle is so quick that it is difficult to catch the profile of the drop, it will be very difficult to model such a situation. At present, a static solution is assumed for simplification purpose.

3.3 Summary

OPERA-2D was used to simulate the potential distribution of the pendant drop in a cylindrical surrounding tube. A series of simulations was used to synthesise the solution and the techniques that were involved in the modelling processes are described. The models are considered to be elementary.

Theories on the formation of the pendant drop charge and profile are introduced and discussed. Most important is that a method of measuring absolute contact potential between a solution and a solid was invented which can be simulated by using OPERA finite element analysis method.

CHAPTER FOUR

JET (STREAMING CURRENT)

After the work on static charge of a pendant drop, we have been investigating further into the hydrodynamic effects on liquid charging. As the pressure pushing liquid through the capillary increases, the dripping rate of the detaching drops increases and finally the liquid becomes a jet. In this chapter the charging phenomenon associated with jets is discussed.

4.1 Introduction

It has been known for many years that petrochemicals become highly charged unless stringent precautions are taken during the handling and transportation of such liquid. The charging phenomena which occur in these insulating hydrocarbon liquids are amongst the most widely studied and understood of all electrostatic charging mechanisms. Clearly, the prime motivation has been to reduce the risk of electrostatically-induced explosions when handling such flammable liquids. Of particular concern to the petrochemical industry is the charging, which occurs during pipeline flow. The origin of the effect is the formation of a double-layer (as mentioned in Section 3.2) of charge at the interface between the liquid and the wall of the pipe. During flow, this double-layer is sheared and charge becomes entrained in the liquid. If this charge is allowed to accumulate in the system a potentially hazardous situation is created.

4.2 Theoretical Background

The term 'streaming current' in pipe flows refers to the presence of a convection current

$$I = \int_0^a qv2\pi rdr \qquad (21)$$

where q is the charge density in the liquid, v is the axial velocity component, and a the pipe radius. All fluids have some electrical conductivity, even if very small, because of the contamination during handling. The equilibrium condition between the charged species and a bounding wall generally induces a finite charge density in the fluid adjacent to the wall (which is known as double layer, the schematic diagram is shown in Fig.28) and hence a convection current will occur whenever flow takes place.

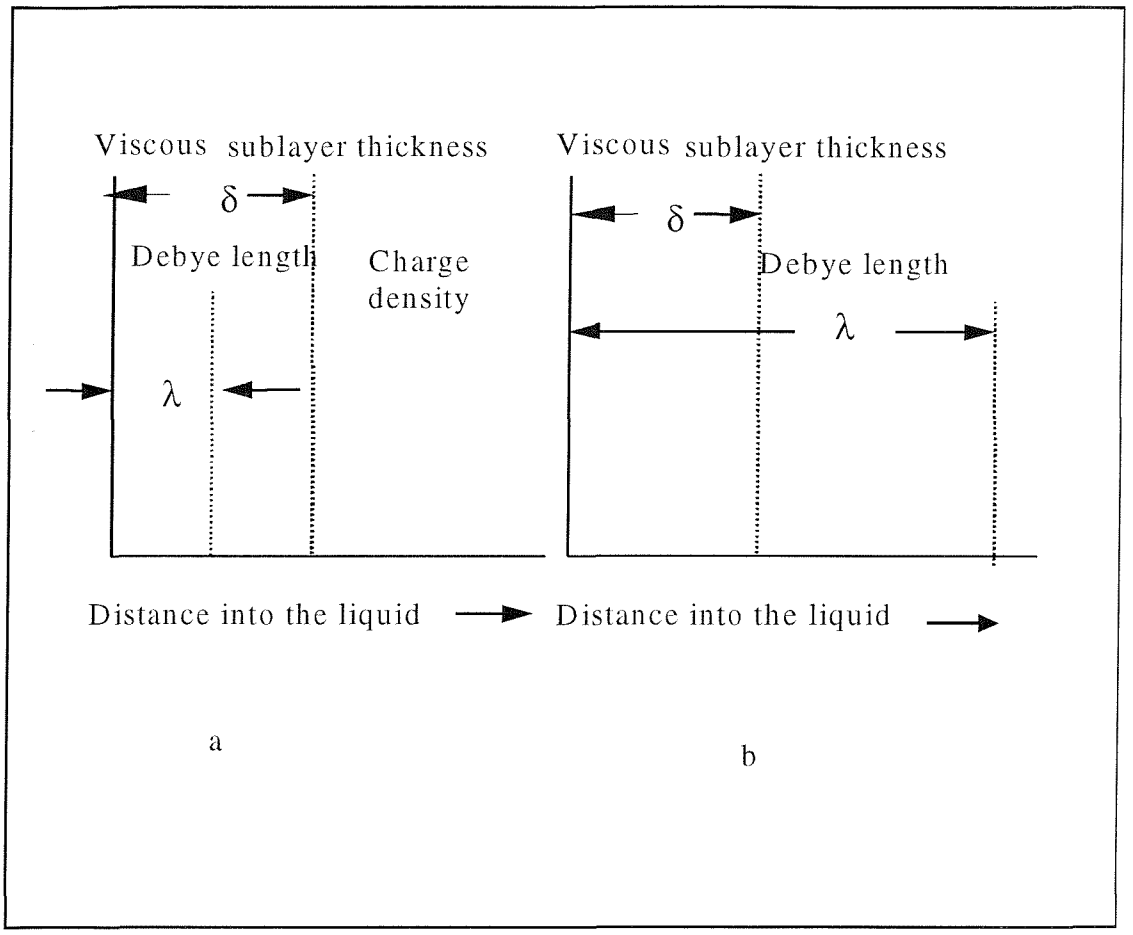

Fig. 28 Sketch of charge distribution near wall for (a) λ<<δ and (b) λ>>δ

A general theoretical description of charging is available for laminar pipe flows (Pribylov & Chernyi 1979) [18] [65].

$$I_{lam.} = -8\pi\varepsilon\varepsilon_o\zeta v \qquad (22)$$

$$v = \frac{Q}{\pi a^2} \qquad (23)$$

where v is the bulk velocity of the liquid; ε is the relative permittivity of the liquid, ε_0 is the permittivity of free space, ζ its electrokinetic potential, Q the volume flow rate.

The electric charges in liquid are in a diffuse layer close to the wall; in laminar flow, the speed of the liquid near the wall is proportional to the distance from the wall; hence, under conditions of laminar flow the electric charges in the liquid move at very low speeds.

However, for turbulent flows the situation is not extremely complex. Contributions have been made by Cooper (1953) [66] [67], Klinkenberg (1959, 1964) [18] and Koszman & Gavis (1962a) [68].

Applications where the flow is turbulent involve at least four characteristic lengths: the diffusion sublayer thickness δ, the Debye length λ (or double layer thickness), the tube radius a and the tube length L. In a turbulent flow, liquid flow becomes turbulent through a core constituting most of the tube, and in this core the velocity is nearly constant. Only in a thin sublayer near the walls does the flow remain laminar, hydrodynamic theory (Rouse and Howe) [69] gives ($\lambda^2 << \delta^2 << a^2$, as shown in Fig.28)

$$\delta = 118 a R_e^{-7/8} \qquad (24)$$

where the Reynolds number $R_e = 2a\rho v/\eta$ is large enough to guarantee the turbulent flow. Here, ρ is the mass density of the liquid. The Debye length, which

characterizes the thickness of the unperturbed charge double layer at the liquid-capillary interface,

$$\lambda = (\varepsilon D_m / \sigma)^{1/2} \qquad (25)$$

brings in the average ion diffusivity D_m and conductivity σ.

The molecular diffusion coefficient, D_m, is related to charge mobility by Einstein relation

$$\frac{D_m}{\mu} = \frac{kT}{e} \qquad (26)$$

$$\mu \approx \frac{2\times10^{-11}}{\eta} \qquad (27)$$

where μ, k, T, e and η are ion mobility [70] [71], Boltzmann constant, temperatur, charge of an electron and viscosity of the liquid,. Implicit in this definition is the assumption of an essentially uniform conductivity, which requires that positive and negative ion concentrations remain close to their quiescent liquid bulk values, with the net volume charge arising from a small imbalance in these concentrations.

The velocity gradient in the laminar sublayer during turbulent flow is much higher than in Eq.22, since most of the velocity gradient occurs in this region. If we rewrite Eq.22 with a velocity gradient v/δ, we obtain the approximate relation

$$Iptur = -\frac{2\pi\varepsilon\varepsilon_o a\zeta v}{\delta} \qquad (28)$$

where I_{ptur} is the streaming current in transition flow.
In the fully developed turbulent flow the viscous sublayer thickness based on the Blasius friction-factor correlation

$$\delta = 118 a R_e^{-7/8} S^{-1/3} \qquad (29)$$

is uniform over the length of the tube. Schmidt number $S=\eta/\rho D_m$ is large, being greater than 500. In this case the Debye length exceeds the diffusion sublayer thickness,

$$\lambda^2 >> \delta^2 \qquad (30)$$

so some of the ionic atmosphere will extend into the turbulent core, the volume charge entrained in the flowing liquid is distributed well into the core of the flow by turbulent diffusion. If the whole double layer is assumed approximately to be swept away with liquid, then the streaming current I*ftur* under fully turbulent flow condition is given

$$I_{ftur} = -2\pi aqv = -\frac{2\pi\varepsilon\varepsilon_o\zeta a}{\lambda}v \qquad (31)$$

For pure HPFP, its permittivity at 25°C is 23 ε_o and conductivity is 7.87E-10 S/m, which is between water ($80\varepsilon_o$) and good insulator (~ $2\varepsilon_o$). Therefore, a certain extent of dissociation of the molecules is expected. But the ionic species are difficult to predict. They might be polynuclear ions.

In order to avoid accidental impurities playing a predominant part in the interfacial phenomena between liquid and solid, a deliberately chosen antistatic agent (Ca-Dips) with acetone as a surfactant was used in which these ions were supplied in a number sufficient to build up a diffuse layer.

4.3 Measurements on Streaming Currents

4.3.1 Aqueous solutions

In this investigation, needle Gauge 22 (length 180 mm), a stainless steel tube (diameter 33 mm) and stainless steel wires were used. Flow rate from 6 to16 ml/min was employed to give laminar and turbulent flow. Various aqueous solutions were used. The same set-up as the one used in studying pendant drops was used.

4.3.1.1 Flow rate dependence

Fig.29 shows the pattern of streaming current against time (flow rate) of tap water. In this study it was found that one minute of flow is enough to give a stabilised flow as shown in the figure. Fig.30 shows the results obtained from measurement of streaming current against flow rate of DI water. It can be seen that the streaming current, Is, increases linearly as flow rate increases as expected.

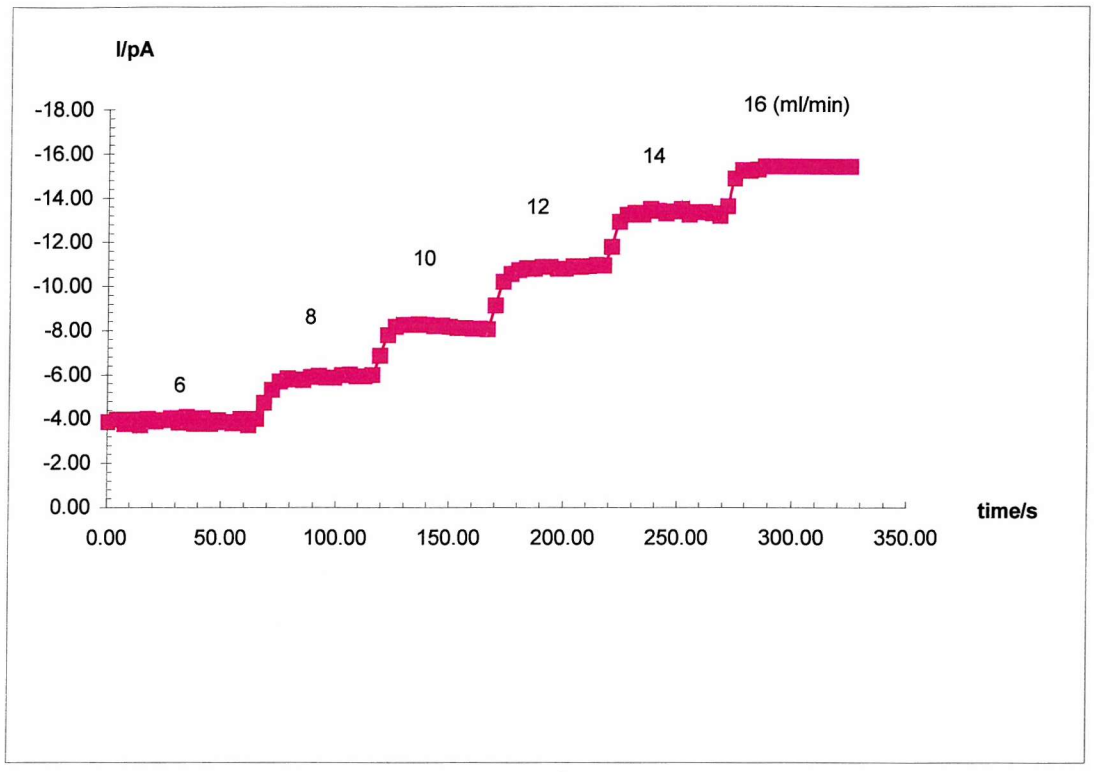

Fig.29 The flow pattern of the pump-streaming current against time (flow rate) for tap water

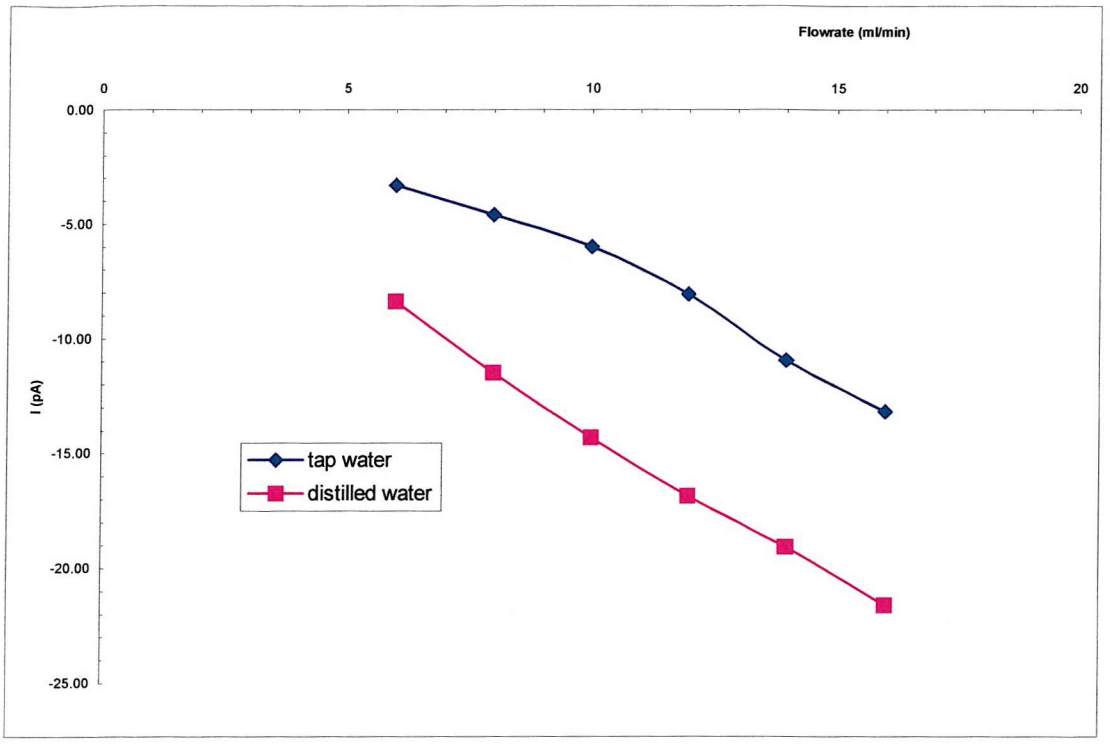

Fig.30 Streaming current against flow rate for DI water and tap water

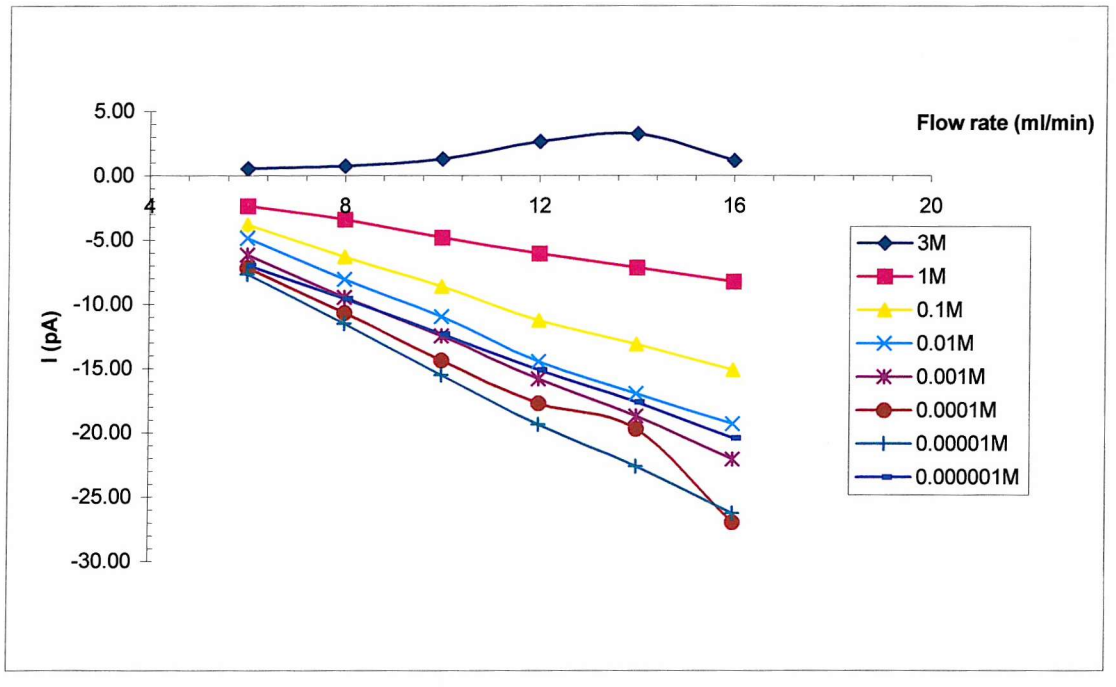

Fig.31 Streaming current against flow rate of KCl solutions

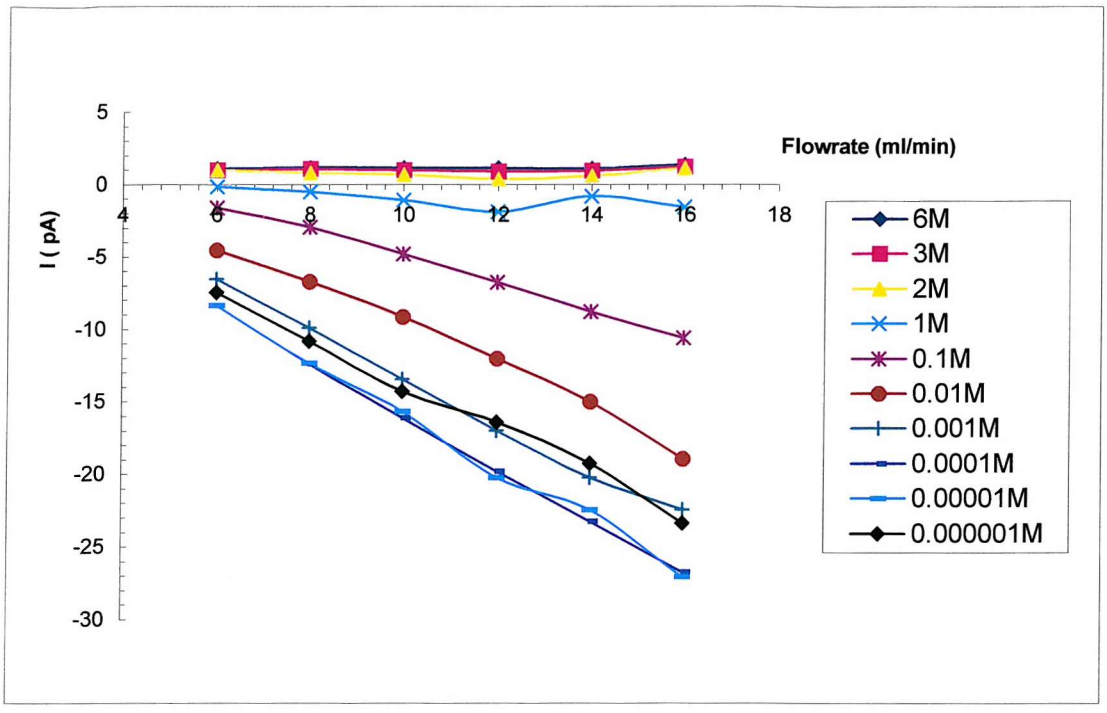

Fig.32 Streaming current against flow rate for NaCl solutions

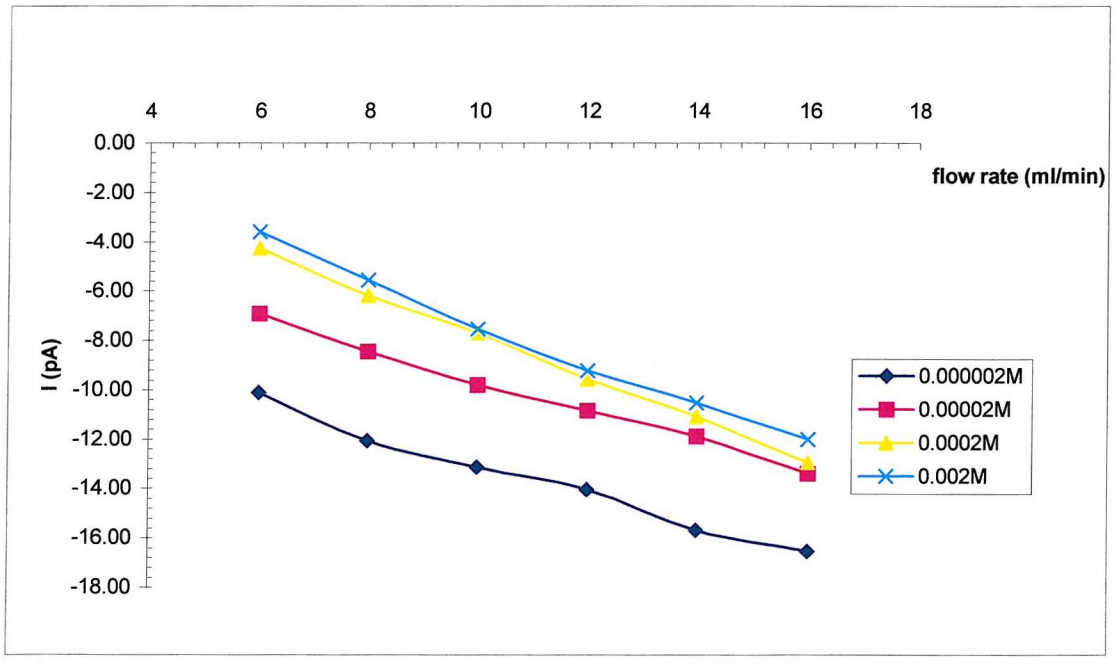

Fig. 33 Streaming current against flow rate for KOH solutions

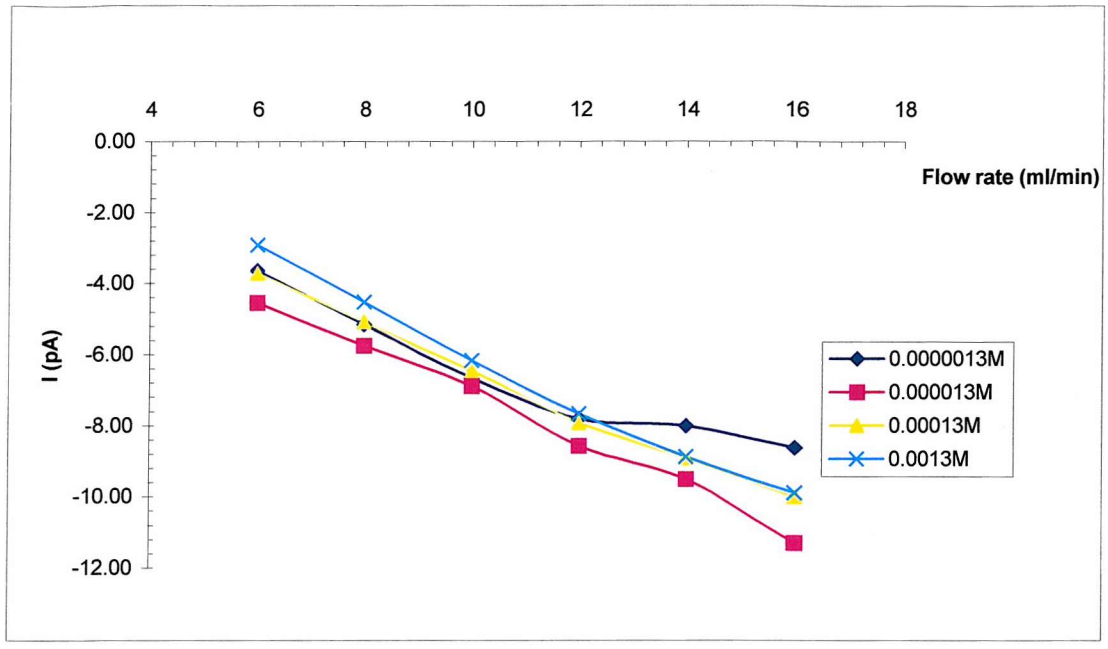

Fig.34 Streaming current against flow rate for NaOH solutions

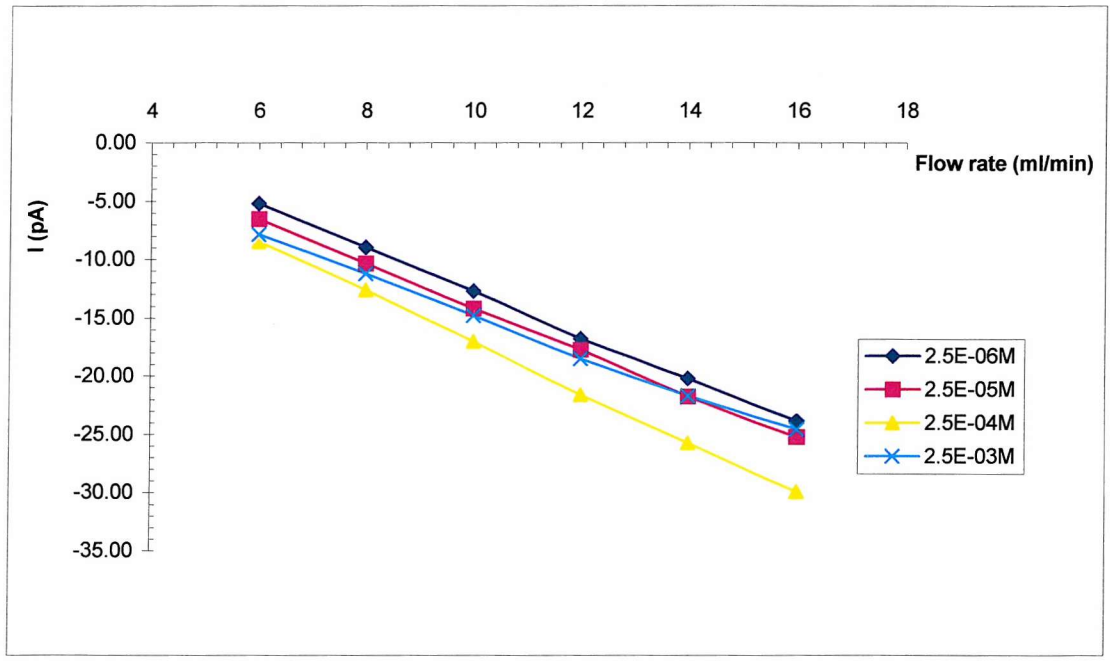

Fig.35 Streaming current against flow rate for H_2SO_4 solutions

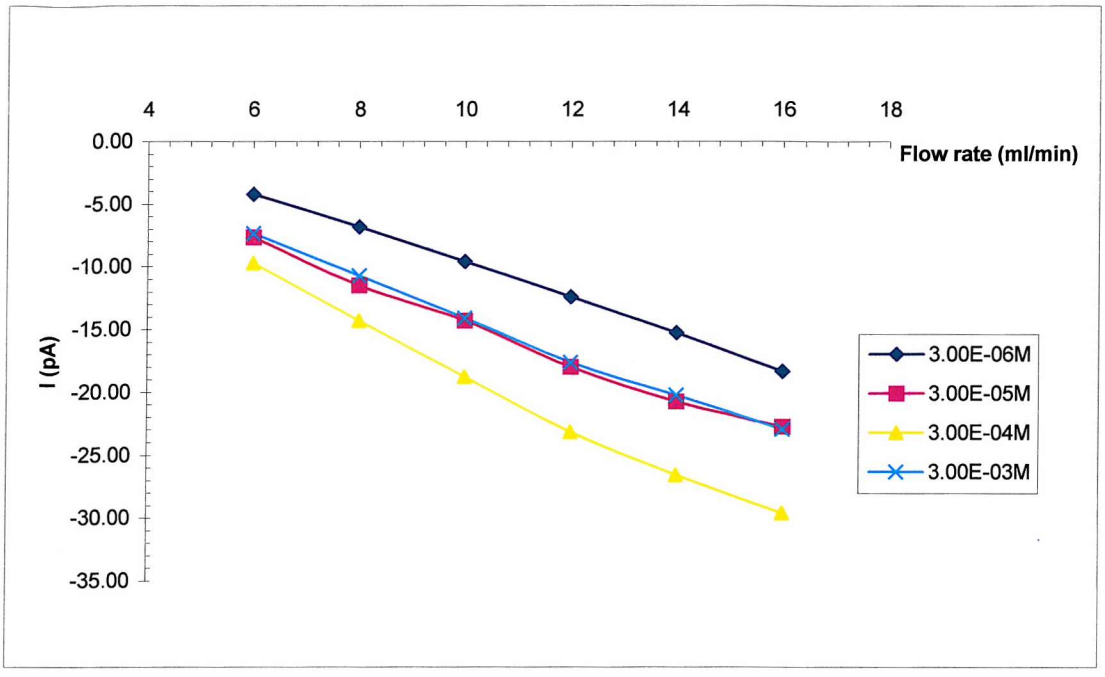

Fig.36 Streaming current against flow rate for HCl solutions

Fig.31 to Fig.36 show the streaming current against flow rate of solutions of KCl, NaCl, KOH, NaOH, H_2SO_4 and HCl at different concentrations respectively. It can be seen that the relationship between the streaming current and flow rate for all solutions are linear, as expected for aqueous solutions. This is because the double layer is so thin that it always under the laminar flow layer.

4.3.1.2 Concentration of electrolytes dependence

This section describes the relationship between streaming current and the concentrations of various aqueous solutions: salts, acids and alkalis.

4.3.1.2.A Salts

Fig.37 and Fig.38 show the relationship of streaming current vs concentration of solutions of Potassium Chloride and Sodium Chloride respectively from 10^{-6} to 3 M at different flow rates (6 ml/min to 16 ml/min). From the graphs, it can be seen that streaming current is negative at all flow rates at dilute concentrations and there is a slight increases in magnitude, then a decrease in magnitude as the concentration increases and reversal of its sign at around 1 M and becomes positive at 3 M.

It is interesting to notice that the trend of charge density with salt solution concentration is almost the same as that in pendant drop. This should give the information of contact potential between salt solution and the inner wall of the needle. This will be discussed further in the conclusion section.

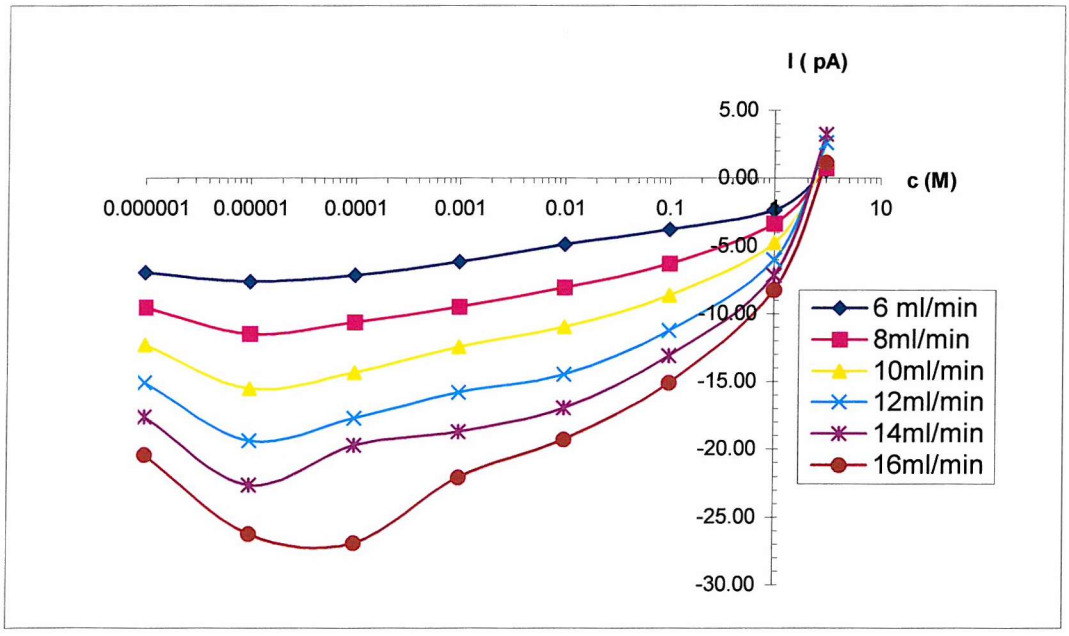

Fig.37 Streaming current against concentration of KCl solutions

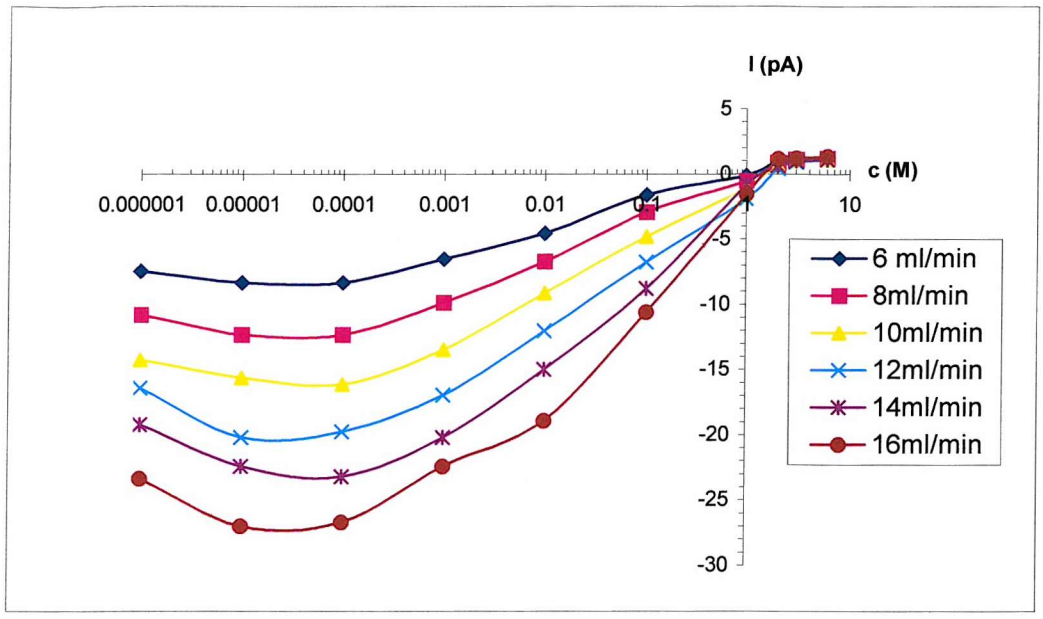

Fig.38 Streaming current against concentration of NaCl solutions

4.3.1.2.B Alkalis

Fig.39 and Fig.40 show the results obtained from the streaming current measurement against the concentration of Potassium hydroxide and sodium hydroxide respectively. From the graphs it can been that, in the case of NaOH, as concentration increases the streaming current, first, increases in magnitude, then at concentration around 10^{-4} M decreases and after that almost keeps constant while for the case of KOH, the streaming current decreases at the beginning and then tends to keep constant. The streaming current is always negative at all concentrations.

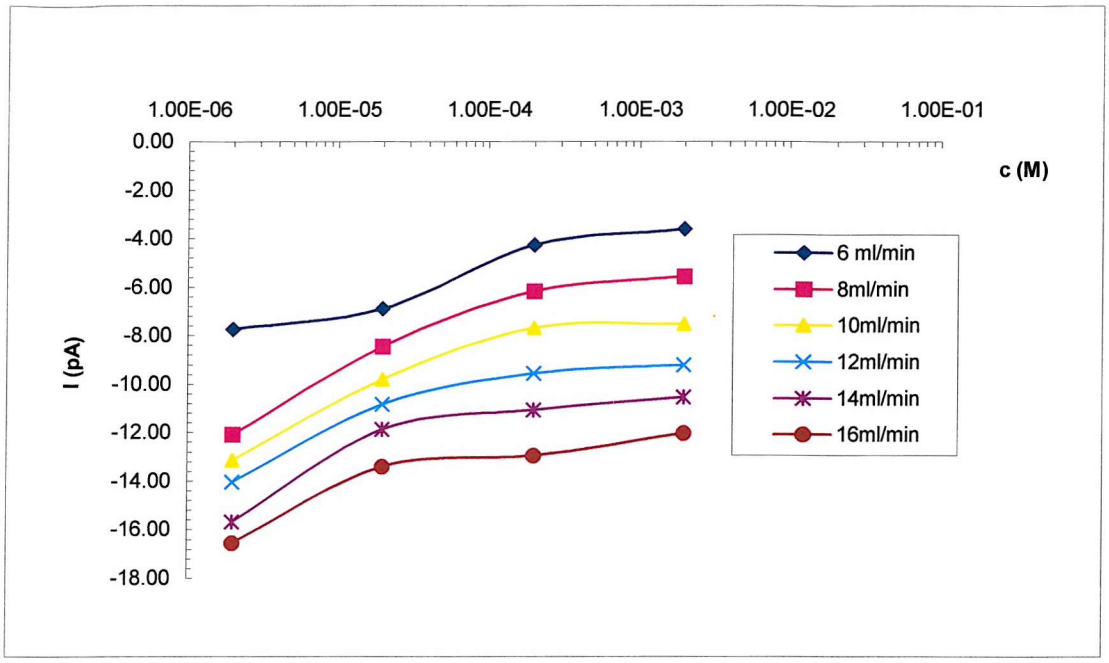

Fig. 39 Streaming current against concentration of KOH solutions

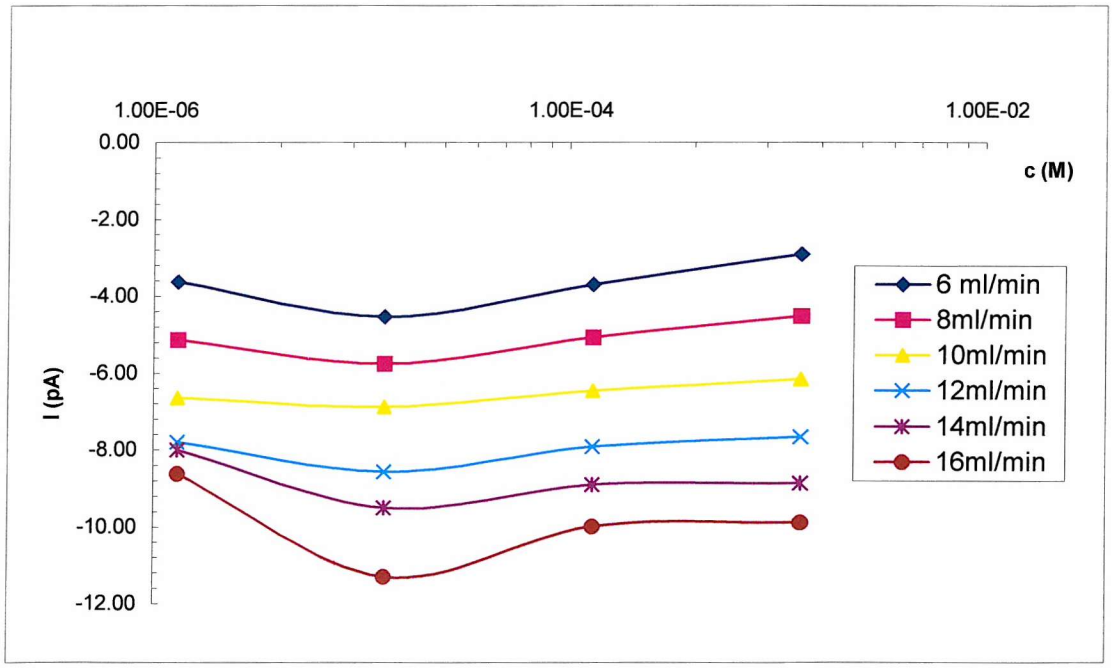

Fig.40 Streaming current against concentration of NaOH solutions

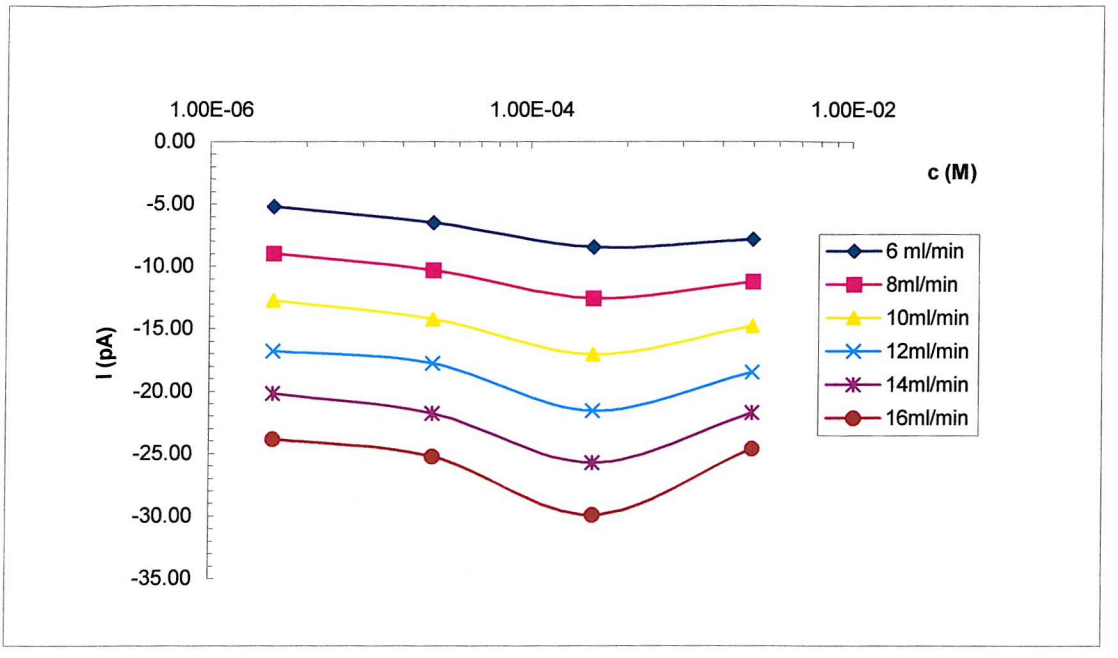

Fig.41 Streaming current against concentration of H_2SO_4 solutions

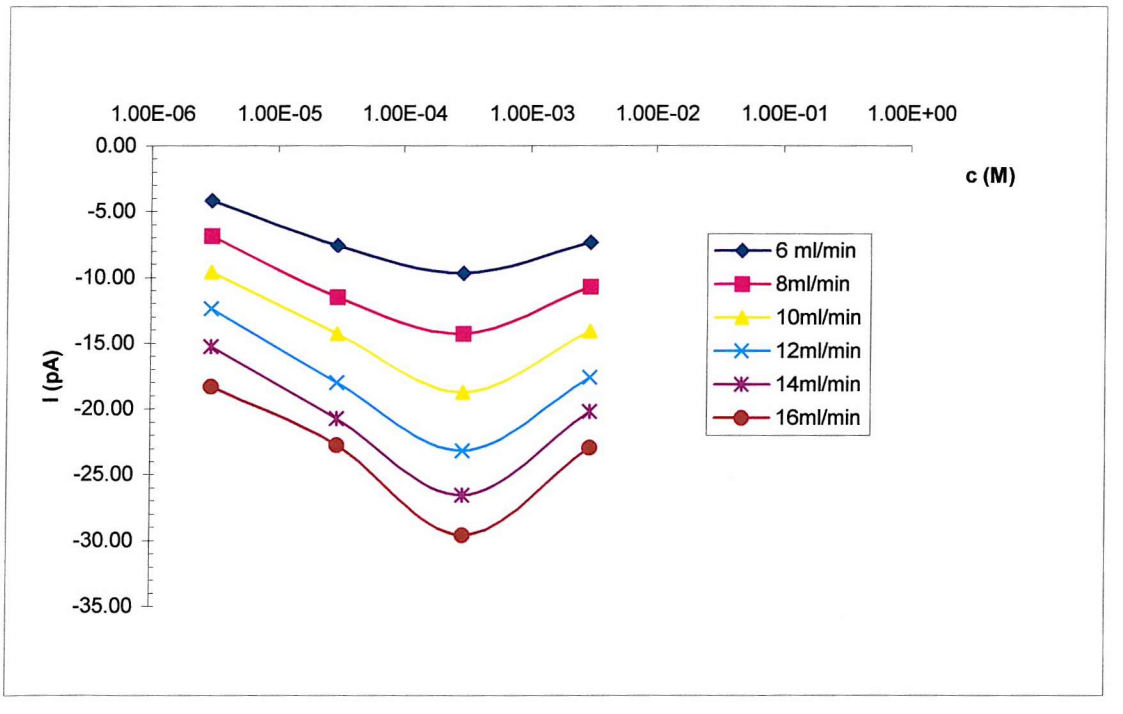

Fig 42 Streaming current against concentration of HCl solutions

4.3.1.2.C Acids

Fig.41 and Fig.42 show the relationship between the streaming current and the concentration of sulphuric acid and hydrochloric acid respectively. It can be seen that the streaming current increases in magnitude as the concentration increases, then reaches their maximum at concentration about 10^{-4} M and then decreases. The streaming current is always negative in all cases.

4.3.2 Streaming Current on Model Propellant

It is the aim of this work to investigate the electrostatic properties of aerosols generated using various propellants, with particular interest in inhalation HFA's (i.e. 227 and 134a). HFA 227ea and 134a are highly volatile at room temperature and this poses some experimental difficulties. Preliminary work has therefore been undertaken using the less volatile 2H, 3H-Decafluoropentane (HPFP, mp-80°C, bp-53.6°C and vp330mm@250°C) which is structurally similar to HFA.

In these experiments, the liquid is driven through a capillary tube at flow velocities up to about 50 ml/min. The charges of jets are measured by collection of the liquid in a Faraday Cup. Moreover, in order to obtain information concerning the effect of electrokinetically active substances on charge density, measurements were made using solutions of HPFP with acetone as a surfactant containing increasing concentrations of calcium diisopropyl salicylate (Ca-Dips). Acetone was used as a co-solvent to increase the solubility of Ca-Dips in HPFP. Ca-Dips were deliberately chosen for two reasons: one is that they had previously been used in benzene by Van der Minne and Klinkenberg [18] in electrokinetic measurements on carbon black and copper; the other is no literature is available on solubility of anything in HPFP.

This section describes investigations of the influence of flow rate and conductivity on jet charge tendency. The main objective here is to demonstrate how the

fundamental laws of fluid mechanics and electrostatics can be used to predict the charge tendency of the system.

Material used: Calcium diisopropyl salicylate (Ca-dips) was prepared from the acid, m.p.117°C. (lit. 118.5°C., *Bull. Soc.chim. France* 1948, 68-70) [72].

It is not soluble in HPFP. Therefore acetone solutions of Ca-dips of different concentrations were prepared in the first place. Then 2%(v/v) of different concentration acetone solutions of Ca-dips were added to HPFP to obtain different conductivity HPFP solutions of Ca-dips.

2H, 3H-Decafluoropentane (HPFP, mp-80°C, bp-53.6°C and vp330mm@250°C) was produced from Apollo limited. It was filtrated using syringe filter (PTFE Filter Media with Polypropylene Housing).

Acetone was from the Aldrich Chemical Company had a purity of 99%.

4.3.2.1 Flow rate dependence

The streaming currents measured for needles of Gauge 30 at different concentrations of Ca-dips in HPFP are plotted against flow rate, as shown in Fig.43 and Fig.44. Fig.43 shows all the results for different concentrations. Take Fig.44 as an example, which is the streaming current as a function of Reynolds number (Re $\propto$ v). It can be seen from the graph that in the I against Re (or flow velocity v) curve the dramatic change of slope sets in only at the higher rate of flow (in this case is $v \cong 6m/s$, which corresponds to Re $\cong$ 2000); we also note that at high rates of flow

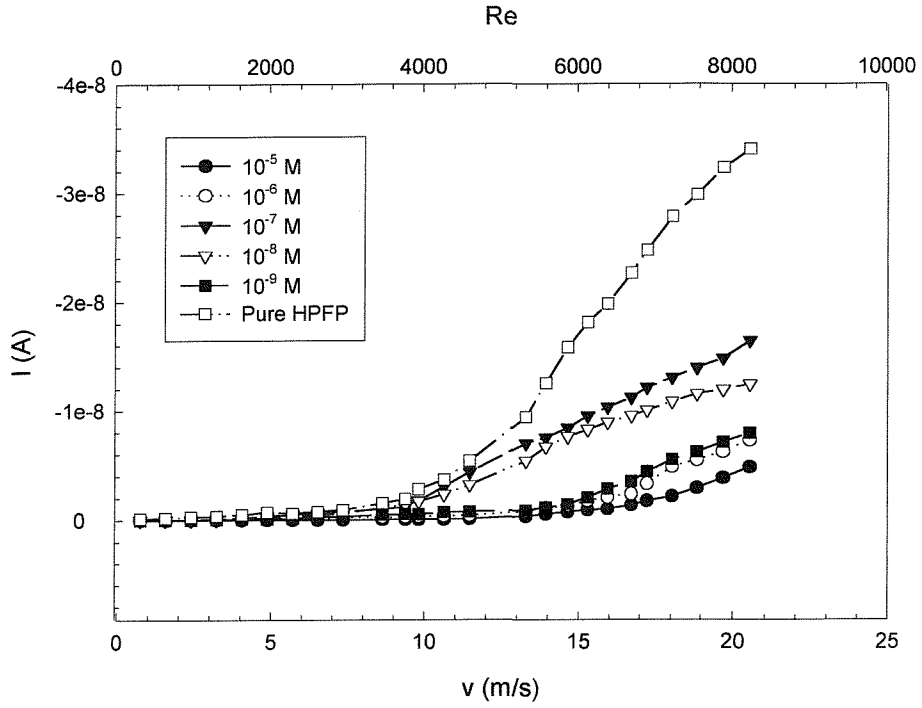

Fig.43 Streaming current I as functions of Reynolds number Re and flow velocity v of solutions of Ca-dips in HPFP of concentrations from 10^{-9}M to 10^{-5}M

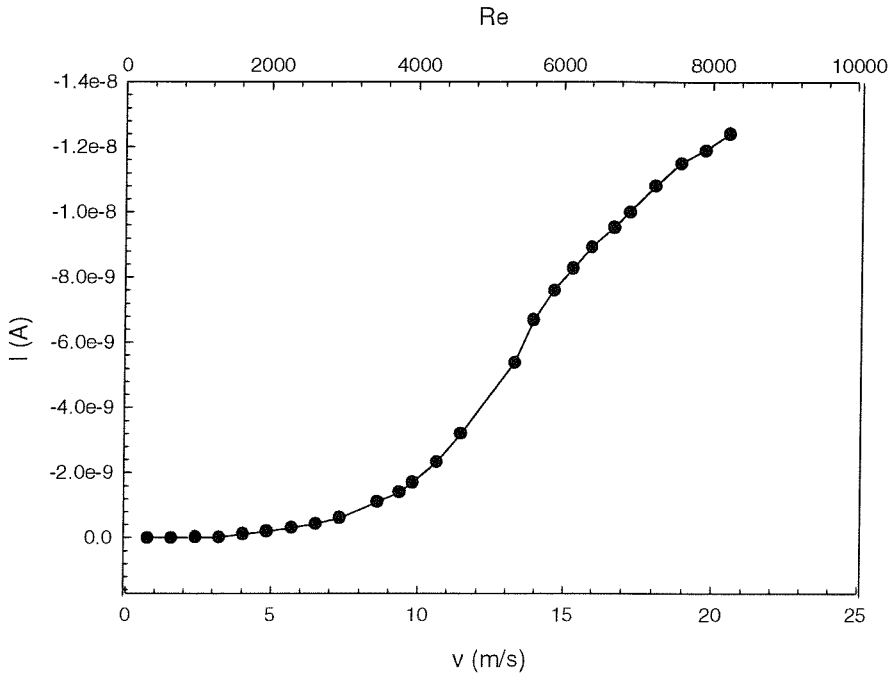

Fig.44 Streaming current I as functions of Reynolds number Re and flow velocity of solution of 10^{-8}M Ca-dips in HPFP

there is a return to linearity between I and Re (or I and v, which in this case is $v \cong 13m/s$, which corresponds to Re ≅ 4000). This we interpret as that the first straight part represents the laminar flow, the second straight part the fully turbulent flow and the intermediate part with a strongly sloping, where the slope change with v, for regions of lesser turbulence.

As indicated in Section 4.2 theory, for laminar flow at low flow rate the current is relative low (0.92 m/s ≤ v ≤ 6 m/s). As flow rate increases (13 m/s ≥ v ≥ 6 m/s, in this case $\lambda^2 << \delta^2$, i.e. the double layer is still lying under the sub laminar layer), liquid flow becomes turbulent through a core constituting most of the tube, the streaming current as indicated by Eq.28 increases dramatically because of the greater velocity gradient in the sublayer region. When the flow rate reaches 13 m/s

(or Re ≅ 4000), here, the $\lambda^2 >> \delta^2$ (δ is determined by Eq.29) limit of this general result is obtained directly by regarding turbulent diffusion in the core of the flow intense enough to render the volume charge density there essentially uniform, while sufficiently diminished in the diffusion sublayer that molecular diffusion completely dominates. In this case, illustrated in fig. 28 (b), the complete diffuse charge (q in C/m^2) is carried off with speed v, we then have Eq.31

$$I_{lam.} = -8\pi\varepsilon\varepsilon_o\zeta v \tag{22}$$

$$Iptur = -\frac{2\pi\varepsilon\varepsilon_o a\zeta v}{\delta} \tag{28}$$

$$I_{ftur} = -\frac{2\pi\varepsilon\varepsilon_o\zeta a}{\lambda}v \tag{31}$$

(22), (28) and (31) describe the relationship of streaming current and flow velocity for laminar flow, transition from laminar to turbulent flow and fully turbulent flow respectively. Therefore, it is expected that the curve would be the shape of fig. 44.

4.3.2.2 Concentration dependence

Streaming currents were measured using different concentrations of Ca-dips in HPFP solutions and relative zeta potentials are calculated from the results. Streaming current and zeta potential are plotted as a function of concentrations (or conductivities) as shown in Fig.45. The zeta potential for pure HPFP is 17 mV. We note that as concentration increases at the beginning both streaming current and zeta potential increases, until a maximum is reached at concentration of ~10^{-7}M and then both streaming current and zeta potential decreases. The change of streaming current with concentration is due to the relationship of zeta potential to concentration (or conductivity) while the curve shape of zeta potential against concentration can be explained in terms of specific adsorption of charged species on the inner wall of the capillary. The streaming currents being negative shows that the stainless steel wall is positively charged, presumably by adsorption of a monolayer of ions such as Ca^+(di-isopropyl-salicylate) [18].

When the concentration of the ions is very low, the ions tend to be adsorbed onto the surface of the inner wall of the capillary. But as the ion concentration in the liquid increases the specific adsorption reaches its saturation of the ion on the wall. Now the counterion adsorption is dominating, which makes the positive charge density on the wall decrease. This means the zeta potential will decrease and so does the streaming current.

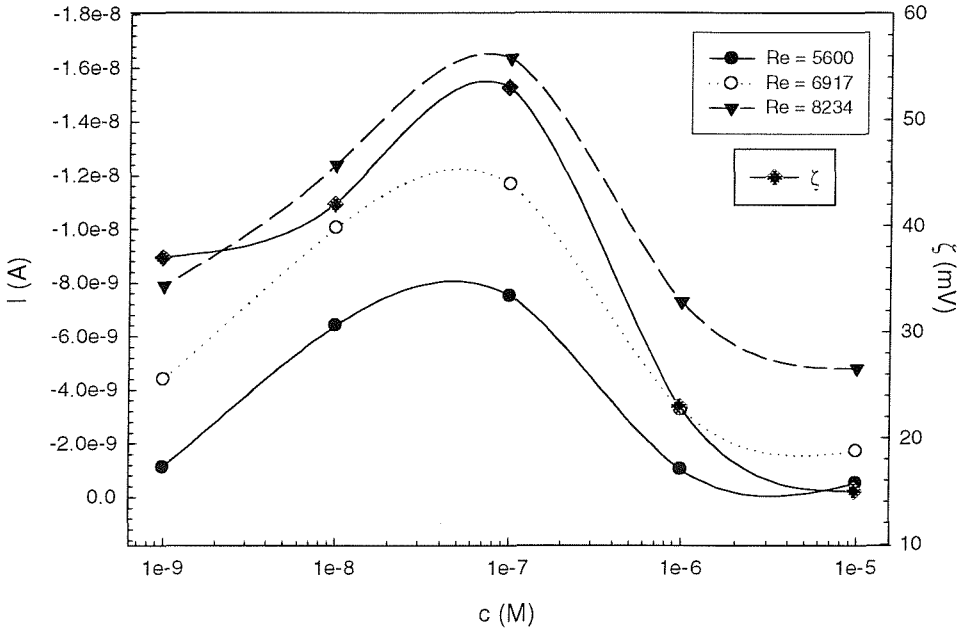

Fig.7 Streaming current I and zeta potential ζ as functions of concentration of solutions of Ca-dips in HPFP.

Fig.45 Streaming current I and zeta potential ζ as functions of concentration of solutions of Ca-dips in HPFP for different Re numbers

4.4 Conclusions

From the results mentioned above we can draw conclusions as the following:

(1) The relationship between streaming current and flow-rate in all cases investigated, except for KCl (3M) and NaCl (2, 3 and 6 M), is linear. This means

the laminar flow pattern can be used to explain the results (Equation (22)) and the resulting zeta-potentials calculated from equation (22) are listed in Table3 below.

Table3.Zeta-potentials (mV) of electrolyte solutions at different concentrations

c (M)	KCl	NaCl	KOH	NaOH	H_2SO_4	HCl
10^{-6}	14.6	7.5	15.8	16.1	11.9	11.6
10^{-5}	14.1	8.0	23.0	18.5	8.8	8.9
10^{-4}	8.9	7.9	18.5	14.5	10.2	7.7
10^{-3}	5.5	7.9	10.4	12.9	7.4	8.6

The zeta potential for DI water is 12.1 mV.

(2) As stated in section 3.2, the zeta-potential between water and inner wall of the stainless steel needle is supposed to be positive, i.e. the diffuse part of the double layer is negative so that the charge carried away by liquid is negative. As the surface of the inner wall is positive charged, increasing positive ions concentration (H^+, Na^+ and K^+) would increase the zeta-potential, i.e. the streaming current would increase. But as the cations adsorb onto the surface of the inner wall of the needle the positions available to be occupied by cations decrease and the thickness of double layer (according to equation (8) $\delta = \left(\frac{\varepsilon\varepsilon_o D}{2ne\mu}\right)^{\frac{1}{2}}$) also decreases. Finally, at a certain concentration the surface is saturated by the cations, which means that the contribution of zeta-potential increase is less than that of the decrease of the double layer thickness δ. This, according to the results from acids and alkalis, is around 10^{-4} M. After the saturation point, the streaming current decreases or keeps almost constant as the concentration of cations increases. On the contrary, as the concentration of anions (Cl^- and OH^-) increases the zeta-potential decreases because of the adsorption of the anions onto the surface of the inner wall of the needle, which cancels out the surface potential-determining ions- positive ions. Finally it reaches the saturation point so that the zeta- potential keeps almost

constant in the case of alkalis or reverses the sign of the surface charge in the case of salts.

(3) The theory of double layer only can be used in dilute solutions as mentioned in section 3.2. Therefore, for concentrated solutions there is still no theory to explain the phenomena. As in the cases of KCl and NaCl solutions, the charge sign reversal at concentration ~ 1 M cannot be explained by double-layer theory quantitatively. But it may be explained qualitatively. Suppose that there is still a double layer for concentrated solutions between the solution and the inner wall of the needle, although very thin. Therefore, as the concentration of Cl^- increases, Cl^- is adsorbed onto the surface of the wall to make the zeta-potential decrease, i.e. the streaming current decrease. As soon as the concentration of the adsorbed Cl^- becomes greater than that of the original surface potential-determining ions, the double layer completely collapses and zeta potential reverses its sign. This qualitative explanation can be used in the cases of both drops and jets.

(4) There are some inconsistent results, such as the relationship between streaming current and flow-rate for solutions of KCl (3M) and NaCl (2, 3 and 6 M) do not seem to be linear as expected but almost constant. This needs to be investigated futher.

(5) The process of flow-induced electrification consists of four stages, charge generation, transport, accumulation and leakage of which an understanding of electrification requires a combining of the laws of electromagnetism, fluid mechanics, heat, and electro-chemistry to describe.

(6) HPFP has larger streaming current than aqueous solutions. This is because HPFP has a larger zeta potential (17 mV) while DI water has a lower zeta potential (12.5mV).

(7) As the conductivity of HPFP solutions increases, the charge density increases first, then a maximum is reached. Afterwards, the charge density decreases. However, there is no polarity change observed as in aqueous solutions. These can be explained in terms of contact potential between liquid and the inner wall of the needle. The explanation would be similar to the aqueous solutions. As for the no polarity change being observed, this might be due to HPFP and its solutions have not enough ions available to adsorb to the inner wall surface of the needle to make the contact potential change its sign.

It can be concluded from the results we obtained that the motion of relatively low dielectric materials such as various propellants relative to a solid surface will generate electrical charge in the liquid, of which the magnitude can be monitored by adding antistatic agents in the liquid. The solid surface has a preferential adsorption to various ions, which determines the sign of the solid surface charge, i.e. the liquid charge sign. There is a balance between the solid surface ion charge density and the ion density in the liquid. Below that value increasing the potential-determining ions will increase the zeta potential and streaming current. After reaching that value, further increasing the same sign ions will decrease the streaming current due to the counter ion adsorption becoming dominant then.

As for the influence of flow rate on streaming currents it is much more complex and which largely consists of three parts- straight parts for laminar and for fully turbulent flow, with a strongly sloping intermediate part for regions of lesser turbulence.

CHAPTER FIVE

SPLASHING CHARGING

5.1 Introduction

There are various ways by which liquid drops can acquire charges. Apart from the methods mentioned in the last two chapters, drops can acquire charges by impact of liquid on solids (electrification by splashing). Lenard (1892, 1915) [22][23] was among the first to notice electrification by splashing near waterfalls, and Zeleny (1933) [25] described a typical experiment with air shattering. The explanation usually put forward is that the effect is due to an electrical double layer within the surface (Chapman 1938) [36] and that when a drop breaks up the outer layer is in some way scraped off, taking its charge and leaving the residue with an equal and opposite charge. Zeleny in fact refers to the production of negative ions.

Lenard allowed various liquids to descend through air, the results for charges found in the liquid being, such as water, positive. He also found that the charge in the air was negative. He also found that different charges were found in liquid when letting different liquids splash against different solid surfaces.

Gill and Alfrey (1952) measured charges on drops breaking up in electric fields. They interpreted the results in terms of ordinary laws of electrostatic induction, with allowance for contact potential differences. They also studied splashing phenomena and they also explained their results in terms of contact potential between liquid and solid.

Matsuyama and Yamamoto [73] [74] studied the impact/contact of a particle with metal plate in both atmospheric conditions and in Ar gas. A model of charge relaxation due to gaseous discharge was proposed by them.

The aim of the study of splashing liquids against solids is to investigate the charges on droplets after splashing against some solid plates. To obtain more information

about contact potentials between different liquids and different material solids; to further consolidate the theory developed in last two chapters.

5.2 Theory

Capacitance: A particularly important concept in electrostatics is the capacitance of a system. Capacitance quantifies the ability of a system to store electrostatic charge and, as will be shown later, quantifies also the electrical energy that can be stored in the system. All electrostatic systems including a particle approaching to a plate have an associated capacitance.

5.2.1. Isolated Sphere Capacitance

The capacitance of two conducting, concentric spheres is readily determined from Gauss' theorem. Consider the situation in Fig.46, where a charge +q has been transferred from the earthed outer sphere to the inner sphere raising its potential to V. From symmetric considerations, the electric field at the surface of an imaginary sphere of radius r enclosing the inner conductor is given by

$$E(r) = \frac{q}{4\pi\varepsilon\varepsilon_0 r^2} \tag{32}$$

The potential of the inner sphere relative to the outer is given by

$$V = \frac{q}{4\pi\varepsilon\varepsilon_0}\int_a^b \frac{dr}{r^2} = \frac{q}{4\pi\varepsilon\varepsilon_0}(1/a - 1/b) \tag{33}$$

from which the capacitance is seen to be given by

$$C = \frac{4\pi\varepsilon\varepsilon_0}{(1/a - 1/b)} \tag{34}$$

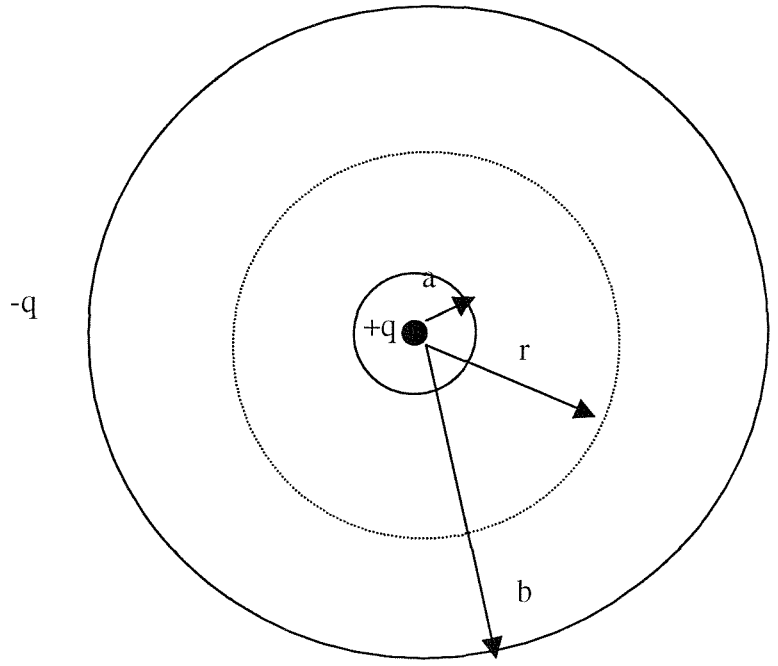

Fig.46 Concentric conducting spheres

If the radius of the outer sphere is much larger than the inner, then equation (34) gives the familiar equation for the capacitance of an isolated sphere, namely

$$C = 4\pi\varepsilon\varepsilon_0 a \qquad (35)$$

Equation 35 shows that accurately machined spheres suspended well away from all other structures can be used as standards for calibrating capacitance measuring instruments.

5.2.2 The Capacitance of Sphere and a Plane

Smythe (1968) shows that the capacitance between two nonconcentric spheres (Fig.47) is given by

$$C = 4\pi\varepsilon\varepsilon_0 ab \sinh a \sum_{n=1}^{\infty} \frac{1}{b \sinh n\alpha + \alpha \sinh(n-1)\alpha} \qquad (36)$$

where

$$\alpha = \cosh^{-1}\left(\frac{d^2 - a^2 - b^2}{2ab}\right)$$

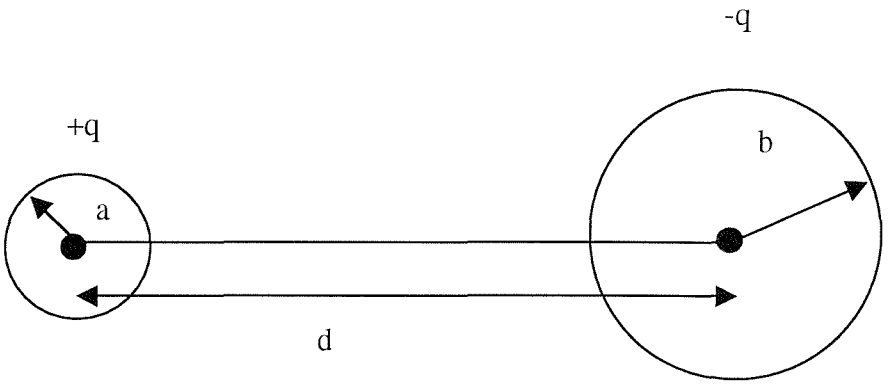

Fig.47 Two spherical conductors of different radii

Often in electrostatic problems, though, we wish to know the capacitance between a sphere and an infinite flat plane as in Fig.48. This case is readily obtained from equation (36) by substituting a=R and b=(d-D) and allowing both d and b to become infinite. Following Smythe the solution is

$$C = 4\pi\varepsilon\varepsilon_0 R \sinh\alpha \sum_{n=1}^{\infty} \operatorname{csc} hn\alpha \qquad (37)$$

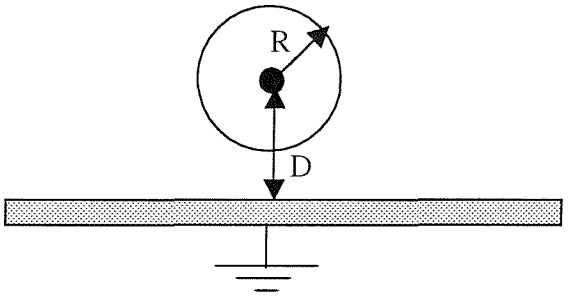

Fig. 48 Conducting sphere above an earthed surface.

where $\alpha=\cosh^{-1}(D/R)$. If D>>R, i.e. the distance of the sphere from the ground plane is large compared with its radius, then equation (37) gives the capacitance of an isolated sphere (cf. equation (35) with a=R) as expected.

5.3 Experimental Method

The same liquid delivery system as the one used to produce drops and jets was used here. As shown in Fig.4 or Fig.5, a metal plate was used as the target against which liquid was splashed. Drops fell from the needle at the rate 1 drop per second.

After falling 1cm the drops encountered an air blast from a tube which shattered them, the spray being blown in the direction of the blast, most of it hitting the target, 10 cm square placed 10 cm from the point of disruption. Most of the spray rebounded from the target but a little collected on the target in drops. The apparatus was contained in a metal cubical box with some holes to let the air and spray out easily, and one to admit the rod holding. The target was insulated from the cage and jointed to a Keithley electrometer. Every thing else was at earth potential.

5.4 Experiments

First, the drops dripping from the tip of the needle without air blast were collected by a Faraday cup which was connected with a Keithley electrometer and the initial charges on the drops were monitored by this Keithley electrometer. This is exactly the same situation as in Chapter Three. Then residual charges on the target were examined after each drop was splashing against it under conditions of: (1) different air blast velocities, (2) different concentrations (conductivities) of electrolyte solutions and (3) different materials of targets.

The effect, as might be expected, depends very much on the surface conditions; the experiments were therefore made with single drops and the target dried each time.

5.5 Experimental Results and Discussion

5.5.1 Effect of air blow rate on Splashing Charging

Fig.49 and Fig.50 show the charges acquired by the target against air blast velocity. It can be seen that in all cases the charge acquired by the target increases rapidly with increase of air blow rate and there is no doubt that this is because the droplets from the shattered drops become smaller as the blast pressure is increased.

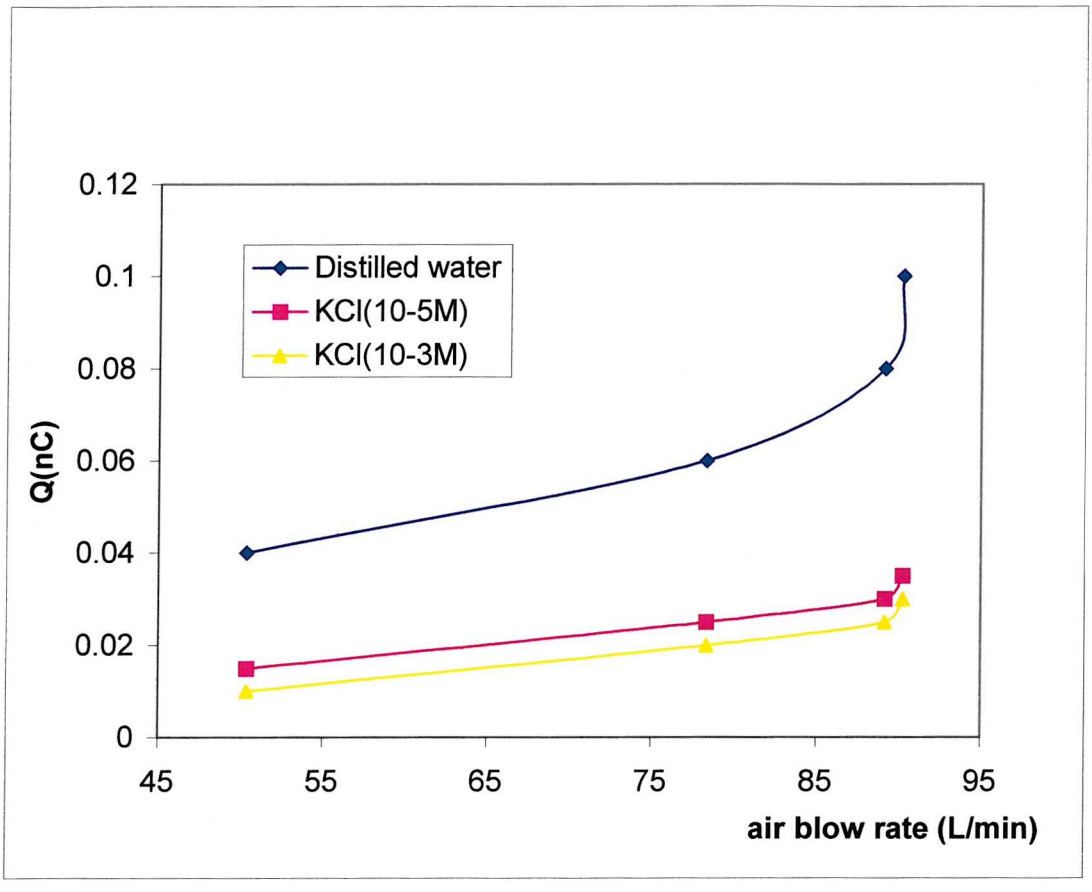

Fig.49 Charge against air blow rate for distilled water and KCl solution with Cu plate

The obvious question of the origin of this charge appears to have three possible answers:

- It was on the original drops before they were shattered by air blast.
- It was produced as Zeleny and others suggest at the moment of shattering.
- It was produced as a result of the droplets rebounding from the target.

The first is easily ruled out. The charge originally on each drop by virtue of its contact potential with the needle was found by turning off the air, insulating the large box and measuring the charge it acquired as the drops fell into it. This was found to be negative and of the order of $\sim 10^{-14}$ C per drop, varying for the different liquids. Not only was this of opposite polarity to the target charge, but the target charge was thousands of times bigger.

As for the second alternative, if the break up of the drops really produces a number of negative ions the residue droplets must carry an equal opposite positive charge. All these negative and positive charges are blown on to the target, and it is impossible to believe that a metal target collects only the positive charge rejecting in some way the negative ions. It seems clear therefore that the third explanation is correct and that the target charge is in some way connected with the rebounding of drops from the target.

An explanation for this is possible based on the simplest principles. A liquid drop touching a metal at earth potential acquires by virtue of the contact potential v (usually negative for distilled water and metal) a charge Q. Q is, of coarse, v multiplied by the capacity C of the drop.

$$Q=vC \qquad (38)$$

It is easy to see that, if the drop is subdivided into a large number of little drops before touching, the aggregate charge collected by the little drops will be far larger than Q because the capacity C depends on the linear dimensions d (diameter of a drop) (Equation 35 or 37) and the volume V on the cube of these dimensions. For example, if divided into 1000 parts each part has one-tenth of capacity of the original but as there are 1000 parts the total charge taken is 100 times as great.

In the experiment the original drop has a charge of the order of magnitude of, say, -Q. When broken up the fragments which hit the target and rebound from it carry away a negative charge many times greater than Q, leaving a corresponding positive charge on the target. The greater the number of fragments the greater the charge transfer, which agree with the curves of Fig.49 and Fig.50.

5.5.2 Effect of solution conductivity on splashing charge

From the two graphs, it can also be seen that the splashing charge decreases as the solution conductivity increases.

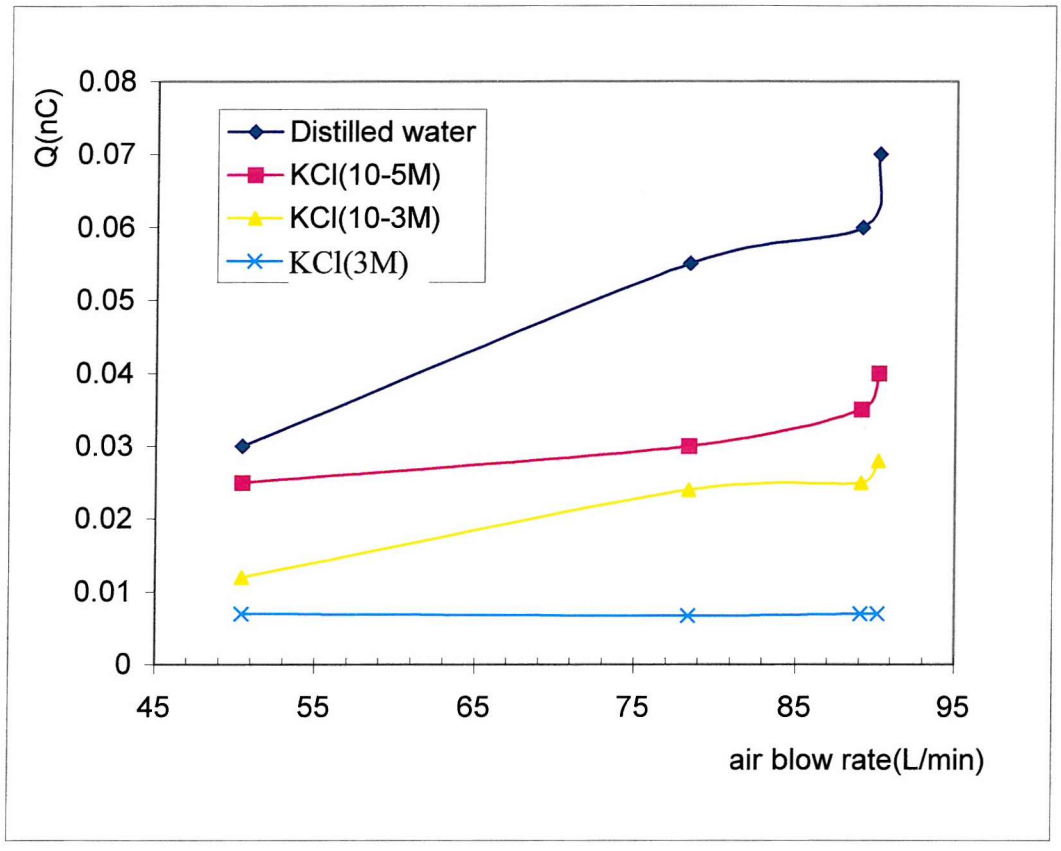

Fig.50 Splashing charge against air blow rate for distilled water and KCl solutions with Pb plate

There is a remarkable difference of splashing charge between distilled water and KCl solutions under like conditions. There is no reason to suppose any particular

variation in the size of the fragments and the contact potentials only differ slightly so that a much more potent reason must be found. There is an attractive hypothesis which is consistent with these results. A drop of liquid placed on a metal assumes a potential v with respect to it, and if its capacity with respect to the metal is C the charge it acquires is vC. But one encounters here the mathematical difficulty that the capacity of two conductors approximates to infinity as they are brought closer and closer together, the infinity being due to the small elements in contact and the rest of the drop having in comparison a negligible effect.

But in practice the whole drop is not at potential v, there is not an abrupt change from 0 to v at the point of contact; instead the potential rises continuously from 0 to v as one proceeds a very small distance into the drop. Therefore at the elements near the point of contact which tend to make the capacity infinite, the potential tends to be zero and the effective capacity of the whole drop is not infinite but depends on the proximity of the equipotentials in the liquid; if they are closely packed then elements of the drop very close to the metal will have an appreciable potential and the effective capacity and charge will be high. If they are more widely spaced the potentials of these near elements will be less and the effective capacity and charge less.

The earliest idea on the origin of contact potentials throw light on the spacing of these equipotentials. The diffusion of ions out of the metal is balanced by a return current through the liquid, which in turn depends on the conductivity and the potential gradient. Hence the spacing of the equipotentials is determined by the conductivity. For poor conductors they are close together, getting further and further apart as the conductivity is increased; or in other words the equivalent capacity is high for poor conductivity and decreases as conductivity increases.

Thus distilled water should have the highest capacity and charge, weak solutions of KCl lower values and strong solutions of KCl should have the lowest values of all for capacity and charge; this is, of the same order as the experimental results. The same variation with conductivity was found many years ago by Sir J.J.Thomson (1894) [75] for a variety of liquids.

5.5.3 Effect of target material on splashing charge

Targets of different materials were next tested, as shown in Fig.49 and Fig.50 but only small variation in results were found for Cu and Pb.

This might be due to the contact potentials for different metal materials being different but the difference is small.

5.6 Conclusions

The experimental results of splashing charge enhance our explanations on drop charging and jet charging mechanisms: contact potentials.

- The splashing charge is caused by contact potential between the impacting drop and the target metal.
- Different materials of solutions and metals have different contact potentials
- The smaller the droplets for a certain amount of liquid the greater the total charge carried by rebounding droplets
- The lower the conductivity the greater the splashing electrification.

CHAPTER SIX

SPRAY CHARGING

6.1 Introduction And Objectives

The use of aerosols was one of the earliest methods by which therapeutic substances were delivered to the lung. The ancient Egyptians are known to have attached cones of burning cotton to the chests allowing them to inhale the acid smoke produced. Since then, inhalation has been used as a route for drug administration by many cultures, Adams, 1844 [76]. Aerosol therapy has advantages over other methods for the administration of some therapeutic agents, since the drug is delivered directly to its required site of action. The therapeutic effect is more rapid than that of an oral dose, a smaller dose may be used and there is a reduced incidence of systemic side effects, Newman, 1983 [77].

Aerosol techniques are now widely used in medicine for: humidification of airways; delivery of drugs to the lung; producing scans of the ventilated parts of the lung; fundamental research into mechanisms of lung disease. The use of clinical aerosols was reviewed by Brian and Valberge, 1979 [78].There are three fundamental devices for producing an aerosol: (1) Dry Powder Inhalers; (2)Nebulizers and (3)Metered Dose Inhalers.

Dry Powder Inhalers (DPIs)

Dry powder systems utilize drug blends in a suitable carrier for delivery to the lungs. Lactose is the single most commonly used drug carrier for DPIs (e.g., Ventolin Rotacaps). Jet milling and spray drying are the two most common techniques to produce fine particles suitable for use in DPIs

Nebulizers

Nebulized systems involve conversion of a liquid formulation into an aerosol with the aid of energy (e.g.ultrasonication), which is then inhaled by the patient. The

formulation may contain cosolvents and other pharmaceutical aids to ensure satisfactory physical and chemical stability of the drug.

Metered Dose Inhalers (MDIs)

Metered dose inhalers are by far the most popular method for pulmonary drug delivery. The charging process of these systems is the subject of this thesis. These systems are tamper-proof and capable of delivering very accurate and reproducible doses of aerosolised drugs to the lung. Typical MDI formulations contain an active ingredient, generally in solution or suspension, along with inactive excipients (e.g., surfactants, suspending agents, protective agents), propellants, and solvents.

Drug Charateristics

Solubility and concentration are two variables that can be altered to improve lung deposition and absorption characteristics of drugs from the lung.

Surfactants

Surfactants generally aid formulation processing and minimize particle aggregation, thus improving physical stability and dose uniformity in pharmaceutical aerosols.

Solvents

Solvents in pharmaceutical MDIs are usually inert and help solubilize drug and surfactant. Solvents in MDIs serve also as carriers for delivering medicament to airways.

Propellants

There are three primary propellant systems in pharmaceutical MDI products. These are trichlorofluoromethane (CFC-11), dichlorofluoromethane (CFC-12), and dichlorotetrafluoromethane (CFC-114). However, due to their ozone-depleting potential, alternative propellants like tetrafluoroethane (HFA-134a) and

heptafluoropropane (HFA-227ea) are being considered as alternative CFC propellants. These non-ozone-depleting propellants possess quite different physiochemical properties compared to CFCs. Of significant importance is the fact that conventional surfactants used in MDIs products cannot be formulated with HFAs. This limitation with HFAs invokes a wide investigation of many aspects of HFAs MDI products in every aspect including the work in this thesis. This also invokes utilization of other formulation adjuncts most of which are solids or non-volatile entities. This could have a significant impact on deposition and absorption of aerosolised drugs.

HFA-134a has a much higher vapour pressure and a correspondingly lower boiling point than most CFC or CFC blends typically used in pharmaceutical MDI products. A higher vapour pressure increases particle velocity and subsequent upper-airway deposition as a result of inertial impaction. This decreases bioavailability of the aerosolised drug. Alternatively, a fine aerosol product formulated with HFA-134a would be quite dry by the time the aerosolised drug particles exit the mouth adapter. Such particles could survive filtration and impaction losses, thus depositing in the respiratory zones of the lung and presenting a significantly higher extrinsic bioavailability.

Aerosols produced by the mechanical disintegration of liquid surfaces are known to carry a net electrical charge; the process has been termed *'spray electrification'*, Loeb, 1958 [79]. In the spray electrification process, charge separation takes place, whereby the net charge carried by the dispersed cloud is accompanied by a charge of opposite polarity on the spray source.

The MDI is an atomizer which produces an aerosol by mechanical forces. Clinical MDIs generate sprays of small mean droplet size, the larger droplets being removed by impaction within the device. The aerosols produced by MDIs are often polydisperse and invariably electrically charged. Charge can play a significant part in aerosol dynamic behaviour and deposition.

The influence of electrical charge on aerosol particles is rarely considered in respiratory medicine. However, there is evidence that, for a given concentration of

therapeutic agent, the fraction of inhaled particles which is actually deposited in the respiratory tract will be greater for charged than for uncharged particles. Increasing the charge on an inhaled particle increases its force of attraction to the lung epithelium[100].

Aerosol electrostatics is an under-investigated feature of pharmaceutical aerosols, even though the various processes of aerosolization are known to produce charges on individual aerosol particles or droplets [80]. To date, research has focused upon three quite distinct areas: electrostatic measurements in powders for inhalation [81]-[83]; the influence of electrostatic charge upon aerosol deposition in the respiratory tract [84]-[87]; the importance of static charge upon aerosol holding chambers, as a factor controlling aerosol drug retention within these devices [88]-[95]. No report has been seen on systematic research on electrostatic charges produced by aerosolization from pressurised metered dose inhalers (pMDIs). This is probably due to the extreme complexity of the charging processes that occur during the production of aerosols from pMDIs, which makes the interpretation exceedingly difficult.

The phenomenon of droplets carrying net charges produced by pMDIs can be utilized in the therapeutic industry once the mystery of the charging mechanisms of aerosol particles generated by pMDIs is solved. The aerosols generated can be charged to a magnitude and sign in a controlled manner.

The airms of this study are to assess the electrostatic characteristics and size of aerosols produced by pMDIs, and to understand the charging mechanisms. It is hoped also to lay down guide-lines for the design of improved pMDIs.

6.2 Theory

6.2.1 Metered Dose Inhalers

A metered dose inhaler is a device capable of converting a suspension or a solution of drug into an aerosol mist.

6.2.1.1 Inhalation Drug Delivery System –Metered-Dose Inhalers

The configuration of a typical MDI delivery system is shown in Fig.51. It essentially comprises four separate components. These are (a) the base formulation (drug, excipient, propellants, etc.), (b) the container, (c) the metering valve, and (d) the actuator (or mouthpiece). All of these are interrelated, and they each have a bearing on the overall performance of the delivery system. Each of these components in turn will be introduced by describing features that are commonly found in marketed MDI products.

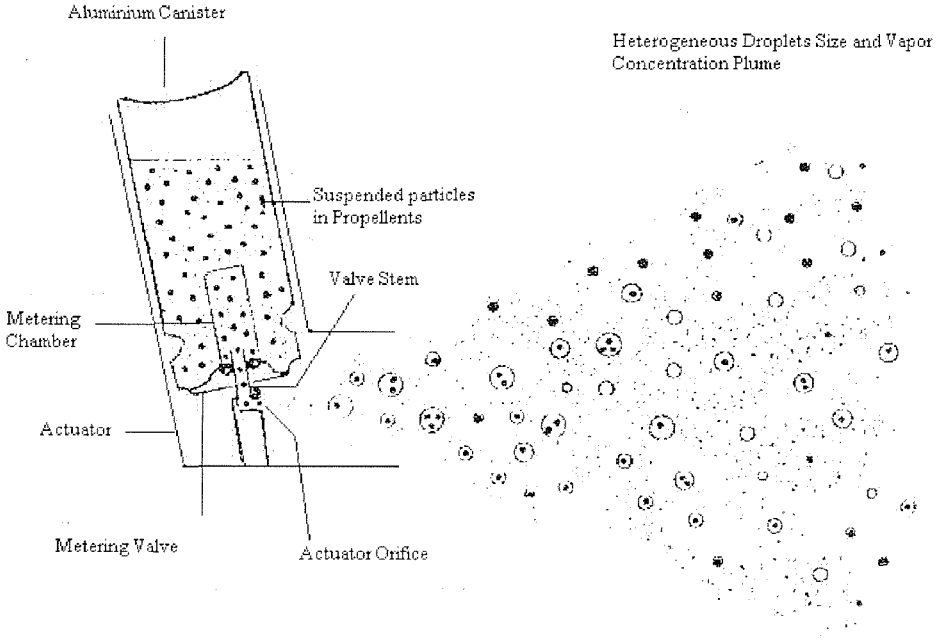

Fig.51 Schematic diagram of the components of an metered dose inhaler and droplet dispersion

Formulation components

There are two types of pMDI formulations: suspension formulations, in which microparticulate drug (invariably, the bulk material needs to be ball milled or micronized) is dispersed in a combination of volatile propellants; and solution formulations, in which the drug freely dissolves in either the volatile propellant or a combination of propellant and an acceptable cosolvent, typically ethanol [96].

Both of these types of formulations have inherent advantages and disadvantages. Suspension formulations are the more common dosage form because they have a much wider applicability. That is, there are only a limited number of drugs that are freely soluble in propellant and cosolvent mixtures.

Typical containers

There are essentially two types of containers that are currently used for MDI products. These are either glass products, which are typically laminated or plastic coated so that they can withstand high pressures, and aluminium products. The latter are generally preferred because they are lighter, nonfragile, and impervious to light. However, in some cases, the inert nature of glass containers makes them a more suitable choice for use in solution formulations. These containers are sufficiently robust to withstand internal pressures of up to 150 psig without deformation. Aluminum containers for use in MDI products are typically in the range of 15 to 30 ml in capacity, with a neck diameter of 20 mm.

Metering valves

The metering valve in an MDI is the critical component in the design of an effective delivery system. The main function of the metering valve is to reproducibly deliver a portion of the liquid phase of the formulation in which the medication is either dissolved or dispersed. The valve also forms the seal atop of the canister to prevent loss of the pressurised contents. The valves generally comprise at least seven components that are constructed from a variety of inert materials. Typical materials of construction are acetal or polyester for the valve body, stainless steel or acetal for the valve stem, generally, anodised aluminium for the ferrule, and butyl, nitrile, or neoprene for the elastomers used in the seals and gaskets.

The valves are essentially designed to work in the inverted (stem down) position, although, with the aid of a dip tube, they can also be used in the upright position. Depression of the valve stem allows the contents of the metering chamber to be dispensed through the orifice in the valve stem. After actuation, the metering

chamber refills from the bulk liquid formulation, once the metering chamber is sealed from the atmosphere and is ready to dispense the next dose. This is essential; otherwise, continuous spray would be achieved. Typical volumes that are dispensed range from 25 to 100 µl.

Actuator

The actuator (or mouthpiece) of an MDI is generally constructed from a range of polyethylene or polypropylene [97] materials by injection-moulding techniques. The actuator is the means by which the valve stem in the metering chamber is depressed, and patients, by cupping their lips around the squat end, inhale the dose. The aerosol cloud generated after the depression of the valve stem is dependent on the vapour pressure of the formulation, the geometric size of the active drug if the

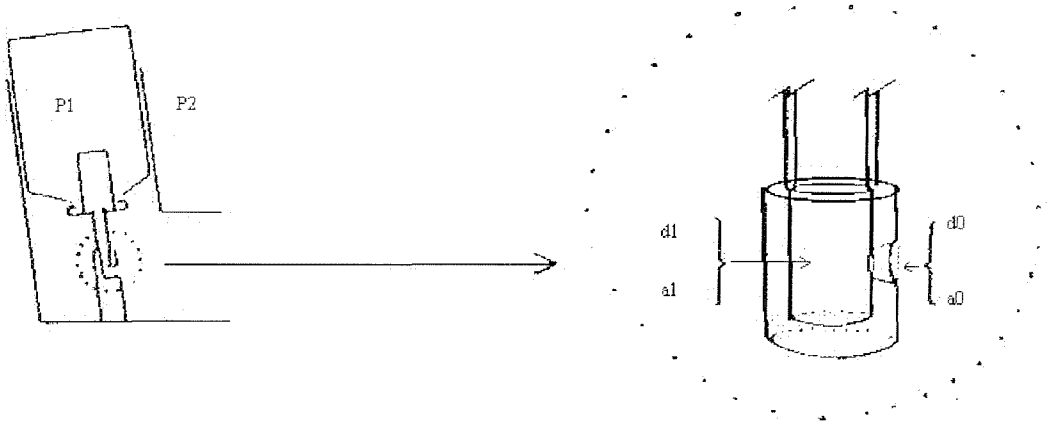

Fig. 52 Schematic diagram of actuator orifice indicating dimensions required to calculate performance characteristics. P_1 and P_2 are canister and atmospheric pressure; d_1, a_2 and d_0, a_0 are expansion chamber and orifice diameter, and areas, respectively.

product is a suspension formulation, the volume of the metering chamber, and, critically, on the diameter of the jet orifice in the mouthpiece. The diameter of this orifice also controls the rate of spray formation. The dead space between the actuator orifice and the metering chamber act as an expansion chamber in which the propellant forms a mixture of liquid and vapour phases before exiting. The orifice geometry and dimension will have an effect on the droplet formation,

therefore an effect on the charge produced on the droplets. Functionally, the orifice of the actuator consists of the "sump," a small region beneath the valve stem in which expansion occurs, and the orifice through which the mixed vapour/liquid phase is emitted, as shown in Fig.52. The dimensions of the expansion chamber and orifice have a significant effect on the output from a metered dose inhaler. Consequently a significant effect on drop charges would be expected.

6.2.2 Factors Affecting MDI Aerosols

6.2.2.1 Particle Size

The *'size'* of droplets in a monodisperse aerosol is completely characterized by a single parameter, the particle diameter. Most aerosols, however, have polydisperse size distributions. It is necessary to accurately characterize these size distributions by statistical means. The 'mass median diameter (MMD)' of an aerosol is defined as the diameter above which 50% of the total aerosol particle mass resides. The MMD may be used as an index to characterize the behaviour of the entire size distribution of an aerosol, Task Group on Lung Dynamics, 1966 [98].

In order to be clinically viable, an aerosol must contain enough fine particles to reach the smaller airways of the lung. If the aerosol has an MDD > 8 μm, a significant amount of drug can be wasted by deposition in the mouth, Lippmann [99]. Further the site of drug deposition within the lung is dependent on the size of the particles being inhaled, Hashish, 1988 [100].

It is quite clear, therefore, that the therapeutic effect of a drug delivered by a MDI device is highly dependent on particle size and that the majority of droplets should be of diameter < 5μm to allow adequate penetration into the airway.

6.2.2.2 Propellant vapour pressure

Because the driving force of a MDI device is the propellant pressure inside the can, the propellant vapour pressure plays a dominant role in aerosol properties

generated by a MDI device. The MMD of aerosol produced using a MDI is dependent on the vapour pressure of the propellant since this determines the energy with which the particles are pushed out of the nozzle of the inhaler. The fall in MMD with high driven pressure is due to the increasing force with which the liquid is disrupted and also due to the high speed of evaporation of the propellant.

6.2.2.3 Nozzle Size

The performance of any given type of atomizer depends on its size and geometry and on the physical properties of the dispersed phase (i.e., the liquid being atomized) and the continuous phase (i.e., the gaseous medium into which the droplets are discharged).

For plain-orifice pressure nozzle (such as MDI devices), the dimension most important for atomisation is the diameter of the final discharge orifice. Theory predicts, and experiment confirms, that mean drop size is roughly proportional to the square root of the liquid jet diameter. Thus, provided the other key parameters that affect atomisation are maintained constant, an increase in atomizer scale (size) will impair atomisation, Lefebvre, 1989 [99].

6.2.2.4 Electrical Charge

According to Vincent et al., 1983 [102], all natural and generated aerosol particles are electrically charged. It follows that the droplets and particles in pharmaceutical aerosols are charged. Such charge may play a significant part in aerosol dynamic behaviour and deposition.

6.2.3 Charging Mechanisms

Although it is well known that Liquid droplets and solid particles generated by MDI devices are inherently charged, to date no completely satisfactory quantitative spray charging model has been formulated.

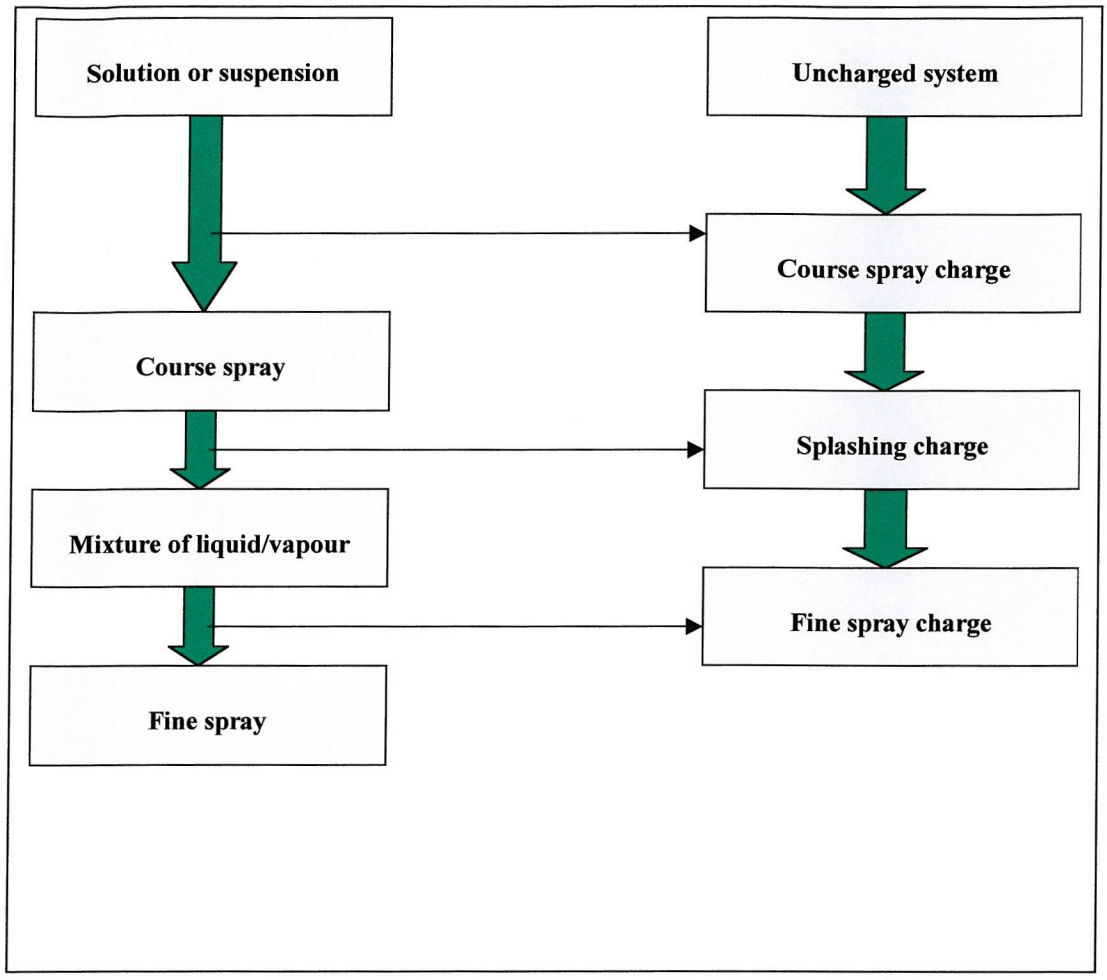

Fig.53 Spray formation and charging processes

Based on the results and understanding of charging mechanisms obtained on drop break-up from the tip of a needle, jet break-up into small droplets, big drops splashing against solid to form small droplets and also the operation principles of a pMDI device, a charging model of a pMDI device is proposed as shown in Fig.53.

6.2.3.1 Spray forming processes

When a pMDI device is actuated by pressing down the valve, the drug solution or suspension is pushed through the valve stem under the propellant vapour pressure. A coarse spray (or a jet) is formed; the formed coarse spray with high kinetic energy splashes against the inner wall of the expansion chamber as shown in Fig52. A mixture of liquid and vapour phases is generated; the mixture of

liquid/vapour phases is emitted from the small orifice of the actuator. A fine spray cloud is finally produced by the pMDI device.

6.2.3.2 Spray charging processes

The spray charging processes are closely related to their forming processes as shown in Fig.53 Before the MDI device is actuated, the device is electrically uncharged. As the MDI device is actuated, the charge separation processes take place. When the drug solution or suspension is pushing its way through the valve stem, an electrokinetic charging process takes place making the solution or suspension carries electrical charge of one sign and the can carries one of the other. After emitting from the valve stem, the formed coarse spray splashes against the inner wall of expansion chamber with its original charge produced by going through the valve stem. During the splashing process, another charging separation process occurs-splashing charging as called by Gill and Alfrey in 1952. This process alone also makes the liquid/vapour phases carries electrical charge of one sign, the actuator itself carries electrical charge of the other. When the mixture of liquid/vapour or liquid/vapour/solid squeezes through the orifice of the actuator' mouth piece, a final electrical charge separation process takes place, which itself makes the final fine spray cloud to carry electrical charge of one sign and the actuator carries charge of the other sign. Therefore the final charge on the whole fine cloud emitted from actuator is determined basically by three processes as described above: *coarse spray charging, splashing charging and fine spray charging*.

In this thesis, the three charging processes are investigated separately under three different systems: aqueous system, non-aqueous system and real MDI system.

PART I COARSE SPRAY

6.3 Measurements

6.3.1 Electrical Charge Measurement

6.3.1.1 Introduction and Objectives

Many types of clinical MDIs are presently in use. However, there is little information available regarding MDI output characteristics, especially in relation to the magnitude and nature of any electrostatic charge that might be present on the aerosol particles.

Whenever aerosols are generated, aerosol particles are electrostatically charged. Whether an aerosol consists of droplets all having the same polarity of charge or both polarities depends upon the aerosol generation device. Many aerosols are bi-polar in nature, i.e., both positively and negatively charged particles are present. The particle charging mechanisms that occur during atomisation are not fully understood to date, which is the reason for starting this study. Some aerosols are found to consist of approximately equal numbers of positively and negatively charged particles having a Gaussian charge distribution [103]. However, some are found to carry a net electrical charge [104]. The level of charge on such aerosol particles is likely to play a part in their deposition within the respiratory tract on the one hand; also to contribute to the dose loss due to drug particle deposition onto the inner wall of mouthpiece on the other hand.

In practice, many atomisation processes produce charged spray with varying charge levels on droplets. Often, the level of charge is found to increase considerably as the energy of the atomisation process is increased. Very fine droplets are required for therapeutic aerosols and so fairly energetic atomisation processes are used for this purpose.

The objectives of this study are to assess and compare the electrostatic characteristics of aerosols produced using the spray system as shown in Fig.54 with aqueous solutions, model propellant, pure HFAs and real MDI devices propelled by HFA 134a and HFA227ea.

The effect of (1) different concentration of electrolyte solutions and (2) different pressures inside cans were also studied.

6.3.1.2. Methods

6.3.1.2.A Coarse spray system with aqueous solutions, model propellant and pure propellants HFA134a and HFA227ea

Two big cans of 100 ml capacity were modified so that different solutions can be filled in and also the inside pressure can be controlled by a nitrogen cylinder. A screen can was purposely made up to actuate the big cans. The screen can was made such that the aluminium plate inside the screen can only depresses the valve stem to actuate it but not to blur the output electrical characters of the aerosols.

In use, the big can was put upside down inside the screen can and was actuated by pushing down the rod, which can be seen from Fig. 54. When it was actuated, a coarse spray came out from the bottom of the screen can. The sprays for aqueous solutions were collected by a Faraday pail which was connected to a Keithley electrometer and the big can was also connected to a Keithley electrometer. Therefore, the charges on the sprays and cans were measured by the Keithley electrometers at the same time. Model propellant HPFP was also investigated using the same spray system as with aqueous solutions. However, only the charge left on the can was examined. The reason for this is the difficulty to capture the whole spray aerosols due to its high volatility. For the same reason only the charge left on the can was measured with pure propellant HFA134a and HFA227ea. However, the pure propellant HFA134a and HFA227ea were filled in the similar cans in AstraZeneca because of the experimental difficulty to handle with their high volatilities. The coarse spray for HFA134a and HFA227ea were produced by using the same spray system but with the pre-filled cans prepared at AstraZeneca.

6.3.1.2.B Coarse spray system with Formoterol pMDI devices with both HFA134a and HFA227ea formulations

Two real pMDI devices were prepared by AstraZeneca. The devices consisted of Formoterol drugs and have HFA134a and HFA227ea as propellants respectively. It was the aim of this work to characterize the electrostatic properties of aerosols generated from the same drug Formoterol with two different HFA based formulations supplied by AstraZeneca.

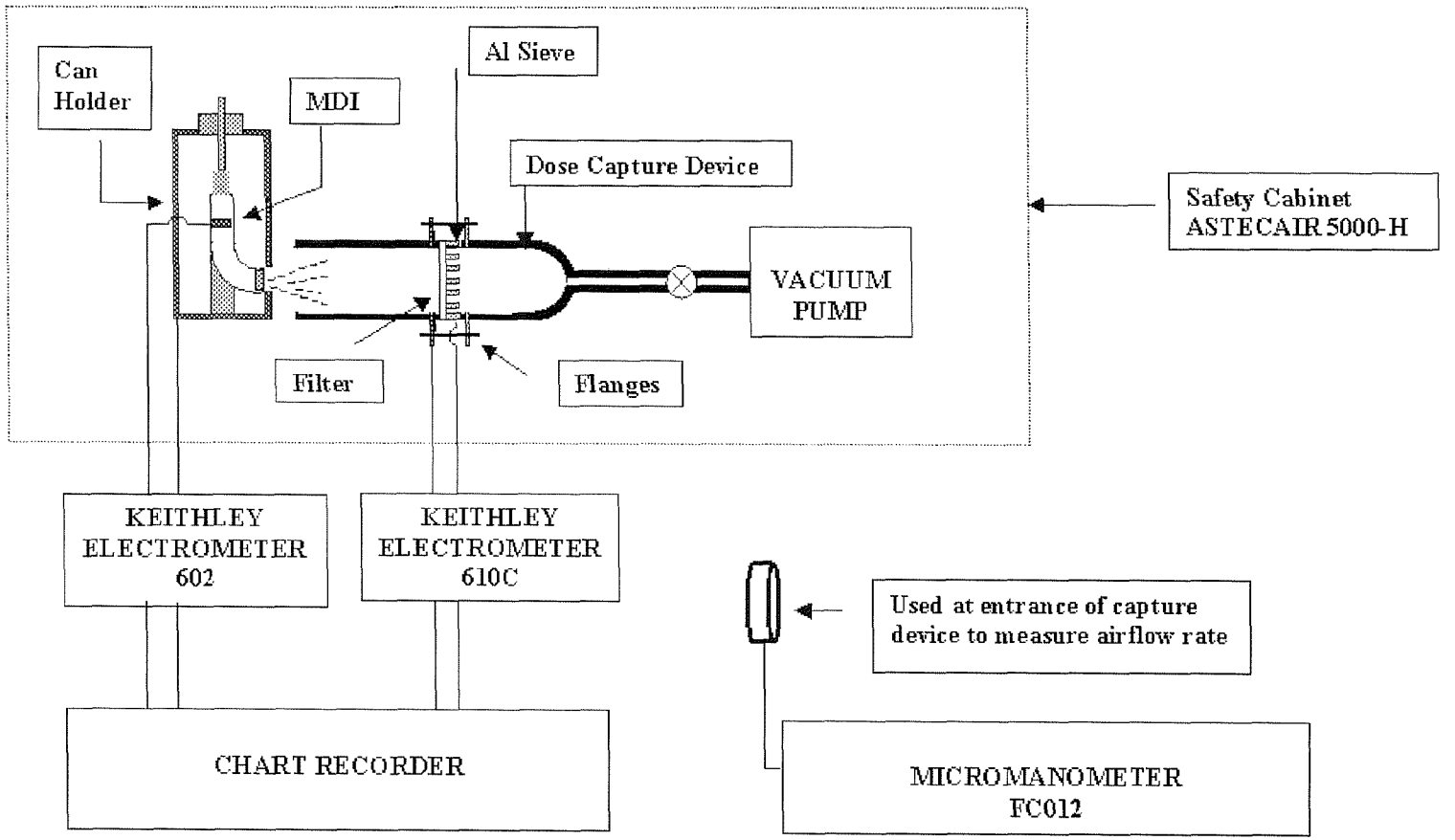

Fig.54 Diagram of spray setup

As shown in Fig.54, a dose capture device (supplied by AstraZeneca) was modified to measure the charge on aerosols produced by pMDIs. A probe connected to a Model 610c Keithley Electrometer was inserted into aluminum sieve, upon which was a filter (GF/A, Diameter 70 mm). A vacuum pump was used to draw air through the capture device at the required constant flow rate of 80 l/min. A purpose built can holder was connected to another Keithley Electrometer (Model 602). Both electrometers were connected to a two-channel chart recorder (JJ Instruments, CR600).

A micromanometer was mounted at the entrance of the dose capture device to measure the flow rate prior to dose measurement.

When the aerosol was produced from MDIs, the drug particles were drawn onto the surface of the filter paper, which was attached to the Aluminum sieve. The charges accumulated on the filter paper and cans were measured by two Keithley electrometers at the same time and recorded on the chart recorder paper as two steps. Throughout this work, the red pen channel recorded the charge on clouds; the black pen channel recorded the charge on cans. The right side steps on the chart recorder paper are negative, the left side steps are positive.
All samples were shaken for 10s and then measured. 6 puffs were measured for each sample.

6.3.1.2. Theory

The methods adopted in the coarse spray charge measurement are based on a single principle. That is the electrostatic charge carried by aerosols emitted from MDIs should be equal in magnitude and opposite in sign to that of the cans. Therefore the charge on aerosols and cans was measured at the same time as a method to double-check the data. So for situations at which the spray aerosols are difficult to catch such as with pure HFA134a, HFA227ea and model propellant HPFP, charges on the cans are examined only. Therefore it can be said that charges on the spray aerosols are the same in magnitude but opposite in sign. All graphs shown in this chapter are charge densities on aerosols calculated upon this principle.

6.3.1.3. Experimental results and discussion

6.3.1.3.A Charge on coarse spray aerosols produced by distilled water system

The aerosols generated using distilled water system were invariably charged and were always negative. The level of the electrostatic charge was increased as the flow rate increased as shown in Fig.55.

This can be explained in terms of contact potential between distilled water and the inner wall of the valve stem. According to the theory introduced in Chapter three, there is a contact potential between the distilled water and the inner wall of the valve stem. From the result that the distilled water spray aerosols are negative charged, we can infer that the inner wall of the valve stem is positive charged and on the water side the water is negative charged. As water flows in such high flow rate inside valve stem, electrokinetic charge takes place. Therefore as flow rate increases, charge density carried by flowing water increases.

6.3.1.3.B Charge on coarse spray aerosols produced by electrolyte solutions

6.3.1.3.B.a Effect of electrolyte concentration on charge of coarse spray aerosols

Experiments were carried out to examine the effect of the addition of electrolytes had on the aerosol charges of coarse sprays. Concentrations from 10^{-6} M to 2 M of sodium chloride and potassium chloride were used. The charges on coarse aerosols produced by these electrolyte solutions were measured. The charge density curves were plotted for different concentrations at different flow rates (or pressures inside the can). Fig.56 shows the charge density against different concentrations of potassium chloride at gas pressures of 3.9 bar and 5.72 bar. The pressures chosen to show in this graph are the vapour pressures of HFA227ea and HFA134a, which are the pressures operating in real HFA formulation MDI devices. These pressures were chosen such that the charge levels could be compared with those charge levels produced by HFA formulation MDIs under similar operating conditions.

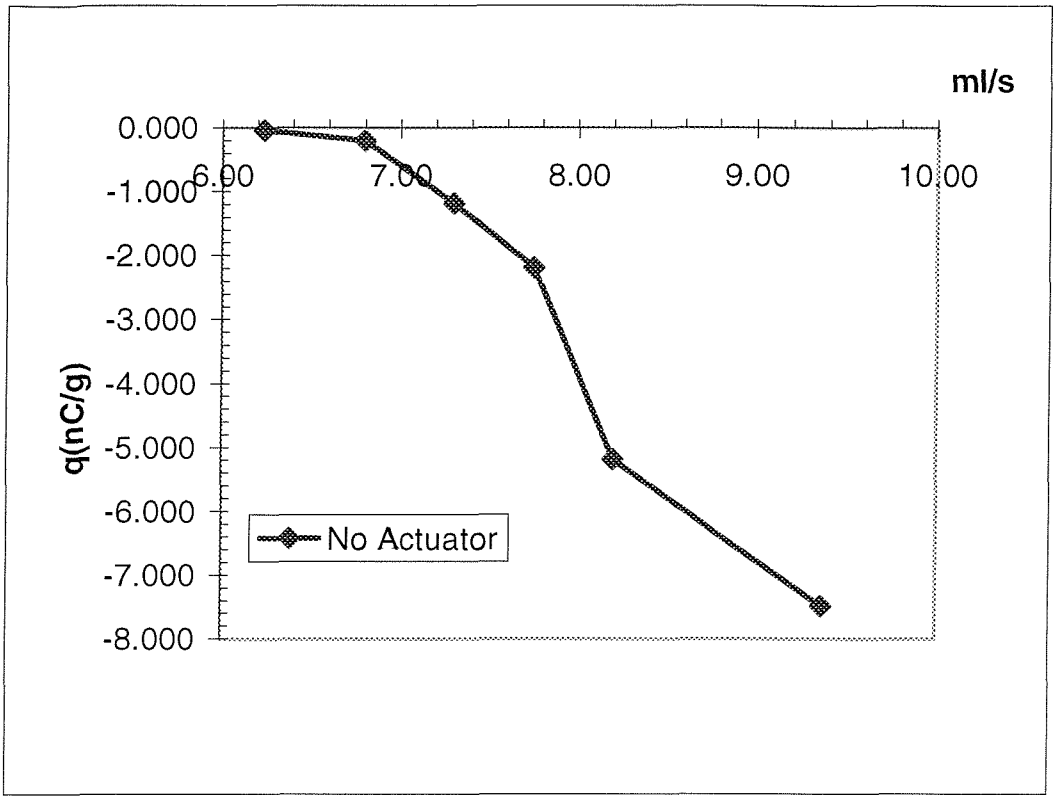

Fig.55 Charge density vs flow rate for distilled water without an actuator*

It can be seen from the graph that the droplets of the aerosols produced by potassium chloride solution carry negative charge at dilute conditions (in these two situations concentration ~ c < 0.01 M) while positive charge is carried by droplet aerosol when concentration increases (c > 0.01 M). On the whole, the droplet aerosol generated by potassium chloride solution is negatively charged at dilute concentrations. As the concentration increases the magnitude of the negative charge of the aerosol decreases until a zero charge point is reached at concentration ~0.01 M; then the charge of aerosol changes its polarity to positive and the magnitude of the aerosol charge increases as the concentration increases.

** No actuator means a specially made actuation system was employed so that the actuation system did not blur spray-charging processes*

The results can be explained in terms of zeta potential formed at the interface between the liquid and the inner wall of the valve stem based on the theory introduced in Chapter Three. From **Section 6.3.1.3.A**, we know that the contact potential at the interface between water and the valve stem is positive at the solid surface and negative inside the water. This means the zeta potential is positive in this case. According to the theory from Chapter Three, we know that zeta potential decreases at dilute concentration of aqueous solution as concentration increases until zeta potential decreases to zero. This corresponds to the magnitude of charge density of aerosol decreasing to zero. After this point, the double layer at the interface of the liquid and inner surface of the valve stem collapses and zeta potential changes its sign. As the concentration continues to increase, the zeta potential increases. Therefore, the charge on the aerosol also changes its sign after zero charge point (ZCP) and the charge density increases as the concentration of the solution continues to increase.

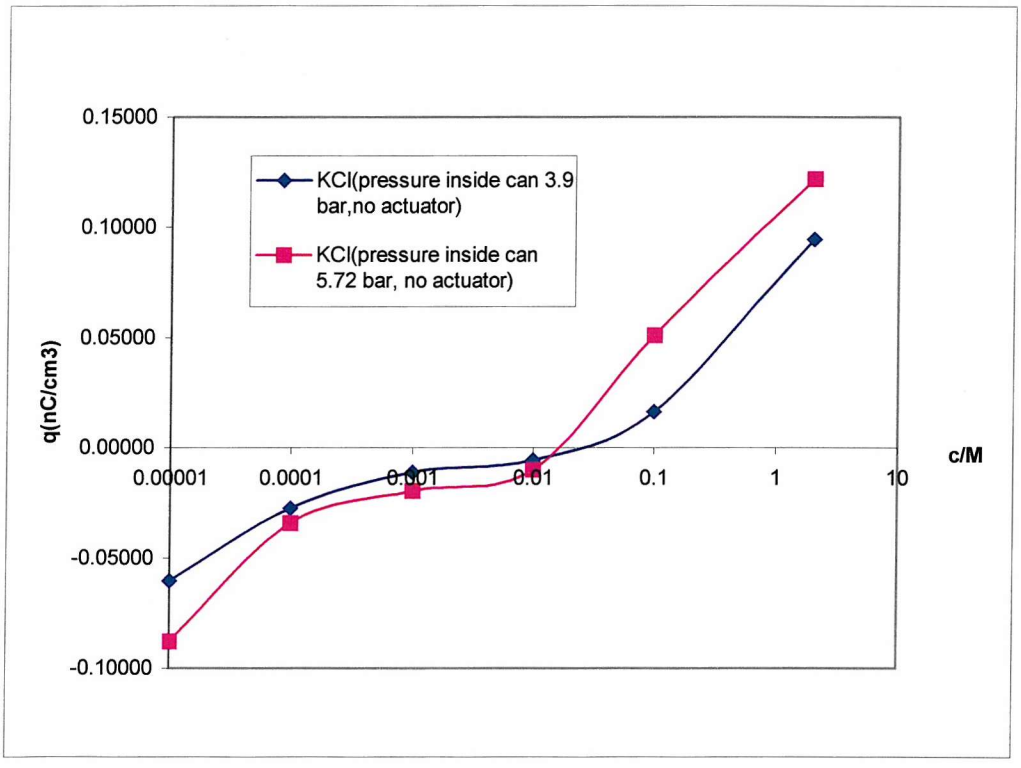

Fig.56 Charge density vs concentration for KCl solutions without actuators

6.3.1.3.B.b Effect of flow rates of electrolyte solutions on charge of coarse spray aerosols

The effect of flow rate (or pressure inside the can) of electrolyte solutions was investigated with potassium chloride. It was found the charge densities on the aerosols at all examined concentrations produced by potassium chloride increase as the flow rate increases, as shown in Fig.57.

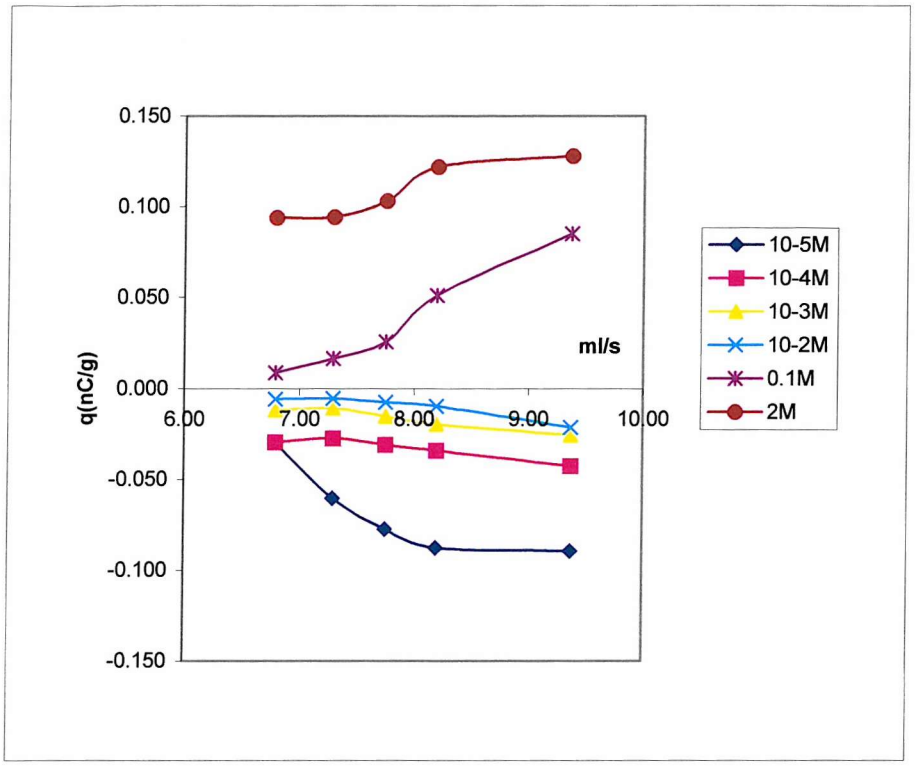

Fig.57 Charge density vs flow rate of KCl solutions without actuators

This result can also be interpreted in terms of double layer formed at the interface between liquid and inner wall of the valve stem.

As pointed out in Chapter Three, the charge density of the double layer at the solution side drops off as it goes into the inside of the solution far away from the interface. In other words, the nearer the liquid to the interface, the larger is the

charge density. Therefore, as flow rate increases, the liquid flow becomes more turbulent, which sweeps closer to the interface so that more liquid with larger charge density is carried with the liquid. This makes the charge density on the liquid aerosol increase as the flow rate increases.

6.3.1.3.C Charge on coarse spray aerosols produced by Model propellant HPFP

The electrostatic charge on Model propellant HPFP was measured at different flow rates. The charge density of the aerosol generated by HPFP is plotted against different flow rates, as can be seen in Fig. 58.

It was found that the charge on the aerosol produced by HPFP was also negative, which means the zeta potential at the interface between HPFP and the inner wall of the valve stem is also positive. However, the charge density on the aerosol produce by HPFP is larger than that by distilled water. It can be seen by comparing Fig.58 with Fig.55 that, at flow rate 7.5 ml/s, the magnitude of the charge density on the aerosol produced by HPFP is 7 times that generated by distilled water at the same flow rate.

From the results obtained in Chapter three, the zeta potential for pure HPFP (17mV) is much larger than that for distilled water (12.5mV). Therefore, it is expected that the charge density produced by HPFP at the same flow rate is greater than that generated by distilled water.

6.3.1.3.D Charge on coarse spray aerosols produced by pure propellant HFA134a and HFA227ea

The charge densities on aerosols generated by pure HFA propellants HFA134a and HFA227ea were examined and the results are shown in Table 4.

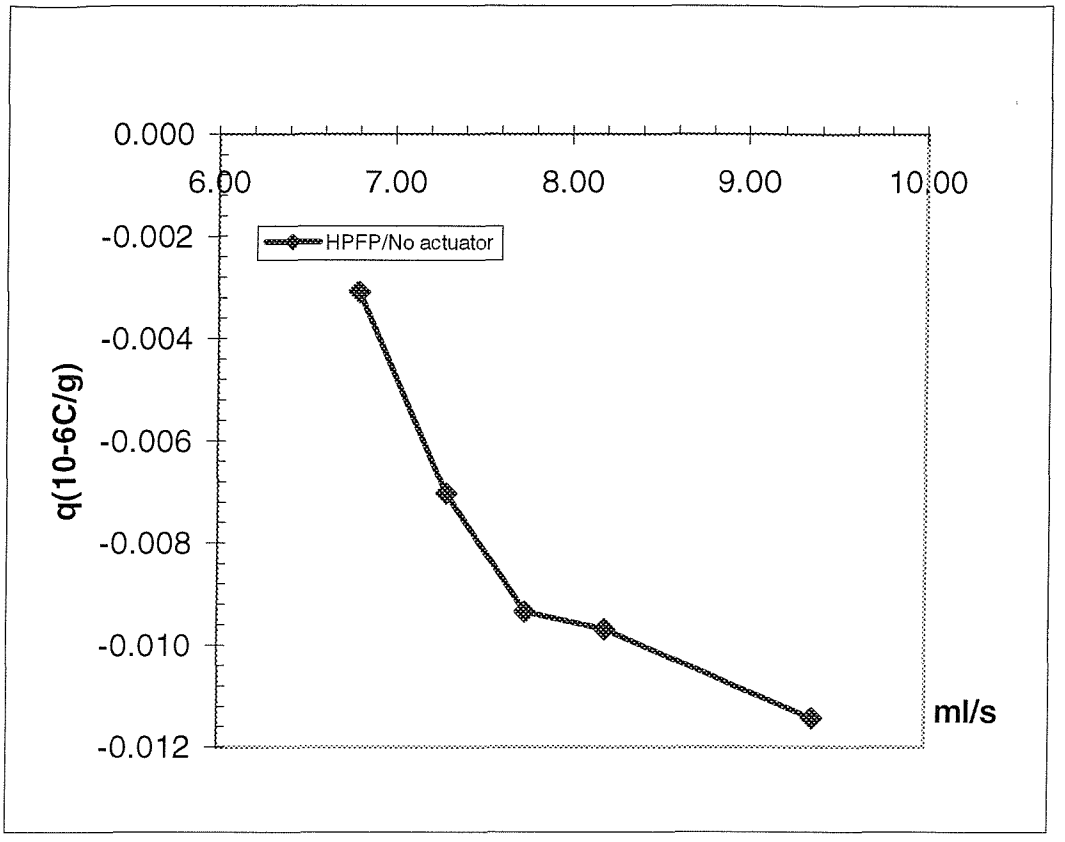

Fig.58 Charge density vs flow rate for HPFP

Table.4 Charge density on the aerosols produced by pure propellants HFA134a and HFA227ea

	HFA134a	HFA227ea	HPFP	HPFP
P(Bar)	5.7	3.9	5.7	3.9
Q(μC/g)	-0.732	-0.019	-0.01	-0.007

From the data shown in Table.4, it can be seen that the charge density on aerosols produced by pure HFA propellants HFA 134a and HFA227ea is also negative. The charge level for HFA134a is much larger than that for HFA227ea. The magnitude of the charge density for HFA134a is over 38 times greater than that for HFA227ea.

This result could be interpreted in terms of vapour pressure. By comparing the vapour pressures of HFA134a and HFA227ea, it can be seen that the vapour

pressure for HFA134a (5.7 bar) is one and half times bigger than the vapour pressure for HFA227ea(3.9 bar). As we know that at same zeta potential, increasing flow rate will increase the charge density carried by aerosols. However, it seems the dramatic difference between the charge density of HFA134a and HFA227ea could not totally be contributed by the flow rate difference alone. The dramatically high charge density on aerosols generated by HFA134a might also be due to the larger contact potential between HFA134a and the inner wall of the valve stem. This cannot be verified due to experimental difficulties.

From the Table, we also can see that at the respective same pressures the charge densities on HPFP are less than those on HFA134a and HFA227ea respectively. These results also imply that the contact potential between HPFP and the inner wall of the valve stem is smaller than those between HFA134a, HFA227ea and the inner wall of the valve stem.

6.3.1.3.E Charge on coarse spray aerosols produced by Formoterol formulation MDIs with propellant HFA134a and HFA227ea

The charge on every puff for each device was examined and the mass of each puff was measured. Then the charge to mass ratio for each MDI product was calculated and shown in the following Table5.

In order to compare the charge to mass ratios with or without Formeterol, pure propellants HFA134a and HFA227ea were prepared in the same way as the two products (P5548 stands for Formeterol formulation with HFA227ea and PS157/9 stands for Formeterol formulation with HFA134a; where P5548 and PS157/9 are the Batches of the devices).

From Table 5, it can be seen that all the products have the same valve material PBT and the same storage condition.

All the aerosols produced by the four products are negatively charged. Before the drug Formoterol was put in, the aerosols produced by pure HFA134a and

HFA227ea are negatively charged and the charge level of aerosol produced by HFA134a is greater than that produced by HFA227ea. After drug Formoterol was

Table.5 Charge to mass ratio on the aerosols

Description	**Batch**	**Charge /Mass (nC/g)**	**Sample Details**	**Storage Condition**
Formoterol pMDI 4.5 μg	P5548	-4.83	PBT valve, HFA227ea	Initial
	PS157/9	-5.49	PBT valve, HFA134a	Initial
	HFA227ea	-2.17	PBT valve	Initial
	HFA134a	-4.23	PBT valve	Initial

put in, the charges on aerosols produced by both HFA227ea and HFA134a formulations are still negative and the charge magnitude for HFA134a formulation is larger than that for HFA227ea formulation. However, the charge level for products of both HFA134a and HFA227ea formulations are higher than that for pure HFA propellants. It seems drug itself has dominant influence on aerosol charges.

PART II FINE SPRAY

6.4 Measurements

6.4.1 Electrical Charge Measurement

6.4.1.1 Introduction and Objectives

Only droplet size less than ~5 μm and greater than ~1 μm particles will contribute to the deposition fraction in the lungs of the particles produced by pMDIs[7][8]. As seen from the last section, the aerosols produced from the valve stems of cans give relatively large size distribution. Therefore, in order to give fine size distribution, an actuator usually is utilized in practice. The structure and operation principles have been described in last section.

In this section, we investigated that the electrostatic characteristics of aerosols generated using actuators of different materials as shown in Fig.54 with aqueous solutions, model propellant, pure HFA134a and HFA227ea and two real MDI devices, examined in last section at conditions without actuators. Comparison is made between with and without actuators in aspects of size distribution, electrostatic characteristics and the effect of size distribution on electrostatic characteristics.

All the effects of electrolyte concentrations and pressure inside the can on electrostatic characteristics under the condition with actuators are also investigated. Furthermore, the effect of actuator material is examined in this section.

6.4.1.2 Methods

6.4.1.2.A Fine spray system with aqueous solutions, model propellant, HFA134a and HFA227ea

The same large cans used in the previous section were used in this study, but a modified screen can with typical plastic actuator was used to produce fine spray aerosols as shown in Fig.54. The operation procedures were the same as previous section.

6.4.1.2.B Fine spray system with Formoterol pMDI devices of both HFA134a and HFA227ea formulations

The same drug cans containing Formoterol of both HFA134a and HFA227ea formulations used in last section were used in this section, but the size distribution and electrical characteristics were examined with a plastic actuator. The electrostatic charge of Formoterol HFA227ea formulation was measured with both aluminium and plastic actuators. The results were compared to give information about the effect of actuator materials on electrostatic characteristics of aerosols produced by MDIs.

6.4.1.3 Experimental results and discussion

6.4.1.3.A Charge on fine spray aerosols generated by distilled water

The aerosols generated using distilled water with plastic actuator were always charged. The charge on the aerosols produced by distilled water with plastic actuator is positive; the level of the electrostatic charge was increased as the flow rate increased as shown in Fig.59.

This might be due to the contact potential between distilled water and plastic actuator. The double layer at the interface between distilled water and plastic actuator is such that the layer in water side is positively charged while the surface of the plastic actuator is negatively charged. Therefore, the distilled water aerosols carry positive charge with it and leaves negative charge on the can.

As for the phenomenon that the charge level increases as flow rate increase, it is due to the more violent turbulent flow to sweep more charged liquid layers with higher charge densities as already discussed.

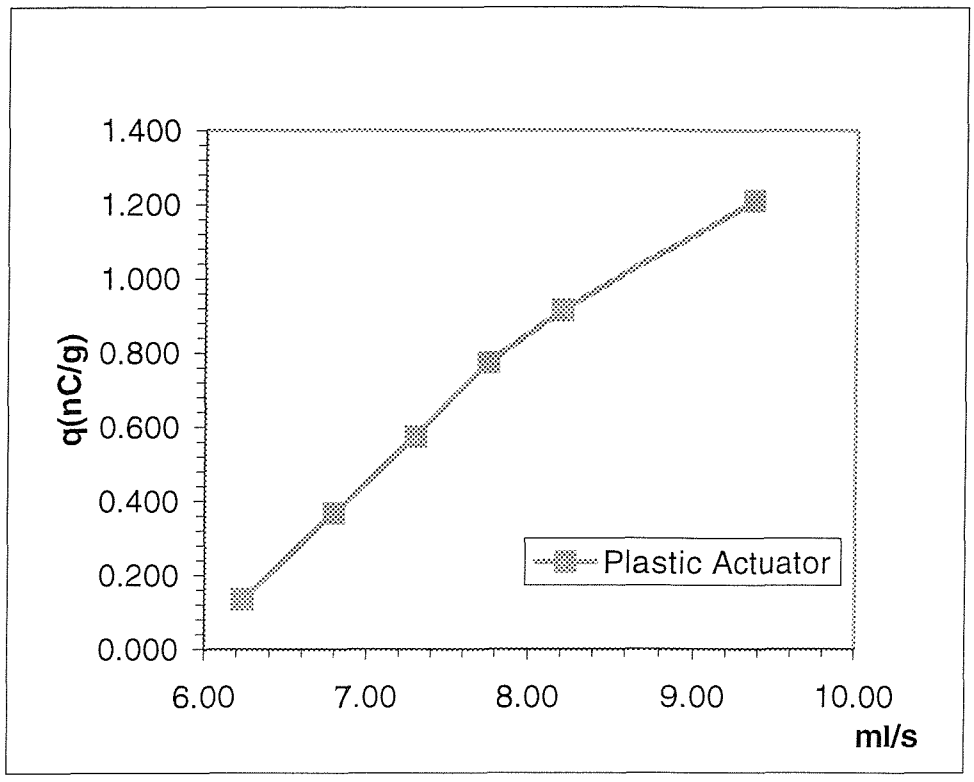

Fig.59 Charge density vs flow rate for distilled water with plastic actuator

6.4.1.3.B Charge on fine spray aerosols produced by electrolyte solutions

6.4.1.3.B.a Effect of electrolyte concentration on charge of fine spray aerosols

Experiments were carried out to examine the effect of the addition of electrolytes had on aerosol electrostatic characteristics of fine spray. Concentrations used in previous section were used here as well. Both potassium chloride and sodium chloride were investigated. The charges on the cans while fine sprays were produced were measured. The calculated aerosol charge density was plotted against different concentrations at different pressure inside cans. Fig.60 and Fig.61 showed the charge density against different concentrations of potassium chloride and sodium chloride at gas pressures of 3.9 bar and 5.72 bar. The pressures were

chosen for the same reason mentioned in previous section. They are the vapour pressures of HFA227ea and HFA134a.

It was found that the curves of charge density against concentration for KCl and NaCl have the same trend. Only KCl situation is discussed here. With different concentrations of potassium chloride by fine spray with a plastic actuator, the charge on the aerosols was first positive at dilute solutions (~ c < 0.01 M); then the charge level decreases as concentration goes up until the point of ZCP (~ c = 0.01M). After ZCP, the charge on aerosol becomes negative until reach a maximum charge point MCP (c is between 0.001 M and 0.01M) (It has to be

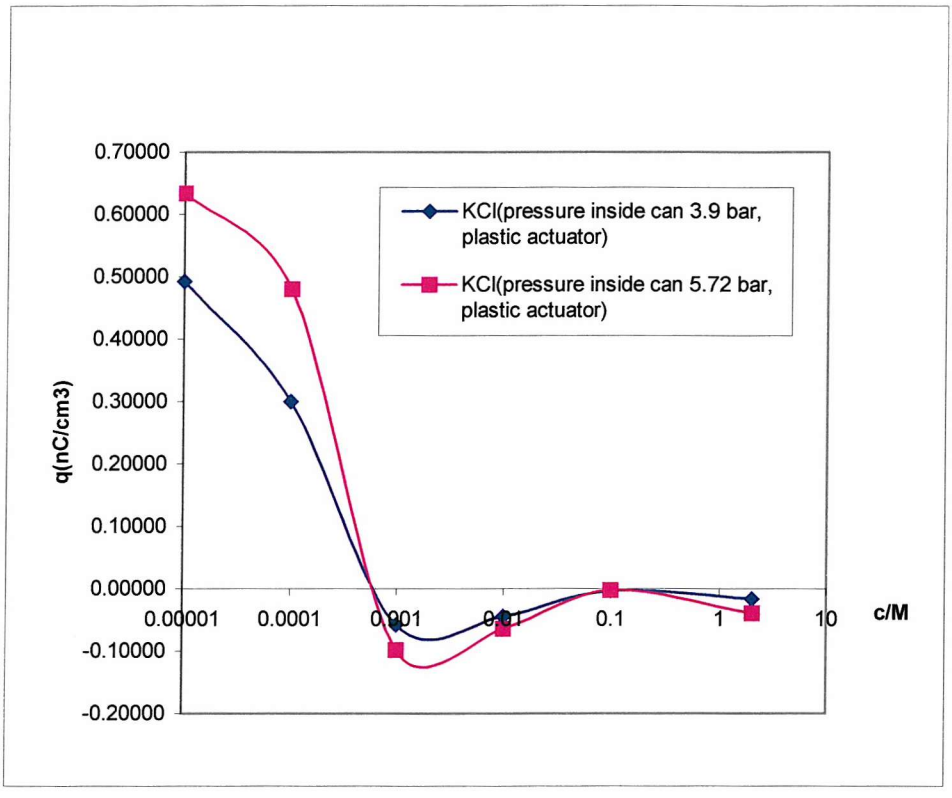

Fig.60 Charge density vs concentration for KCl solutions with plastic actuators

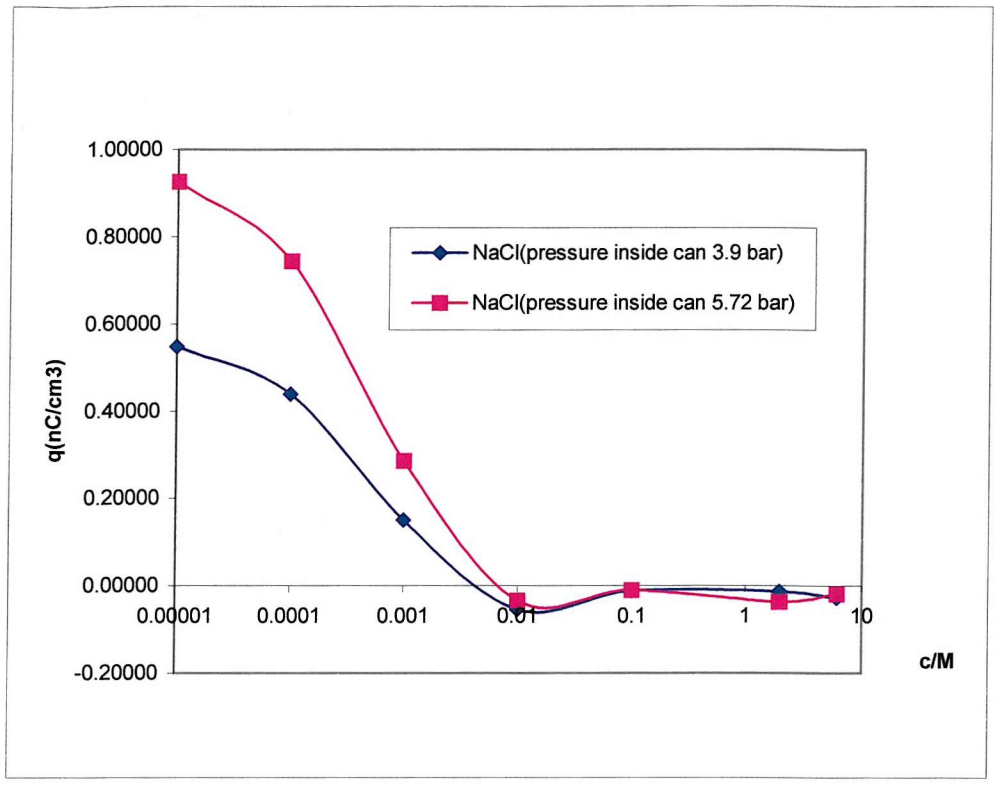

Fig.61 Charge density vs concentration for NaCl solutions with plastic actuators

pointed out that the ZCPs and MCPs for potassium chloride and sodium chloride are little different); then the charge level decrease again as concentration increases, but this time the charge does not change its polarity and only stops at another ZCP (c~0.1 M); after that the charge goes up again. It seems that the charge would go dampening with increasing concentration.

This result is very interesting in every aspect. It will be discussed in detail in next section.

6.4.1.3.B.b Effect of flow rates of electrolyte solutions on charge of fine sprays

The effect of flow rate (pressure inside a can) of electrolyte solutions on fine aerosol charge was examined with KCl and NaCl. It was found that the charge

densities on the fine aerosols at almost all concentrations increase as flow rate increases, as shown in Fig.62 and Fig.63 for both KCl and NaCl solutions.

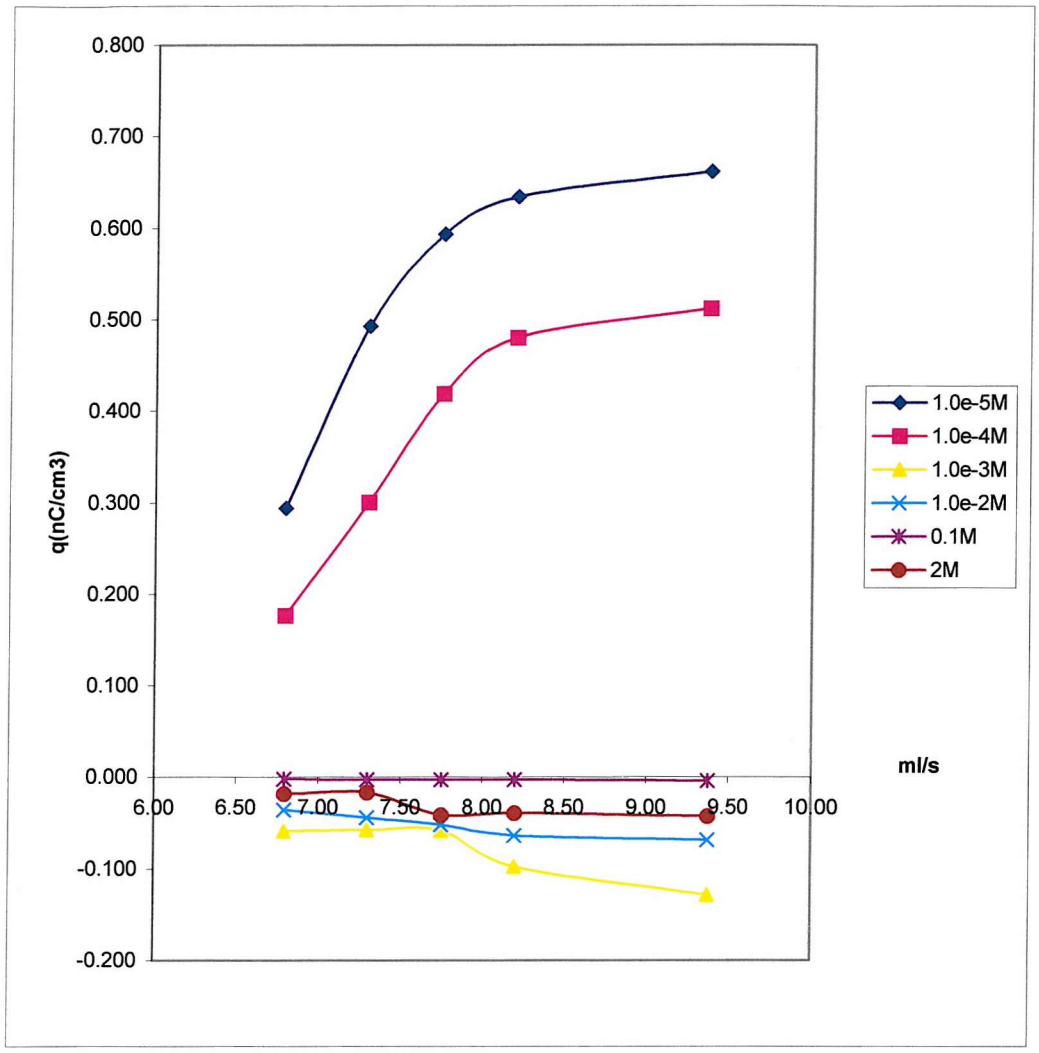

Fig.62 Charge density vs velocity flow rate for KCl solutions with plastic actuators

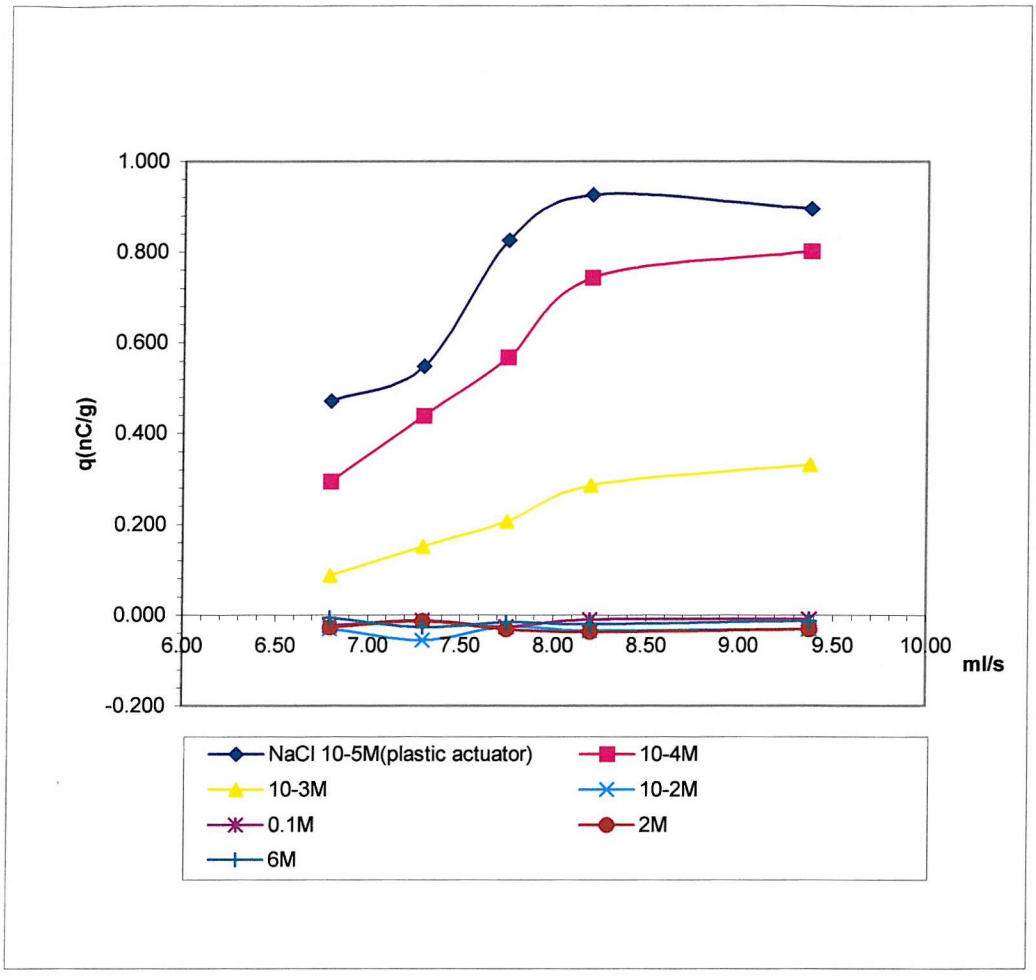

Fig.63 Charge density vs flow rate for NaCl solutions with plastic actuator

This can be explained in terms of turbulent extent. At the same concentration, zeta potential should keep constant. Therefore, at the same zeta potential, as flow rate increases the turbulent flow goes deeper inside the double layer to carry more charge with it.

However, as shown in Fig.62 and Fig.63, after the charges of aerosol change its sign, the charge density seems not to be influenced by the flow rate. This is still beyond explanation with existing theories.

6.4.1.3.C Charge on fine spray aerosols produced by Model propellant HPFP

The electrostatic charge on the can of fine spray of model propellant HPFP was measured at different flow rates. The negative charge density of fine aerosols is plotted against flow rate, as shown in Fig.64.

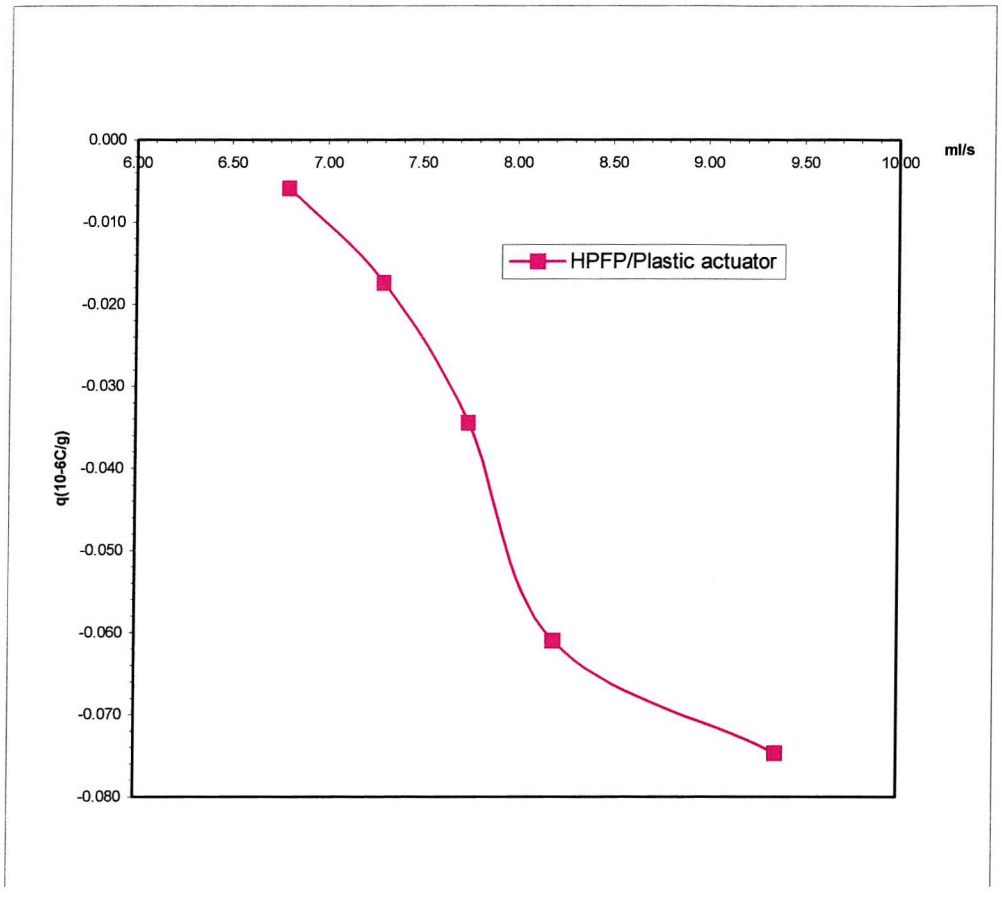

Fig.64 Charge density vs flow rate with plastic actuator

It was found that the charge on the fine aerosol produced by HPFP was negative and the charge level on the fine aerosol increases as flow rate increases as expected. The charge level is much higher than without actuators.

6.4.1.3.D Charge on fine spray aerosols produced by pure HFA134a and HFA227ea

The charges on the can generated by pure propellants HFA134a and HFA227ea were measured and the results are shown in Table 6.

Table 6 Charge density on the aerosol for HFA134a and HFA227ea with plastic actuators

	HFA134a	HFA227ea	HPFP	HPFP
P(Bar)	5.7	3.9	5.7	3.9
Q(μC/g)	-1.098	-0.034	-0.061	-0.017

From the data shown in this table, it can be seen that pure HFAs give higher charge level than HPFP at same gas pressures. The charge on the aerosols for all four cases is negative. The charge level for HFA134a is the highest, HFA227ea the second and HPFPs are the lowest. All data are greater than those without actuators.

6.4.1.3.E Charge on fine spray aerosols produced by Formoterol HFA134a and HFA227ea formulations

The charges on both cans and fine aerosols generated by Formoterol HFA134a and HFA227ea formulation devices were measured. The charge to aerosol mass ratio were calculated and shown in the following Table7. Again, pure HFAs charge to mass ratio were also shown in the table to give comparisons.

Table.7 Charge to mass ratio on the cans for fine sprays

Description	Batch	Charge /Mass (nC/g)	Sample Details	Storage Condition
Formoterol pMDI 4.5 μg	P5548	13.79	PBT valve, HFA227ea	Initial
	PS157/9	-16.48	PBT valve, HFA134a	Initial
	HFA227ea	-21.14	PBT valve	Initial
	HFA134a	-117.42	PBT valve	Initial

From the table above, it can be seen that as Formoterol was added to HFA134a, the charge level decreases dramatically while for HFA227ea it even changes the charge polarity.

These results further prove that the drug itself is the dominant factor in determining electrostatic charges on aerosols produced by MDI. It will also be interpreted in detail in the next section.

6.4.1.3.F Charge on fine spray aerosols produced by Al actuator with Formoterol HFA227ea formulation (P5548)

The effect of actuator materials on spray charges was investigated. An aluminium actuator was used to produce fine spray. Both the charges on cans and aerosols were measured using the set up described as Fig54. The results are shown in Fig.65. From the graph, it can be seen that the charge level on the can is higher than that on the aerosol cloud. This is not as expected. It is beyond our explanation at the moment. The results for Formoterol HFA227ea formulation with aluminium and plastic actuators will be discussed in next section.

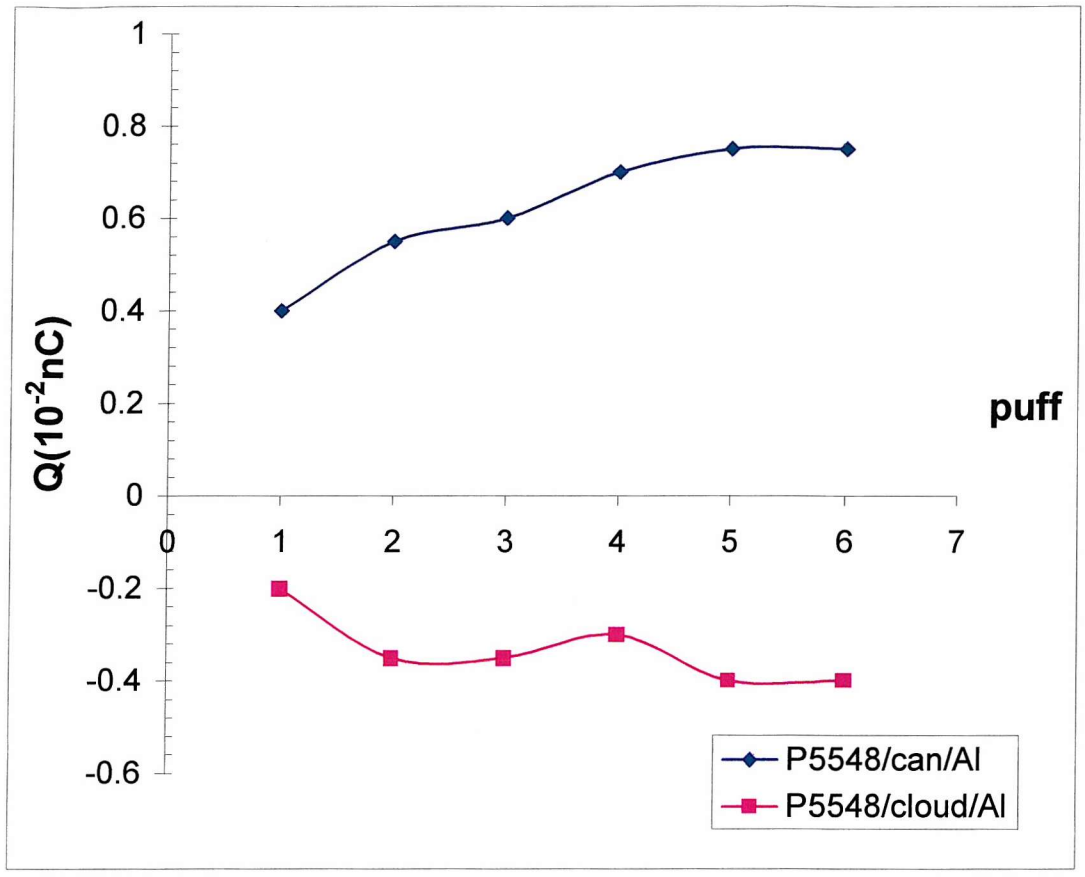

Fig.65 Charge on the can for Formoterol HFA227ea formulatio with Al actuator

6.4.2 Size Measurement

6.4.2.1 Introduction and Objectives

The therapeutic effect and electrical charge of an atomized drug cloud produced by MDI devices is highly dependent on particle size distribution. The size distribution of an aerosol may be assessed by different techniques, Bailey, 1974 [105]. The requirements for particle size analysis, in this study, were that the technique should be able to measure particle size in real time, at a position equivalent to the mouthpiece of the MDI device, and that sampling problems should be avoided. An item of equipment which fulfilled these requirements was the Malvern Particle Size Analyser, based on the technique developed by Swithenbank et al., 1977 [106].

6.4.2.1.A Malvern Particle Analyser

The Malvern Particle Size Analyser can be used to measure the size distribution of particle or droplet ensembles having diameters ranging from about 1μm to 1000μm. The technique is based on the Fraunhofer diffraction principle.

A 2 mW He/Ne laser beam (6 mm in diameter) is used as a coherent light source. A particle in the measuring volume diffracts the laser radiation by an amount which depends on particle size but which is independent of particle speed.

A spherical particle diffracts maximum energy at an angle inversely proportional to its diameter (see Fig.66 a and b). A Fourier transform lens (receiving lens) is used to focus the diffracted light pattern onto a photo-detector consisting of 30 concentric rings.

The size range may be varied by changing the focal lens of the Fourier transform lens; however, there is a lower limit of ~1μm in diameter for He/Ne laser light. This is due to the fact that the required diffraction pattern is only formed when the particle diameter is greater than the wavelength of the laser radiation (λ = 0.6328 μm). The output of the photo-detector is processed by a micro-computer which is controlled by a keyboard. The measured energy distribution is compared with a calculated energy distribution based on known models of particle size distribution (e.g. normal, log normal and Rosin-Rammier distributions or model independent) and a *'best fit'* to the model obtained by the method least squares. Calculation of the particle size distribution is performed using model independent or two-parameters software.

The apparatus is calibrated by the manufacturers (Malvern Instruments Ltd., Malvern, Worcestershire) and the computed mean diameter has an accuracy of ±4% when the total size distribution lies within the measuring range of the

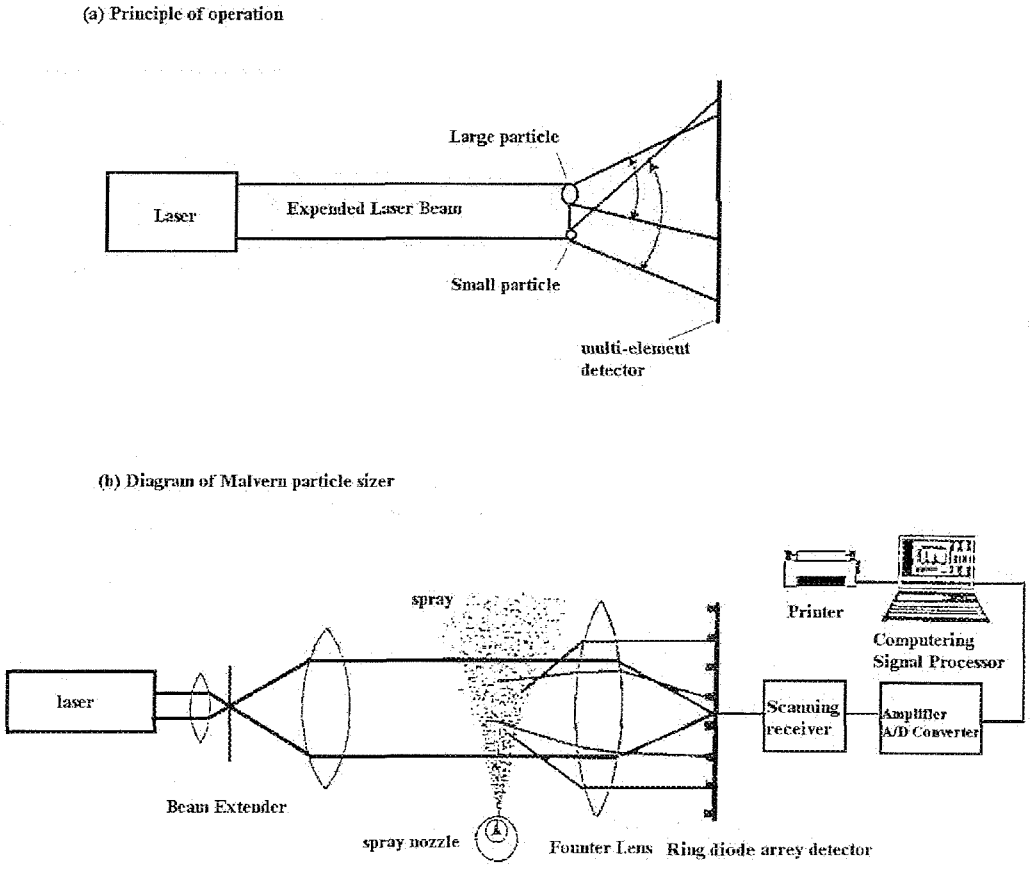

Fig.66 Malvern particle size analyser (a) Principle of operation and (b) Diagram

equipment. Automatic compensation for background particles counts is incorporated into the procedure after an initial background reading has been taken. The sampling time may be varied from a minimum of 30 msec to 50 msec, the time chosen being sufficient long to obtain a representative sample. The sample time in this study was taken as ~5 sec (equivalent 11 puffs) since the high volatility of the propellants makes it impossible to just take one puff as a sample.

The Malvern Particle Size Analyser was used to assess the effect on aerosol particle sizes of: (1) vapour pressure propellants HFA134a and HFA227ea and (2) gas pressure inside the can containing model propellant HPFP.

6.4.2.2 Methods

A Malvern Particle Size Analyser (Model 2600HSD), fitted with a 63 mm focal length lens, was used to measure aerosol droplet size distributions. The aerosol MMD and percentage volume of droplets of diameter were then calculated from the distributions. The experimental sampling time was typically 5 sec (11 puffs) and the resultant data were recorded on magnetic disc for subsequent analysis, using model independent or two-parameter software.

Clamping the spray system in a vertical position enabled the aerosol, released from the spray system, to cross the laser beam between the lens and its outer focal plane (the focal plane region is the most sensitive area for detecting drops of different sizes, Swithenbank et al., 1977 [105]). The spray system for model propellant was driven by compressed nitrogen, from a cylinder, and the pressure was regulated using a reducing valve and monitored by barometer. Nitrogen pressure was measured using a pressure gauge. The aerosol was produced into the laser beam, at a point corresponding to the mouth of the subject. HFA134a and HFA227ea were driven by their own vapour pressures.

6.4.2.3 Results and Discussion

The aerosols measured were all found to have polydisperse size distributions. The use of model independent software, to represent such distributions, is appropriate. No analytical model for the weight distribution of the sample is assumed. Instead, the software considers a set of 15 weight bands, chosen according to focal length of the receiver lens used in the measurement. Using the least squares technique, the sizer optimises 15 independent parameters and can accommodate any type of size distribution.

6.4.2.3.A Repeatability of Droplet Size Measurements

The aims of these experiments were to investigate the repeatability of MDI performance, using the same MDI under identical conditions of atomisation.

Two samples each of pure HFA134a and HFA227ea were prepared by AstraZeneca. For both HFA134a and HFA227ea, one of each was tested 6 times under identical conditions. The data are summarized in Table 8 for HFA134a and HFA227ea.

Table 8 Repeatability of drop size measurement for HFA134a and HFA227ea

Test No	HFA134a	HFA227ea
	MMD (μm)	MMD (μm)
1	3.1	3.2
2	2.9	3.3
3	3.0	3.1
4	3.1	3.2
5	3.0	3.3
6	3.1	3.1
Mean MDD	3.0	3.2

6.4.2.3.B Effect of Gas Driven Pressure and Different Vapour Pressure of Different HFAs on Droplet Size

Model propellant HPFP was driven at pressures of 2.5 bar to 7 bar while propellant HFA227ea and HFA134a were driven at their own vapour pressures. The pressure range was chosen such that vapour pressures of HFA227ea and HFA134a are included. All aerosols were generated by standard AstraZeneca plastic actuators.

The MMD's of the aerosols generated by spray systems were strongly influenced by the driving gas pressure inside the can, see Table.9. As gas pressure increases the MMD of model propellant HPFP decreases.

Table 9 MMDs of droplets of HPFP at different gas pressures

Pressure (bar)	MMD (μm)
2.5	6.8
3.9	6.3
4.5	5.9
5.7	5.6
7	4.7

The difference of vapour pressures between HFA134a and HFA227ea causes a slight difference in MMD, which can be seen in Fig.67 a & b.

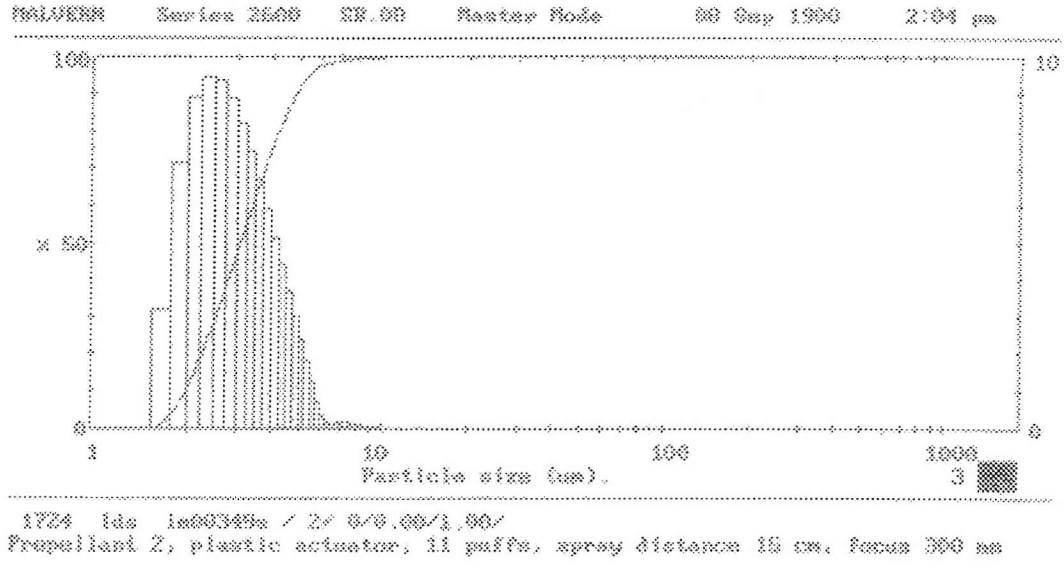

Fig.67 (a) Size distributions for HFA227ea

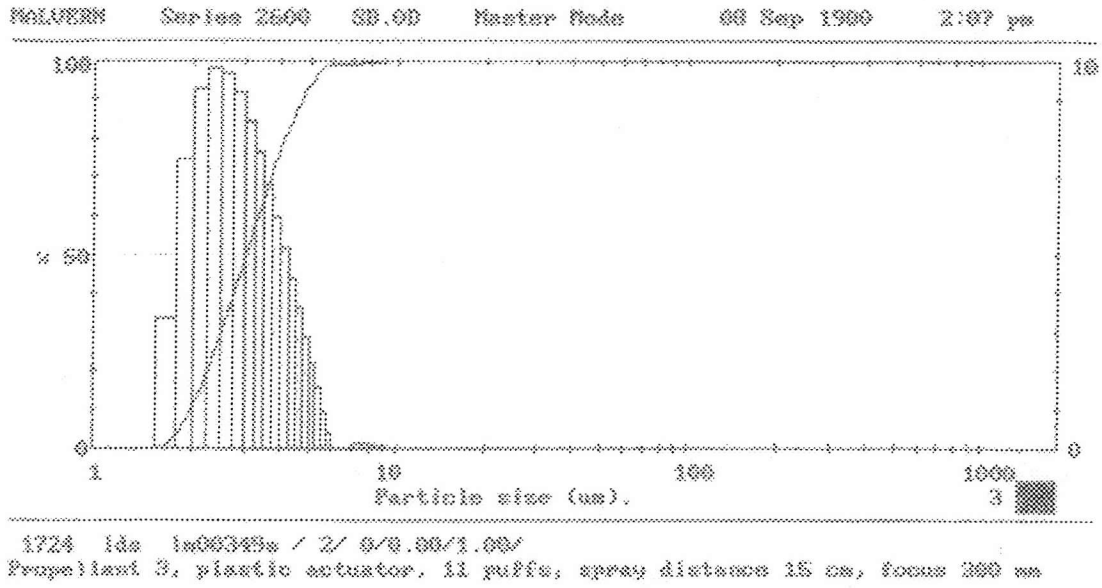

Fig.67 (b) Size distribution for HFA 134a

6.5.1 Experimental Result Comparison Between Coarse and Fine Sprays

6.5.2 Electrical Experimental Result Comparison

6.5.1.A Distilled Water Systems

The charge on the aerosols produced with and without a plastic actuator is plotted against flow rate, as shown in Fig.68.

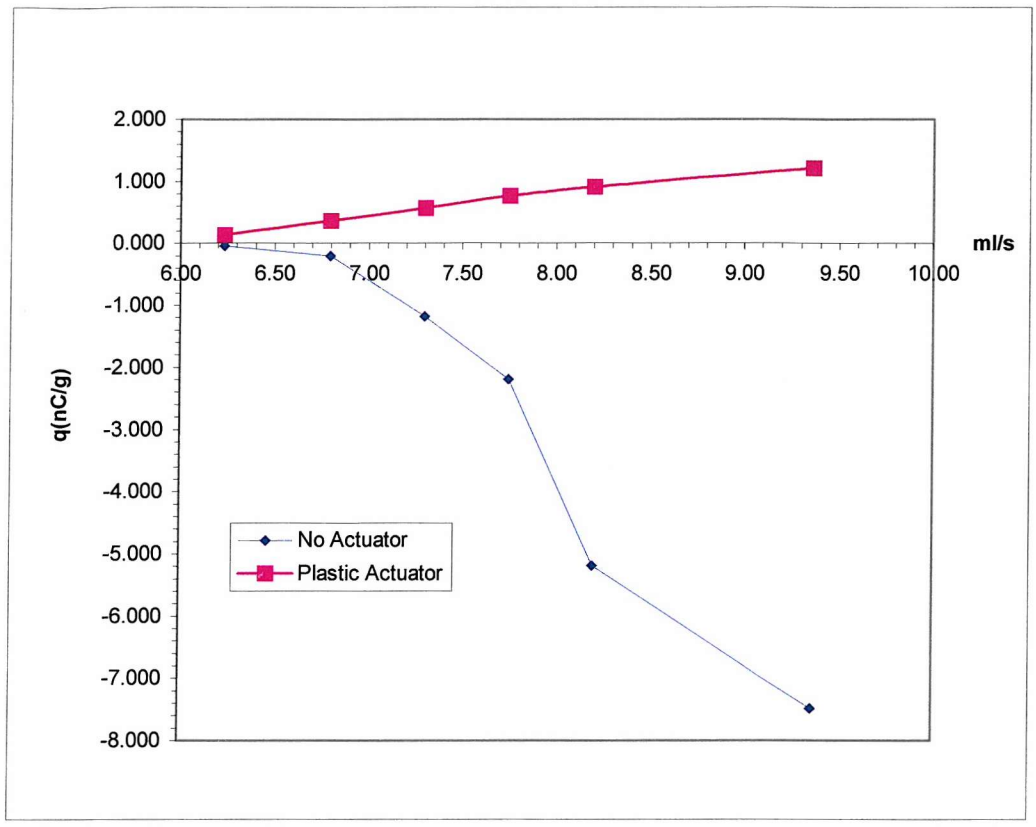

Fig.68 Charge density of aerosol vs flow rate for distilled water with and without plastic actuators

It can be seen from the graph that the polarity on the aerosol charge is changed as a plastic actuator is used. Also the charge magnitude at the same flow rate with a plastic actuator decreases dramatically.

This can be explained in terms of contact potential between distilled water and the valve stem and the plastic actuator. After the liquid flows out of the valve stem, it carries negative charge, which is because the zeta potential is positive between distilled water and the valve stem. As the coarse spray carrying negative charge with it splashes against the plastic actuator and comes out of the orifice of the actuator, it becomes positive charged. This might be due to the zeta potential at the interface between distilled water and plastic actuator is negative, which means the plastic actuator surface is negative charged while the liquid is positive charged. Because there is initial negative charge on the distilled water, the positive charge on the distilled water caused by negative zeta potential at the interface between

distilled water and plastic actuator is compensated partially. However, because splashing against the plastic actuator makes originally zero charged big droplets into highly charged small droplets as described in last chapter, the total charge on the fine spray in magnitude is greater than that on coarse spray. Therefore, the positive charge on fine aerosols caused by interfacial potential between distilled water and plastic actuator and splashing is only partially neutralised. This means the final fine spray carries positive charge and the magnitude on fine spray is less than that the originally negatively charged on coarse spray.

6.5.1.B Electrolyte Solution Systems

In order to compare the results of electrical charges on aerosls produced by electrolyte solutions of KCl with and without actuators at gas pressures of 3.9 bar and 5.7 bar, the charge density on the aerosol is drawn against concentration for both electrolyte solutions. The results for KCl solutions is shown in Fig.69 and Fig.70

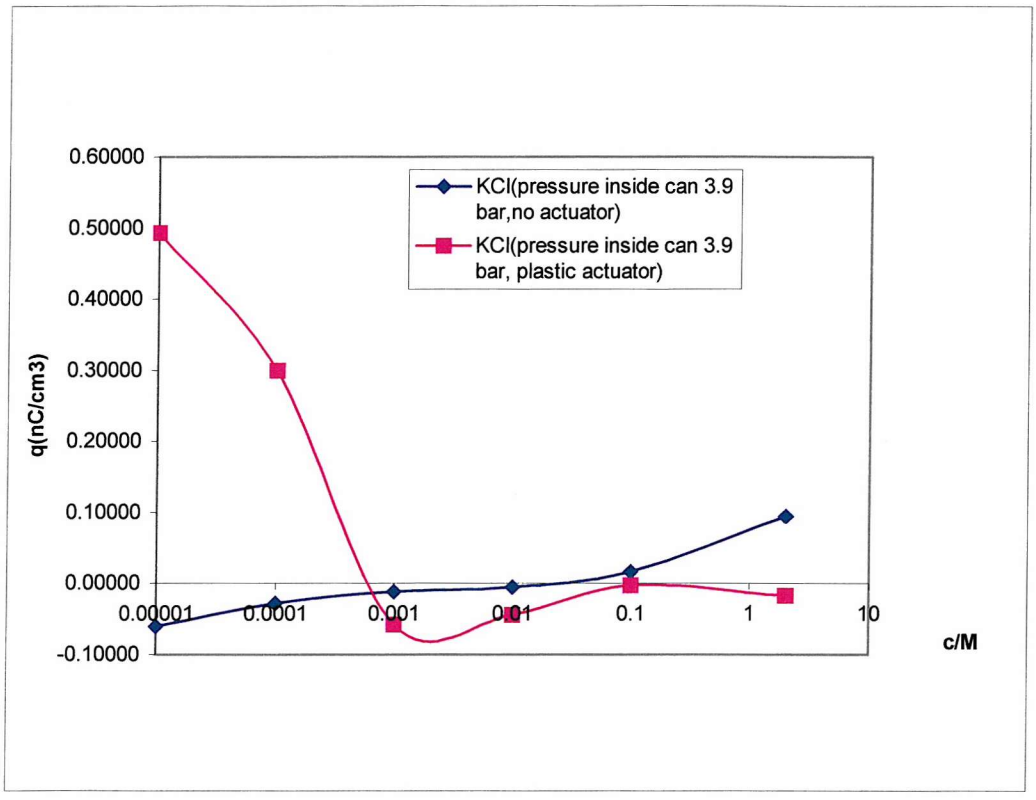

Fig.69 Charge density vs concentration for KCl solutions comparison between with and without plastic actuators (3.9 bar)

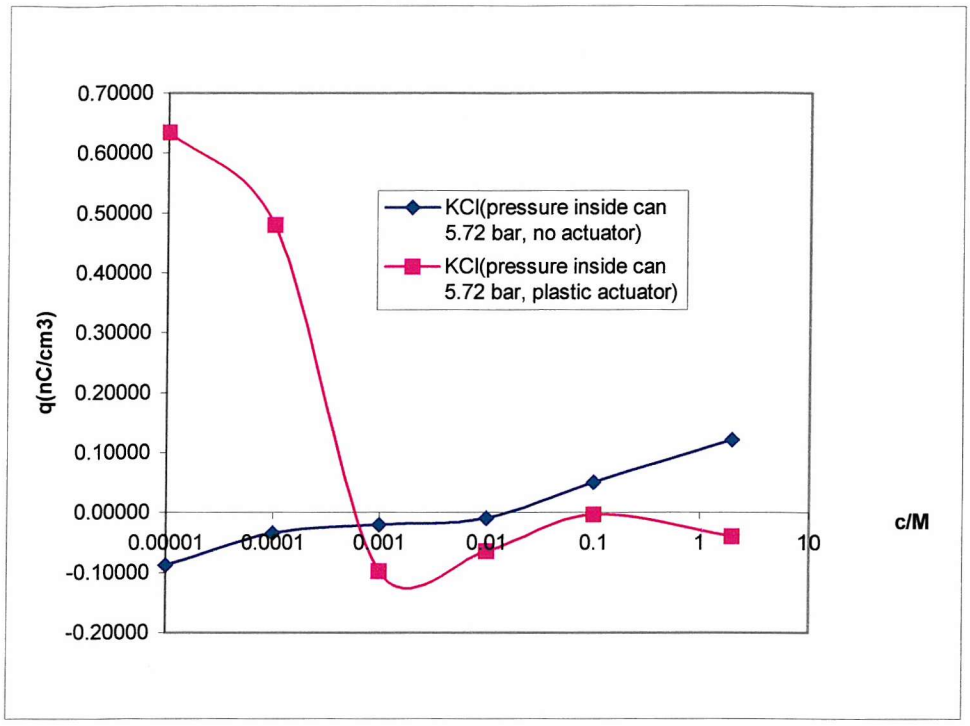

Fig.70 Charge density vs concentration for KCl solutions at 5.72 bar comparison between with and without plastic actuators

From the graphs, it can be seen that as KCl is added to distilled water the negative charge level on the coarse aerosol decreases because of the decrease of the zeta potential at the interface between the solution and the valve stem. Then a ZCP is reached (between 0.01 and 0.1 M); after this point the charge on the coarse spray becomes positive. However as pointed out in **Section 5.5.1**, the zeta potential between distilled water and plastic actuator makes distilled water positively charged while the zeta potential at the interface between distilled water and valve stem makes distilled water negatively charged. The same is true for dilute KCl solutions ($c < 0.001M$). There is a compensation between coarse spray charging process and fine spray charging process. Because splashing process generates highly charged fine sprays than coarse spray charging process, the outcome of the two charging processes compensation is the splashing charging overcome electrokinetic coarse spray charging. Therefore, at dilute conditions ($c < 0.001M$), the final fine spray is positively charged for KCl solutions. Then a point is reached which the magnitude of the charge on the aerosol caused by V_{SV} (the interfacial

potential between solutions and valve stem) equals with that caused by V_{SP} (the interfacial potential between solutions and plastic actuator). This makes the total charge on the fine spray zero. After this point, both V_{SP} and V_{SV} make the aerosol negatively charged, which makes the charge on the fine aerosol the addition of the charge caused by V_{SP} and V_{SV}. Therefore, the magnitude of the fine spray charge increases as concentration goes up. However, as concentration increases continually the magnitude of charge on coarse spray decreases. So the addition of the two charges caused by splashing and electrokinetic processes reaches a maximum charge point MCP. After that the magnitude of total charge on the fine spray reduces until another ZCP (c ~ 0.1M) is reached. At this point, the charges on the spray caused by splashing and electrokinetic processes are equal in magnitude but opposite in sign. However, at this ZCP, the splashing process makes the fine spray negatively charged while electrokinetic process makes it positively charged. After this point, the charge on fine spray seems leveling off as concentration continually increases. This might be due to the charge on aerosols caused by splashing process just levels off along the concentration line while the charge on aerosols caused by electrokinetic process becomes more positive.

6.5.1.C Model Propellant HPFP Systems

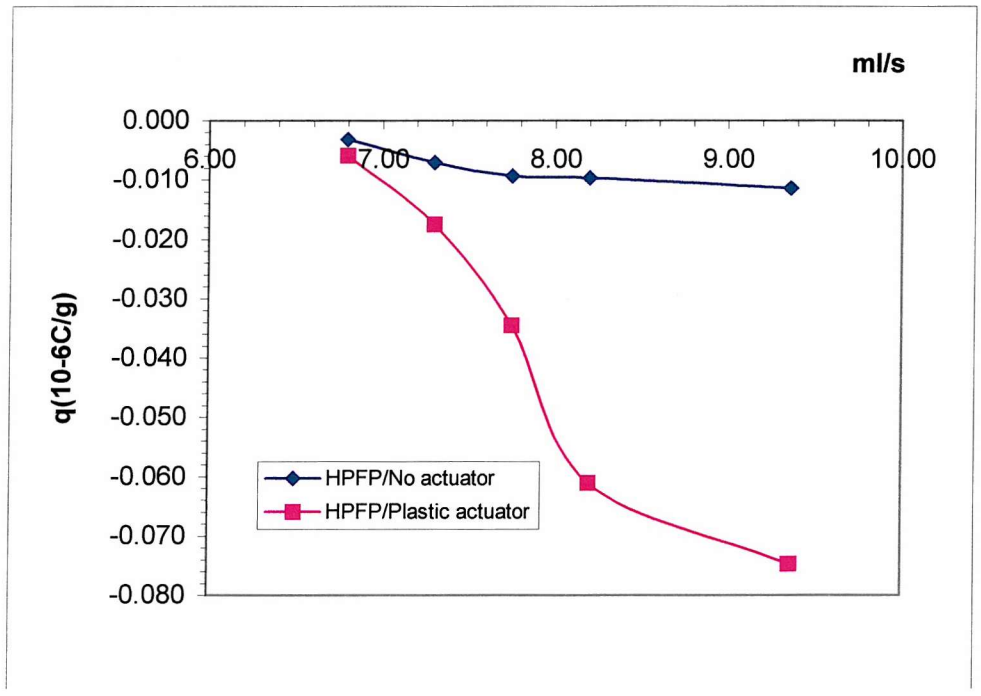

Fig.71 Charge density vs flow rate for HPFP with and without actuators

Fig.71 shows the charges on the cans produced by HPFP system at different flow rate with and without plastic actuators.

Form the graph, it can be seen that the charge on the aerosols produced by HPFP systems is negative with and without using plastic actuators. This means both electrokinetic and splashing processes make the aerosols carry negative charge. This may be due to the contact potentials between HPFP and the valve stem and the plastic actuator all make the liquid sides negatively charged.

6.5.1.D HFA134a, HFA227ea and Formoterol MDIs of HFA134a and HFA227ea Formulation Systems

The charge to aerosol mass ratios for pure HFA134a, HFA227ea and Formoterol MDI devices of HFA134a and HFA227ea formulations with and without plastic actuators are compared in Table 10.

Table.10 Charge on aerosol to mass ratio Q/M (nC/g) for coarse and fine sprays

Description	Batch	Coarse spray Q/M (nC/g)	Fine spray Q/M (nC/g)	Sample Details	Storage Condition
Formoterol pMDI 4.5 μg	P5548	-4.83	13.79	PBT valve, HFA227ea	Initial
	PS157/9	-5.49	-16.48	PBT valve, HFA134a	Initial
	HFA227ea	-2.17	-21.14	PBT valve	Initial
	HFA134a	-4.23	-117.42	PBT valve	Initial

From the data in the table10, it can be seen that the charges on the coarse aerosols for pure HFA134a, HFA227ea and Formoterol MDIs of both HFA134a and HFA227ea formulations are all negative. As Formoterol is added to both HFA134a

and HFA227ea, the coarse aerosol charges increase for both cases. This means the addition of Formoterol enhances the charge on aerosols. For fine sprays, as Formoterol is added to HFA134a, the charge level on fine aerosol decreases while for the case of HFA227ea, the charge on the fine spray even changes its polarity. This might be due to that the contact potential between Formoterol and the plastic actuator in polarity is opposite to that between Formoterol and the valve stem. That is the zeta potential at interface between Formoterol and plastic is negative, which makes the particles carry positive charge; the zeta potential at interface between Formoterol and valve stem is positive, which makes the particles carry negative charge. Therefore, a compensation occurs when using plastic actuator, which makes the particle charge level for HFA134a Formoterol formulation decrease while for HFA227ea case even change the polarity of the charge on particles on fine aerosols.

6.5.1.E Actuator Materials

The following graph shows the effects of actuator materials on aerosol electrostatic charge. The charges for each puff on both the aerosol and the can produced by Formoterol HFA227ea formulation are compared, which includes using both aluminium and plastic actuators.

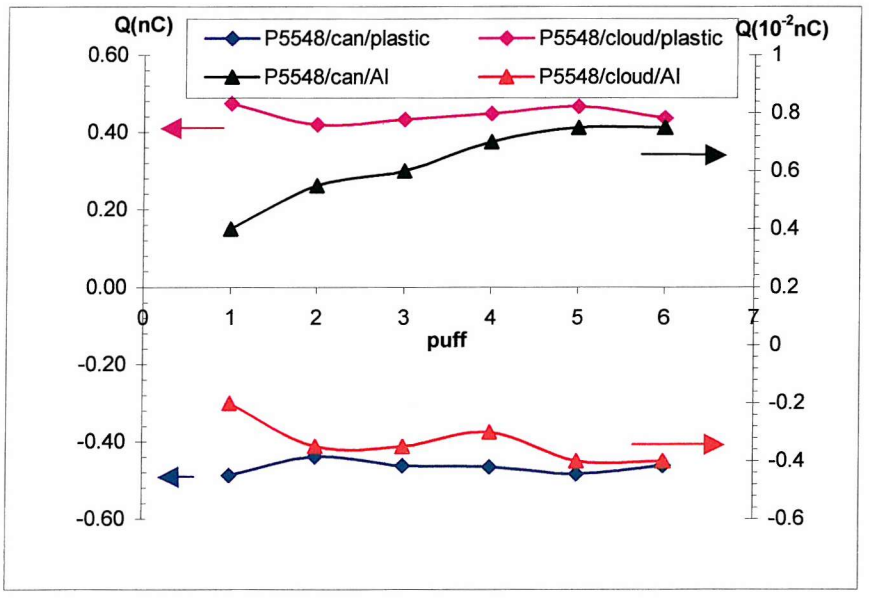

Fig.72 Charges on both the cans and aerosols with Formoterol HFA227ea formulation with both plastic and Al actuators

From graph 72, it can be seen that with the aluminium actuator, a reversal of charge polarity on the cloud and can of batch P5548 was measured and the charge on the cloud was greatly reduced compared with the plastic actuator. The electrostatic charge on the can also decreased, but the charge on the can was almost twice as large as that on the cloud. The electrostatic charge of aerosol emitted from this MDI actuated by the aluminium actuator was two orders less in magnitude than that produced by the plastic actuator.

For the reversal of polarity from plastic actuator to aluminium actuator, the reason almost certainly lies in the different materials having different contact potentials.

As for the dramatic reduction in charge magnitude with the aluminium actuator, it can be explained in terms of contact potential between the particles and the actuators. With aluminium actuator, as the drug particle approaches very close the surface of the Al actuator so that a contact potential is formed temporarily. In this case, the Al surface is positively charged while drug particle surface is negatively charged. As the drug particle approaches further closer to Al surface, the electric field density increases dramatically because the nature of the metal. As a point is reached, the electric field is broken down and the charges at the interface between the drug particle and Al actuator redistribute between the particle and Al actuator. This makes the charge level on both particles and the can with Al actuator is much lower than that it would be otherwise. With the plastic actuator, the electric field between the particle and the surface of the plastic actuator might not go through the breaking down process like the one with Al actuator. Because both drug particles and plastic actuator are non-metal material. They are insulators. Therefore, the charges at the interface need not to accumulate at the very surface to make the electric field too high to break down. There might not be a charge redistribution process, which would make the charge level decreases otherwise.

As for the charge level on the Al can is almost twice as high as that on the aerosols, it still remains unexplainable at this stage.

6.5.2 Size Measurement Comparison for Coarse Spray and Fine Spray

For coarse sprays of HFA134a and HFA227ea, the sizes of the droplets are quite big (MMD ~300μm). Therefore, a photograph would be efficient to show the size difference of drops between coarse sprays and fine sprays. The photos below show the coarse spray produced by HFA227ea without an actuator looks more like a jet (Fig. 73 a) while the fine spray generated by HFA227ea with a plastic actuator looks more like a cloud (Fig.73 b) (MMD ~6μm). This means the sizes of droplets for coarse spray are much larger than the ones for fine sprays (Fig.73 b).

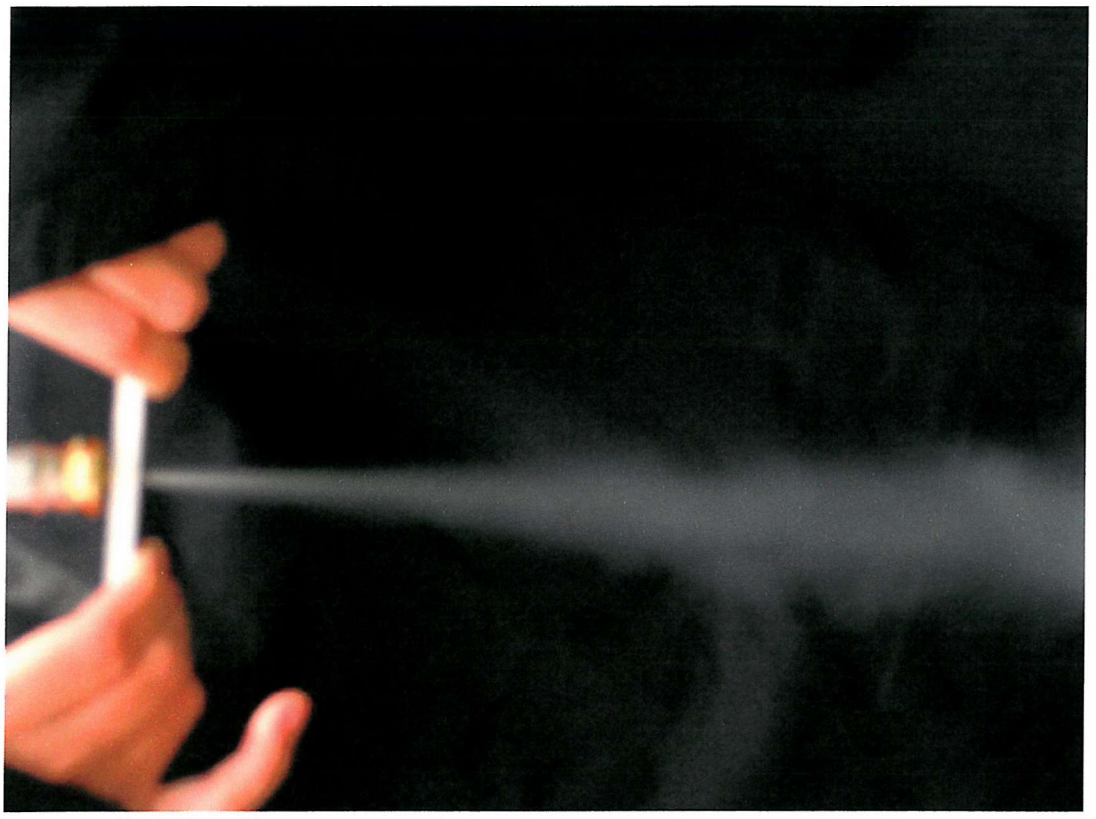

Fig.73(a) Photo taken from HFA 227ea coarse spray without actuator

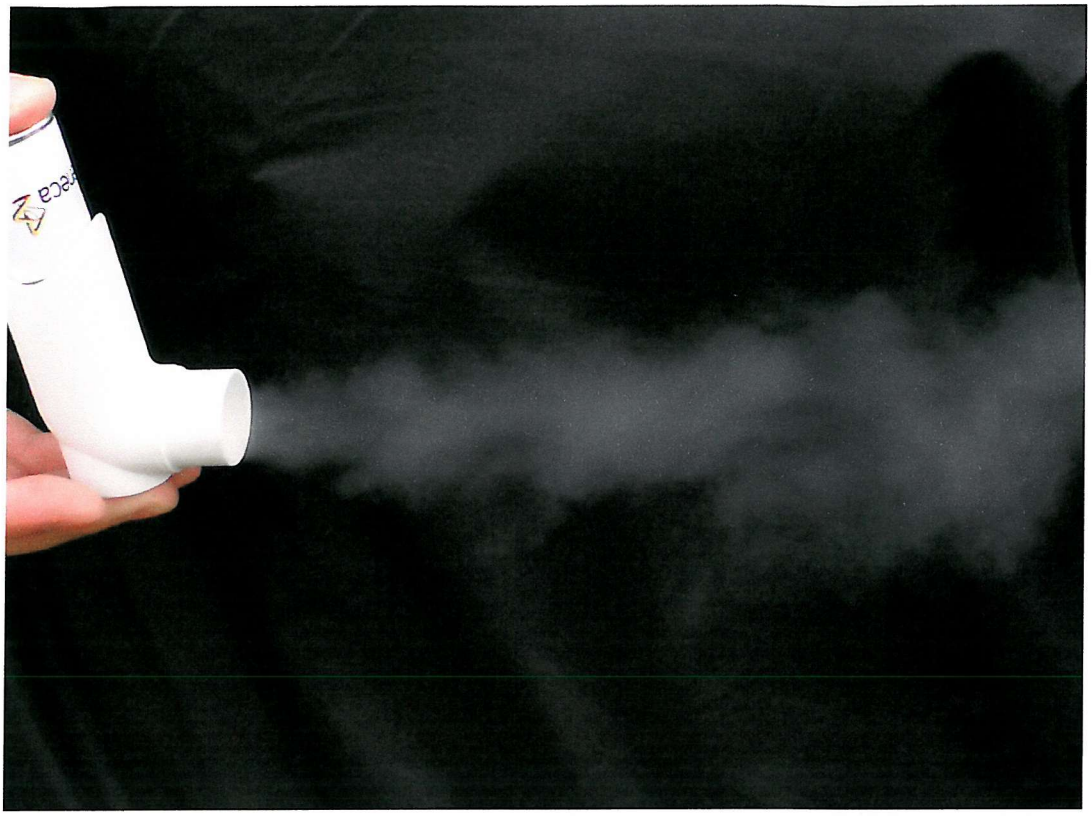

Fig.73 (b) Photo taken from HFA 227ea fine spray with actuator

6.6 Conclusions

- The spray charging process of a pMDI includes: static charging, coarse spray charging, splashing charging and fine spray charging.
- For aqueous solutions examined in this study, fine spray gives a polarity change on aerosols compared to coarse spray. This means the contact potential between these liquids and stem valve has opposite sign to that between these liquids and the actuator. Moreover, splashing charge and fine spray charge levels is higher than coarse spray charge.
- Complex charging processes were observed as aqueous liquid concentration changes. As discussed in previous section, this proves further the concept of the contact potential between a liquid and a solid, which was used to explain drop charging and streaming current phenomena.

- HPFP and pure HFA134a and 227ea as well as their Formoterol formulations give higher charge on aerosols. This means the contact potential between these liquids and the stem valve and actuator is higher than that between aqueous solution and the stem valve and the actuator.
- Coarse spray charges the aerosols much lower than fine spray. This might be due to two reasons: one is that coarse spray produces larger droplets than fine sprays and the other is that splashing charging tends to produce higher charge on aerosols.
- The addition of Formoterol drug into HFAs makes the charge processes even more complex. However, from our experimental results, it seems the drug itself is the dominant factor in aerosol charging phenomenon.
- Actuator materials also play an important part in aerosols charging processes. This is because different materials have different contact potentials. However, for the case of Al actuator, the charge on the can is much higher than the charge on the aerosols. It cannot be explained at the moment.
- HFA134a produces more charge on aerosols than HFA227ea. This is because of the higher vapour pressure of HFA134a, which not only generates a more dynamic flow process inside the can but also produce a finer aerosol cloud. Both of the factors would contribute to the higher charge on aerosols.

6.7 Theoretical Prediction of Spray Charge

Based on the all results obtained in this study, theoretical explanation has been given to every charging process. Therefore, the sum of the charge of each process would give a theoretical prediction of the charge on aerosols and single average drop generated by MDIs.

As pointed out in Chapter Six and Chapter Two, the total charging processes include as following:

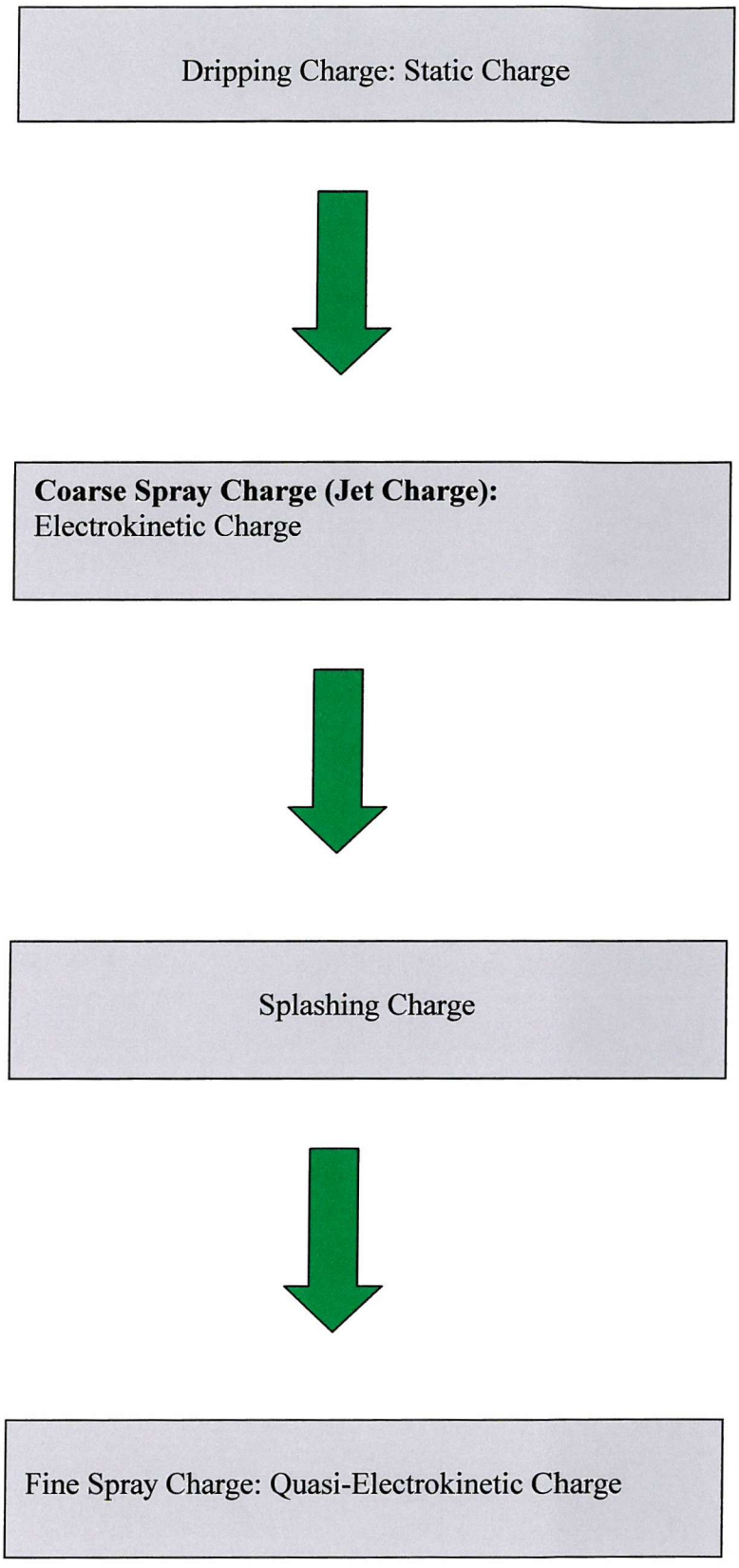

Fig.74 Spray charge processes of a pMDI

Thus, they total current I_t a MDI would produced is:

$$I_t = I_{st} + I_{cs} + I_{sp} + I_{fs} \quad (39)$$

Where I_{st} stands for static charge, which could be calculated by OPERA if the contact potential could be known; I_{cs} for coarse spray current, which could be calculated by equation (31); I_{sp} for splashing current, which would need finite element analysis method to calculated if the contact potential could be known and I_{fs} for fine spray current, which could be calculated by equation (31) as well if the physical properties of the state of a mixture of a vapour and liquid are known.

Equation (39) can be simplified reasonably based on the study results we have obtained.

Among the four components, static current I_{st} is negligible compare to the other three. Substituting the relevant equation into equation (39), it becomes:

$$I_t = \frac{2\pi\varepsilon\varepsilon_0\zeta_0 a_0}{\lambda} v_{cs} + I_{SP} + \frac{2\pi\varepsilon\varepsilon_0\zeta_1 a_1}{\lambda} v_{fs} \quad (40)$$

where a_o, a_1, v_{cs} and v_{fs} are the radius of the valve stem, radius of the orifice of the actuator, flow velocity inside the valve stem and flow velocity inside the orifice while ζ_o, ζ_1 and λ are zeta potential between liquid and the valve stem, zeta potential between the mixture of the liquid and vapour and orifice and Debye length (double layer thickness), where,

$$\lambda = (\varepsilon D_m / \sigma)^{1/2} \quad (25)$$

$$\frac{D_m}{\mu} = \frac{kT}{e} \quad (26)$$

$$\mu \approx \frac{2\times10^{-11}}{\eta} \quad (27)$$

Equation (40) is just a theoretical model, in which the second item needs to be solved using finite element analysis method. This is beyond the range of this study.

CHAPTER SEVEN

CONCLUSIONS

Single drop charge

Experimental results

With external field applied between the needle and the surrounding tube, the dripping drops of DI water carry electrical charges. The relationship between the applied voltage and the magnitude of the dripping charge is linear. This phenomenon can be explained by ordinary electrostatic law. When a potential difference is applied between the needle and the surrounding tube, an electrical field is set up between the needle and the surrounding tube. This electrical field induces charge onto the pendant drop surface and the magnitude of the drop charge is proportional to the applied voltage between the needle and the surrounding tube and the sign of the drop charge is the same as the sign of applied voltage to the needle.

The straight line fails to pass through the origin, giving as intercept the potential that must be applied so that the drop carries no charge. This means that even when the applied voltage to the needle is small positive or zero, the drop carries negative charge. This is because there is an internal system interfacial potential difference, which sets up an electrical field between the needle and the surrounding tube. This induces charge onto the drop surface as well. Its magnitude is determined by the value of the interfacial potential difference and its sign is opposite the applied external voltage in the region between origin and the zero charge point. Therefore when the external field is small positive, the internal field overshadows the external field or the only dominating field in the system under the condition of external field-free. This makes the pendant drop surface carry net negative charge even when the external potential is slightly positive to the needle or zero.

The interfacial potential difference between the liquid and the inner wall of the needle is the dominating factor in the built-in interfacial potential differences in the system. In other words, using the drop-producing system we employed the absolute

interfacial potential difference between a liquid and a solid can be measured. This may be very useful in many ways.

Because an interfacial potential difference is determined by the two surface work functions different materials of the solutions and the solids will be expected to produce difference values of interfacial potential differences. Therefore, the charge on the drop will be expected to be different in both magnitude and sign. This is proved to be true from the experimental data. Because it is easy to change the liquid different electrolyte solutions with different concentrations are employed during the experiments. It is found that, under conditions free of an external field, adding small amounts of electrolytes (uni-valent or multi-valent) to DI water still produce negative charge on drops. The magnitude of the drop charge increases first until a maximum point is reached. Then the magnitude of the drop charge decreases as the concentration increases until a zcp is reached. Then continuing adding electrolyte to DI water makes the drop carry positive charge. This can be interpreted in terms of interfacial potential (or contact potential) between liquid and the needle. The contact potential between liquid and the inner wall of the needle is positive on the metal surface and the liquid is negatively charged. As more electrolyte is added in the water there are more cations to be adsorbed onto the metal surface. This makes the magnitude of the contact potential between the liquid and the metal surface increase until a maximum point is reached. Then the anion adsorption onto the metal surface increases. This makes the contact potential decrease until zcp is reached. Now adding more electrolyte in the solution will make the double layer between the solution and the metal collapse and the contact potential changes its polarity, which makes the drop charge reverse its sign.

Computational simulation on drop charge under conditions of field-free

The computer simulation model on single drop charge is established using OPERA. The contact potential between solution and needle which is obtained from experiments, is used as boundary conditions in the model. Then the electrical field is set up inside the surrounding tube, which induces electrical charge onto the pendant drop surface. The drop charge along the surface is calculated using OPERA.

The computer simulation data on single drop charge is compared with experimental data. The simulation data are in accord with experimental observations and correctly predict that the negative charge carried by drops would increase as the capillary diameter increases and the surrounding tube diameter decreases. Therefore, if the contact potential between a liquid and a solid is obtainable, the charge on the drop can be calculated using this model.

The computer simulation data are always greater than experimental results. And the bigger the drops, the greater the difference. This might be due to the dynamic effect during the drop breaking away process. Two factors might contribute to the lower drop charge phenomenon:

a) During the process of drop formation, a very narrow neck is formed at the final stage of the drop formation. At the moment of the drop breaking away from the tip, a flow of liquid having a net positive charge passes through the constricting neck into the forming drops and as a result the charge on detached drops may be less negative than would otherwise be the case.

b) If satellite drops are formed during this process, as is sometimes observed in practice, they arise from the pinched-in portion which has surfeit of negative charge and hence such satellite drops are likely to be negatively charged, leaving the detached drop even less negative than would be otherwise.

It is clear that these factors, mentioned above, would contribute more as the drop size increases, which explains why the error between experimental results and computer simulation data increases as the capillary diameter goes up.

In order to decrease this error between experimental results and simulation data, the model needs to be improved to include the dynamic process of the drop breaking away from the tip of the needle.

Streaming current

Aqueous solutions

The streaming current always increases linearly as flow rate increases for all dilute solutions. This is because the conductivities of aqueous solutions are higher than insulators (non-aqueous solutions). Therefore the double layer between the solution and the metal is so thin that it always lies under the viscous sub layer.

The streaming current for concentrated solutions (concentration near their saturated point) almost keeps constant as flow rate increases. This is beyond our understanding.

The pattern of the streaming current against solution concentration is very similar to that of the drop charge against solution concentration. The streaming current is negative when the solution is dilute. As electrolyte is added to DI water, the streaming current increases in magnitude first until a maximum point is reached, then the streaming current decreases in magnitude until the zcp is reached. After that the streaming current reverses its polarity. This can be interpreted in terms of contact potential between the solution and the metal, which is similar to the explanation given for drop charge against solution concentration.

For some of the electrolyte solutions (acids and alkalis) the reverse sign point is not observed. This is because concentrated solutions (acids and alkalis) would react with metal, which makes the charging process more complicated. Therefore, with acids and alkalis only very dilute solutions are used.

Model propellant (HPFP) and its Ca-dips solutions

The streaming current for HPFP and its Ca-dips solutions is always negative. As flow rate increases, the streaming current with HPFP and its Ca-dips solutions increases linearly first, then increases dramatically and finally reaches another linear relationship. This is because at low flow rate, the liquid flow can be treated as laminar flow. As flow rate increases, the laminar flow layer is becoming thinner than double layer. This means the double layer becomes exposed to the turbulent

flow, which makes the streaming current increase dramatically. As the flow rate goes up more, the fully turbulent flow stage is reached. Then another linear relationship between streaming current and flow rate is reached.

As more additive (Ca-dips) is added to HPFP, the streaming current increases in magnitude first until a maximum is reached at concentration of ~10^{-7} M and then the streaming current decreases in magnitude. This can also be explained in terms of the relationship between the concentration and the contact potential between the solutions and the needle. The streaming current being negative shows that the stainless steel wall is positively charged, presumably by adsorption of a monolayer of ions such as Ca (di-isopropyl-salicylate)$^{+}$.

There is no charge polarity observed in this case as concentration increases. This might be due to HPFP being non-conductive liquid and the concentration of free ions in the solution being very low. Even when the concentration almost reaches its saturation point, there are still not enough ions in the solution to make the double layer to reach zcp (zero charge point).

Splashing charge

When a falling drop is splashed against a solid plate by gas blast, the rebounding droplets acquire charges, which leaves the solid plate charge (target charge) equal in magnitude and opposite in sign. The value of the target charge depends on the value of the contact potential between the plate, the gas blow rate and the conductivity of the liquid.

Different materials of solutions and solids have different contact potentials, which influence the target charge.

For the metals we used (Cu and Pb), the target charge difference between them shows only small variation. This might be due to the contact potentials for different metal materials being different but the difference is small.

The smaller the droplets for a certain amount of liquid the greater the total charge carried by the rebounding droplets.

The lower the conductivity the greater the splashing electrification.

Spray charging

Coarse spray (without actuators)

Aqueous solutions

The aerosols generated using DI water system are invariably charged negatively. The level of the electrostatic charge increases as pressure inside the can increases.

The aerosols produced using electrolyte solutions are charged except at the zcp but the polarity depends on the concentration of the solutions. At low concentrations the aerosols carry negative charge. As concentration increases the level of the aerosol charge decreases until zcp is reached. Then aerosol charge reverses its polarity and the charge level increases as concentration increases.

The magnitude of the aerosol charge density produced by aqueous solutions increases as can pressure increases.

All these can be explained in terms of double layer at the interface of liquid/solid of the can nozzle as concluded for streaming current.

Fine spray (with actuators)

Aqueous solutions

The fine aerosol generated using DI water with a plastic actuator is positively charged; the level of the charge increases as can pressure increases. With a plastic actuator the aerosol charge reverses its polarity for DI water. This might be due to the polarity of the contact potential between DI water and the nozzle of the can is the opposite that between DI water and the actuator. The final charge process dominates the whole process to make the aerosol charge sign change.

The aerosol charge density level increases with electrolyte solutions as can pressure increases. The aerosol charge is positive for dilute solutions and then decreases as concentration increases until zcp is reached, then the polarity of the aerosol charge changes and the charge level increase as concentration continue to increase until a maximum point is reached, then the charge levels off as the concentration increases. With a plastic actuator employed the charging process becomes more complex because more interfacial potential is involved. It seems that the contact potential between electrolyte solutions and the can nozzle is opposite that between electrolyte solutions and the actuator at low concentrations. Therefore there are two dominating charging processes in the same system, which compete with each other. Also, both of the contact potentials change as solution concentration changes. Before zcp is reached, the fine aerosol carries positive charge. This means that the contact potential between the solution and actuator is dominating. As concentration increases the charge level decreases as discussed in the splashing charging section. Then the zcp is reached when all charging processes cancel out. As concentration continues to increase the contact potential between solution and actuator collapses, which contributes electrical-negatively to the aerosol charge. At this time the contact potential between solution and can nozzle still contributes electrical-negatively to the aerosol charge. Two contributions together make the aerosol negatively charged and the charge increases as concentration increases until the contact potential between solution and can nozzle reverse its sign, which means it contributes positively to the aerosol charge. This make the aerosol charge level decreases as concentration increases. As concentration continue increasing, the interfacial potential difference in the system keeps saturated, which make the aerosol charge level off as concentration increases.

HPFP, HFA134a, HFA227ea and Formoterol formulation MDIs of HFA134a and HFA227ea

The charge on the aerosols produced with a plastic actuator using HPFP, HFA134a, HFA227ea and HFA134a Formoterol formulation systems are all negative, the same sign as without the plastic actuator. This might be due to the contact potential polarity being the same between these liquids or particles and can

nozzle and between them and the plastic actuator. Only HFA227ea Formoterol formulation gives positive charge on aerosols. This is beyond our explanation.

Actuator materials

Actuator materials can both change aerosol charge level and signs. With a plastic actuator Formoterol HFA227ea formulation produces positive charge on fine aerosol particles while with Al actuator it generates negative charge on aerosol particles. This proves again different materials give different contact potentials.

Size distribution effect on aerosol charge

The aerosol charge to mass ratio is higher for HFA134a than that for HFA227ea. This is because HFA134a has higher vapour pressure than HFA227ea and also the droplet size in HFA134a aerosol is smaller than that in HFA227ea. As dicussed in splashing charging and streaming charge sections, the higher the pressure and the greater amount of droplets to a certain amount of liquid, the greater the charge level.

For all charging processes, dripping, jetting, splashing and fine spraying, the contact potential between liquid and solid surface plays a dominant role. The polarity of the contact potential determines what sign of charge the aerosol might carry while the magnitude of the contact potential determines the level of charge presented on aerosols produced by MDIs. The set-up used in this study can be used for measuring an absolute contact potential between a liquid and a solid. The model set up in this study can be used to compare with experimental results or predict drop charge.

In all, MDI spray charging processes can be divided into four basic components: static dripping charging, jet charging, splashing charging and fine spray charging. Amongst the four components, static dripping charge contribution upon aerosol charge can be omitted because of its insignificance in value. Therefore, the final charge presented on aerosols generated by an MDI depends on the three charging processes. Amongst the three, splashing creates more charge than the other two.

APPENDIX I: PUMP CONTROL PROGRAMME AND FLOW CHART

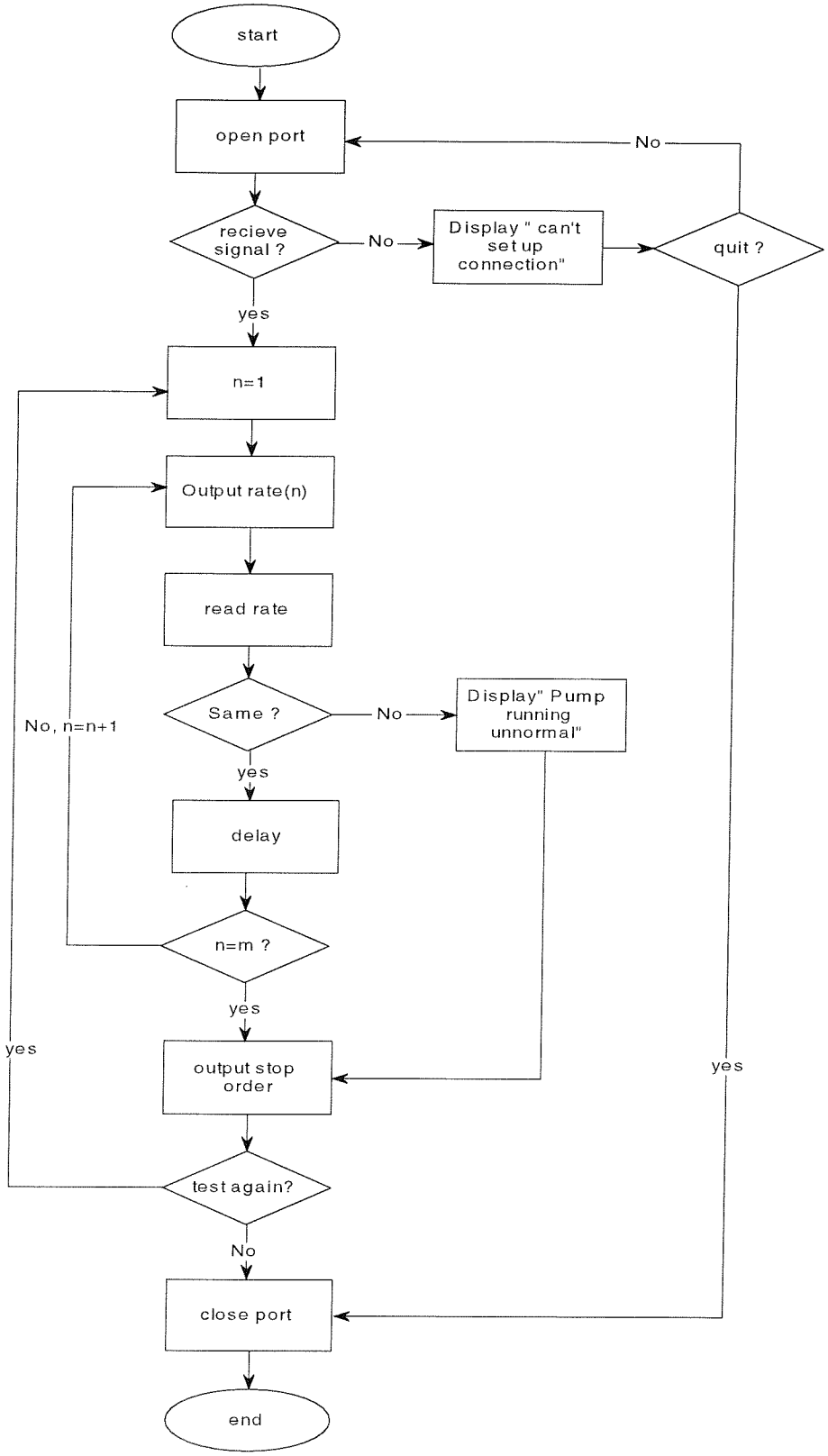

```
#include <dos.h>
#include <stdio.h>
#include <conio.h>
#include <time.h>
#define PORT0 0x3F8 /* COM1*/
int main(void)
{
 void trans_order(const char*string);
 void trans_order(const char*string)
 {
  while(*string!='\0')
  {
   outportb(PORT0,*string++);
   delay(1);
  }
 char str1[]={"RUN\x0d"};
 char str2[]={"STP\x0d"};
 char rate[n] ={" MLM(2+2*n)\x0d " };
 int n,cp=0;
 outportb(PORT0 + 1 , 0);   /* Turn off interrupts - Port1 */
 outportb(PORT0 + 3 , 0x80);  /* SET DLAB ON */
 outportb(PORT0 + 0 , 0x0C);  /* Set Baud rate - Divisor Latch Low Byte */
 outportb(PORT0 + 1 , 0x00);  /* Set Baud rate - Divisor Latch High Byte */
 outportb(PORT0 + 3 , 0x07);  /* 8 Bits, No Parity, 2 Stop Bit */
 outportb(PORT0 + 4 , 0x0B);  /* Turn on DTR, RTS, and OUT2 */
 clrscr();
 printf("\nRun Test Profile\n");
 do
 {
  trans_order(str1);
  delay(10);
  for (n=0;n<5;n++)
  {
```

```
    trans_order(rate[n]);
    printf("pump rate is %d  ml/min\r",2*n+2);
    delay(30000);
   }
   printf("\nTest finish!! Press ESC to quit and Others repeat!");
   trans_order(str2);
   cp=getch();
   clrscr();
 }
   while (cp!=27);
   return 0;
 }

}
```

APPENDIX II: DATA TRANSFER FROM KEITHLEY PROGAMME AND FLOW CHART

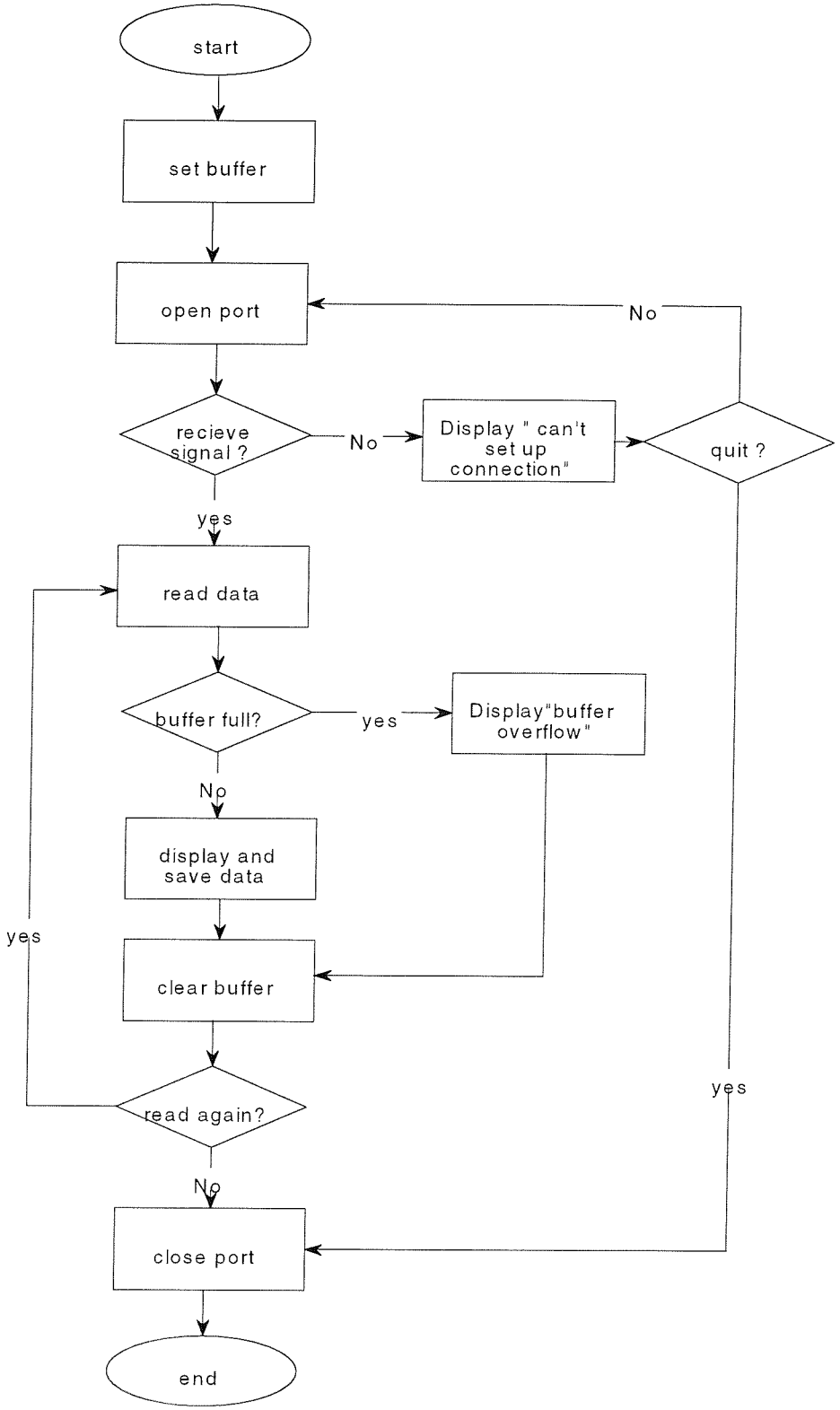

```
#include <dos.h>
#include <stdio.h>
#include <conio.h>
#define COM4 0x2F8 /* COM2*/
#define  INTVECT 0x0C

int bufferin = 0;
int bufferout = 0;
char ch;
char buffer[10240];
void interrupt (*oldads)();
void interrupt COM2INT()  /* Interrupt Service Routine (ISR) for PORT1 */
{
 int c;
 do
 {
  c = inportb(COM2 + 5);
  if (c & 1)
  {
    buffer[bufferin] = inportb(COM2);
          bufferin++;
    if (bufferin ==10239 )
    {
     bufferin = 0;
     printf("data overflow, please increase buffer!");
    }
  }
 }
 while (c & 1);
 outportb(0x20,0x20);
}
void trans_order(const char*string);
void trans_order(const char*string)
{
 while(*string!='\0')
 {
  outportb(COM2,*string++);
  delay(1);
 }
 delay(15);
}
char str1[]="*RST\n";
char str2[]=":FORM:ELEM READ,TIME\n";
char str3[]=":CURR:RANG:AUTO ON\n";
char str4[]=":TRAC:DATA?\n";

int main(void)
```

```
{
 FILE*kf;

 int c, n=0;
 if((kf=fopen("current.dat","w"))==NULL)
 {
  printf("Cannot open file.\n");
  return 1;
 }
 outportb(COM2 + 1 , 0);   /* Turn off interrupts - COM2 */
 oldads = getvect(INTVECT);
 setvect(INTVECT, COM2INT);
 outportb(COM2 + 3 , 0x80);  /* SET DLAB ON */
 outportb(COM2 + 0 , 0x0C);  /* Set Baud rate 9600 - Divisor Latch Low Byte */
 outportb(COM2 + 1 , 0x00);  /* Set Baud rate - Divisor Latch High Byte */
 outportb(COM2 + 3 , 0x03);  /* 8 Bits, No Parity, 1 Stop Bit */
 outportb(COM2 + 4 , 0x0B);  /* Turn on DTR, RTS, and OUT2 */
 outportb(0x21,(inportb(0x21) & 0xE7));  /* Set Programmable Interrupt
Controller */
 outportb(COM2 + 1 , 0x01);  /* Interrupt when data received */
 clrscr();
 printf("\nSample Test Measurement\n");
 trans_order(str1);
 trans_order(str2);
 trans_order(str3);
 trans_order(str4);


 printf("Total Reading Received! Press ESC to quit \n");
 do
 {
   if (bufferin != bufferout)
   {
    ch=buffer[bufferout];
    if(bufferout==10239)
    {
     bufferout=0;
    }
    if ((n+1)==((bufferout+1)/28))
     {
      fprintf(kf,"%c",ch);
      printf("%c\n",ch);
      n++;
     }
     else
      {
       fprintf(kf,"%c",ch);
      printf("%c",ch);
      }
    bufferout++;
```

```
      }
      if (kbhit())
      {
        c = getch();
      }
    }
     while (c !=27);
 outportb(COM2 + 1 , 0);   /* Turn off interrupts - COM2 */
 outportb(0x21,(inportb(0x21) | 0x08));  /* MASK IRQ using PIC */
 setvect(INTVECT, oldads); /* Restore old interrupt vector */
 fclose(kf);
 return (0);
}
```

PUBLICATIONS AND REPORTS

1. Yanyang WANG and Adrian G. BAILEY(1999). Drop charging during liquid dispersion. Electrostatics 1999.

2. Yanyang WANG and Adrian G. BAILEY (1999). The natural charging of liquid jets. AstraZeneca's PhD Student Review Day.

3. Yanyang WANG and Adrian G.BAILEY (1999). Determination of the electrostatic charges on aerosols emitted from pMDIs and cans. Oral presentation and Report for AstraZeneca.

4. Yanyang WANG, Adrian G. BAILEY, and Philippe ROGUEDA (2000).Natural charging of pMDI aerosols. AstraZeneca's PhD Student Review Day.

REFERENCES:

1. Sciarra, J.J. and Cutie, A.J.: Modern Pharmaceutics, Second Edition, G.S.Banker and C.T.Rhodes (eds.), Marcel Dekker, Inc., New York, NY, p.605 (1990).

2. Staniforth, J.N., Aerosol Sci. Technol., **22**, p346 (1995).

3. Molina, M.J. and Rowland, F.S., Nature, **249**, p810 (1974).

4. D'Souza, S: J. Aerosol Med., **8** (suppl.1). S-13 (1995).

5. Noakes, T.J.: J. Aerosol Med., **8** (suppl. 1). S-3 (1995).

6. Tzou, T.T., Pachuta, R.R., Coy, R.B., and Schultz, R.K.: J.Pharm. Sci., **86,** p1352 (1997).

7. Niven, R.W.: Inhalation Aerosols: Physical and Biological Basis for Therapy, A.J.Hickey (ed.), MarcelDekker, Inc., New York, NY, p.273 (1996).

8. Adjei, A.L. and Gupta, P.K.: Inhalation Delivery of Therapeutic Peptides and Proteins, A.L.Adjei and P.K.Gupta (eds.), Marcel Dekker, Inc. New York, NY, p.625 (1997).

9. Newman, S.P., Moren, F. and Crompton, G.K.: A New Concept in Inhalation Therapy, Medicom Europe BV, Bussum, The Netherlands (1987).

10. Hickey, A.J. (ed.): Inhalation Aerosols, Marcel Dekker, Inc., New York, NY, p273 (1996).

11. Hickey, A.J. (ed.): Pharmaceutical Inhalation Aerosol Technology, Marcel Dekker, Inc., New York, NY, p154 (1992).

12. Kelvin Lord, T. W., Proc.Roy.Soc. (Lond.) **16,** p67 (1867).

13. Chalmers, J. A. and Pasquill, F., Phil. Mag. **xxiii**(Ser.7), p88 (1937).

14. Gill, E. W. B. and Alfrey, G.F., Nature **164**, p1003 (1949).

15. Gill, E. W. B. and Alfrey, G.F., Proc.Phys.Soc.Lond., **B65**, p546 (1952).

16. Iribarne, J. V. and Klemes, M., J. Atmos.Sci. **27**, p927, (1970).

17. Boumans. Physica, 's Grav. **23**, p1007,1027,1038,1047 (1957).

18. Klinkenberg, A. and Van Der Minne, D. M., J.L., Electrostatics in the petroleum industry, Elsevier publisher company, Chpt.2, (1958).

19. Rutgers, A. J. and de Smet, M., Trans. Farad.Soc. **48**(part 7), p635 (1952).

20. Rutgers, A.J., de Smet, M. and de Myer, G. Trans. Farad. Soc. **53,** p393 (1957).

21. Simpson, G.C., Phil.Trans. Roy. Soc., A**209**, p379 (1909).

22. Lenard, P., Ann. Der. Physik, Lpz., **46**, p584 (1892).

23. Lenard, P., Ann. der. Physik **47,** p463 (1915).

24. Lenard, P., Ann. Der. Physik **65**, p629 (1921).

25. Zeleny, J., Phys. Rev. **44**, p837 (1933).

26. Iribarne, J. V., J. de Recherches Atmospherique **6**, p265 (1972).

27. Nolan, J. J., Phil.Mag. **46**.No272, p225 (1923).

28. Aganin, M., Ann. der. Physik **45**, p1013 (1914).

29. Thomson, J. J., Phil.Mag. **38**. No.233: p358 (1894).

30. Becker, A., Ann. der. Physik. **31**, p98 (1910).

31. Aselmann, E., Ann. der. Physik. **19**, p960 (1906).

32. Kahler, K., Ann. der. Physik **12**, p1119 (1903).

33. Rey, Sur l'ionisation der l'air par les chutes d'eau, Gauthier Villiers, Paris (1912).

34. Faraday, Experimental Researches (1843).

35. Nolan, J. J. and Enright, J. Scient. Proc. Roy. Dublin Soc. **17**, p1 (1922).

36. Chapman, D.D., Phil. Mag. **25**, p475 (1913).

37. Millikan, R. A., Phy. Rev. **2**, p109 (1935).

38. Byrne, M. J., Ph.D. Thesis, National Univ. of Ireland (1977).

39. Iribarne, J. V. and Mason, B. J., Trans. Faraday Soc., **63**, p2234 (1967).

40. Carter, P. A., Rowley,G., Burdon, M. and Suggett, J., Drug Delivery to the Lungs IX, The Aerosol Society, 14th and 15th, p112 (1998).

41. Clayborough, R. and Nichols, S. C., Drug Delivery to the Lungs IX, The Aerosol Society, 14th and 15th, p108 (1998).

42. Peart, J., Magyar, C. and Byron, P., Respiratory Drug Delivery VI, p227 (1998).

43. Peart, J. and Byron, P., Electrostatics 1999, p77 (1999).

44. Buss, W., Ann. der. Phys., Lpz. **76**, p493 (1925).

45. Matteson, M. J., J. Colloid and Interface Sci. **37**, p879 (1971).

46. Onsager, L. and Samaras, S., N. J. Chem. Phys. **2**, p528 (1934).

47. Harper, W. P., Advanced in Physics, **6**, p202 (1967).

48. Fletcher, N. M., Phil. Mag. **7,** p255 (1962).

49. Bach, N. and Gilman, A., Acta Physicochimica, URSS **9**, p1 (1938).

50. Jonas, P. R. and Mason, B.J., Trans. Farad. Soc. **64**, p1971 (1971).

51. Bailey, A. G.: Electrostatic Spraying of Liquids, Research Studies Press Ltd. England, p3 (1988).

52. Von Helmholts, H.L., Wied. Ann., **7**, p337 (1879).

53. Gouy, G., J. Physique **9**, p457 (1910).

54. Chapman, S., Phsics **5**, p150 (1934).

55. Stern, O. Z., Elektrochem. **30**, p508 (1924).

56. Grahame, D. C., J.Chem.Phys. **18**, p903 (1950).

57. Davies, J. T..: Interfacial Phenomena, Academic Press, p140 (1963).

58. Mitchell, A. R. and Wait, R.,: The finite element method in partial differential equations, A Wiley-Intersicence Pulication, Chpt.1 (1977).

59. Bashforth, F. and Adams, J.C.: An attempt to test the theories of capillary attraction. Cambs. Univ. Press (1883).

60. Lohnstein, T., Ann. Phys. **22**, p767 (1907).

61. Paddy, J. F. Phil. Trans. **269**(A.), p265 (1971).

62. Andreas, J. M., Hauser, E.A. and Tucker, W.B., J. Phys.Chem. **42**, p1001 (1938).

63. Pitts, E., J. Fluid Mech. **63**, p487 (1974).

64. Borzabadi, E. and Bailey, A. G., J. Electrostatics **5** p369 (1978).

65. Pribylov, V.N. and Chernyi, L.T., Fluid Dynamics **14**, p844 (1979).

66. Cooper, W.F., Brit, J. Appl. Phys. **4** (Suppl. 2), S-11 (1953).

67. Klinkenberg, A. and Poulston, B.V., J. Inst. Petrol., **44**, p379 (1958).

68. Koszman, I. and Gavis, J., J. Chem. Engng Sci. **17**, p1013 (1962a).

69. Rouse and Howe,: Basi Mechanics of Fluid, Chapman and Hall, New York, p137 (1953).

70. Morin II, A. J., Zahn, M. and Melcher, J. R., IEEE Trans. Electrical Insulation, **26** (5), p870 (1991).

71. Adamczewski, I, Ionization, conductivity and breakdown in Dielectric liquids, Talylor and Francis, London, p224 (1969).

72. M^{me} et Martinet, M. J., *Bull. Soc.chim. France*, p68 (1948).

73. Matsuyama, H. and Yamamoto, H., J. Phys. D: Appl. Phs. **28**, p2418 (1995).

74. Matsuyama, H. and Yamamoto, H., J. Phys. D: Appl. Phys. **30**, p2170 (1997).

75. Thomson, J. J., Phil. Mag.S.5, **37**, No227, p341(1894).

76. Adams, F., (Trans.) London, Sydenham Society, **1**, p475 (1844).

77. Newman, S. P. and Clark, S. W., Thorax, **38**, p881 (1983).

78. Brian, T. L. and Valberg, P.A., Am. Rev. Dis., **120**, p1325 (1979).

79. Loeb, L. B.: Static electrification, Springer-Verloog, Heidelberg:1, Chpt.1, (1958).

80. Hinds, W. C.: Aerosol technology: properties, behaviour and measurement of airborne particles. Wiley Interscience: New York, p6 (1982).

81. Staniforth, J. N., Byron, P. R., Dalby, R. N. and Farr, S. J. (Eds.), Respiratory Drug Delivery IV, Interpharm Press: Buffallo Grove, **IL**, p303 (1994).

82. Peart, J., Staniforth, J. N., Byron, P. R. and Meakin, B.J. Dalby, R. N., Byron, P. R. and Farr, S. J. (Eds.), Respiratory Drug Delivery **V**, Interpharm Press: Buffallo Grove, **IL**, p85-94 (1996).

83. Byron, P. R., Peart, J. and Staniforth, J. N., Pharmaceutical Research, **14**, p698 (1997).

84. Longley, M.Y., American Industrial Hygiene Association Journal, **21**, p187 (1960).

85. Melandri, C., Prodi, V., Tarroni, G., Formignani, M., De Zaiacomo, T.,

Bompane, G. F. and Maestri, G.: W. H. Walton (Ed.) Inhaled particles **IV**. Pergammon Press: Oxford, p193 (1977).

86. Melandri, C., Tarroni, G., De Zaiacomo, T., Formignani, M. and Lombardi, C. C., Journal of Aerosol Science, **14**, p657 (1983).

87. Balachandran, W., Ahmad, C. N. and Barton, S. A., Institute of Physics Conference Series, **118**, p57 (1991).

88. O'Callaghan, C., Lynch, J., Cant, M and Robertson, C., Thorax, **48**, p603 (1993).

89. Bisgaard, H., Anhoj, J., Klug, B. and Berg, E., Archives of Diseases of Childhood, **73**, p226 (1995).

90. Barry, P. W. and O'Callaghan, C., British Journal of Clinical Pharmacologh, **40**, p76 (1995).

91. Bisgaard, H., European Respiratory Journal, **8**, p856 (1995).

92. Wildhaber, J. H., Devadason, S. G., Hayden, M. J., James, R., Duffy, A. P., Fox, R. A., Summers, Q. A. and Lesouef, P. N., European Respiratory Journal, **9**, p1943 (1996).

93. Dewsbury, N.J., Kenyon, C. J. and Newman, S. P., International Journal of Pharmaceutics, **137**, p261 (1996).

94. Wildaber, J. H., Devadason, S. G., Eber, E., Hayden, M. J., Everard, M. L., Summers, Q. A. and LeSouef, P. N.,. Thorax, **51**, p985 (1996).

95. Clark, D. J. and Lipworth, B. J., Thorax. **51**, p981 (1996).

96. Byron, P. R.: Respiratory Drug Delivey (Byron, P. R. ed) CRC Press, Boca Raton, Fla., p167 (1990).

97. Hickey, A.J. (ed.): Pharmaceutical Inhalation Aerosol Technology, Marcel Dekker, Inc., New York, NY, p174 (1992).

98. Task Group on Lung Dynamics, Health Phys., **12**, p173 (1966).

99. Lippmann W.: Multiple Integrals, Library of Mathematics (Ed. W. Ledermann), Rautlege and Kegon Paul Ltd., London, p36 (1966).

100. Harshish, A. H., Bailey, A. G. and Williams, T. J., Proc. of 2nd Conf. of aerosol Soc., Bournmouth, UK, p121 (1988).

101. Lefebvre, H.: Atomisation and Sprays, Taylor and Francis Inc., p4 (1989).

102. Vincent, J. H., J. Electrostatic, **18**, p113 (1986).

103. Natanson, G.L., Dokl. Akad. Nauk, SSSR, **73**, No. 5, p975 (1950).

104. Moore, A. D. (ed.): Electrostatics and its applications, A Wiley-Interscience Publication, p68 (1973).

105. Bailey, A. G., J. Materials Sci., **9**, p1344 (1974).

106. Swithenbank, J., Beer, J. M., Taylor, D. S., Abbot, D. and McCreath, G. C., Progress in Astronautics and Aeronautics, **53**, p421 (1977).